AD-A094 782 HAWAII UNIV HONOLULU DEPT OF PHYSICS AND ASTRONOMY F/G 20/6
A STUDY OF THE ACOUSTIC-OPTIC EFFECT IN NEMATICS.(U)
DEC 80 C F HAYES N00014-78-C-0417
UNCLASSIFIED 004 NL

1 OF 3
AD A094782

SECURITY CLASSIFICATION OF THIS PAGE (When Data Entered)

REPORT DOCUMENTATION PAGE	READ INSTRUCTIONS BEFORE COMPLETING FORM
1. REPORT NUMBER (14) 004 — 2. GOVT ACCESSION NO. AD-A094782	3. RECIPIENT'S CATALOG NUMBER (2) (3)
4. TITLE (and Subtitle) (6) A STUDY OF THE ACOUSTIC-OPTIC EFFECT IN NEMATICS — FINAL REPORT	5. TYPE OF REPORT & PERIOD COVERED Final Report 1 Sept 1978-Dec. 31, 1980 (1) (8)
	6. PERFORMING ORG. REPORT NUMBER
7. AUTHOR(a) (10) Charles F. Hayes	8. CONTRACT OR GRANT NUMBER(s) (15) N0014-78-C-0417
9. PERFORMING ORGANIZATION NAME AND ADDRESS Department of Physics and Astronomy University of Hawaii Honolulu, Hawaii 96822	10. PROGRAM ELEMENT, PROJECT, TASK AREA & WORK UNIT NUMBERS 121108
11. CONTROLLING OFFICE NAME AND ADDRESS Office of Naval Research Department of the Navy Arlington, VA 22217 (11)	12. REPORT DATE 31 Dec 1980
	13. NUMBER OF PAGES 190
14. MONITORING AGENCY NAME & ADDRESS(if different from Controlling Office) (12) (13)	15. SECURITY CLASS. (of this report)
	15a. DECLASSIFICATION/DOWNGRADING SCHEDULE

AD A094782

LEVEL

16. DISTRIBUTION STATEMENT (of this Report)

Approved for public release; distribution unlimited

17. DISTRIBUTION STATEMENT (of the abstract entered in Block 20, if different from Report)

DTIC ELECTE FEB 10 1981 D C

18. SUPPLEMENTARY NOTES

19. KEY WORDS (Continue on reverse side if necessary and identify by block number)

Acoustic Imaging
Nematic
Acoustic Streaming

20. ABSTRACT (Continue on reverse side if necessary and identify by block number)

The program of this contract has been to study the acousto-optic effect which occurs in nematic liquid crystals when excited by acoustic waves. Both theory and practical application are presented.

DD FORM 1 JAN 73 1473 — unclassified

SECURITY CLASSIFICATION OF THIS PAGE (When Data Entered)

DDC FILE COPY

403697

81 2 09 183

ABSTRACT

Prior to the contract we had proposed an acoustic streaming theory to explain the "acousto-optic" effect which occurs in liquid crystals and had presented experimental data supporting the theory. We subsequently extended the theory to include the simultaneous effect of an applied electric field. During the first year of the present contract we solved the hydrodynamic equations which govern the streaming and obtained a solution for the magnitude of the fluid speed and flow pattern for a small disc-shaped liquid crystal. A sample, doped with grains, was used to test the solution experimentally. A series of cells were constructed and tested which, in fact, showed that an acoustic wavefront pattern can be visualized with this technique. During the second year of the contract we developed and tested a mathematical model which prescribes how a cell should be constructed in terms of: the densities of the cell walls, liquid crystal, and surrounding fluids; the thickness of the cell walls and liquid crystal layer; the acoustic speeds in cell wall (shear and longitudinal), liquid crystal, and surrounding fluids; acoustic frequency; and the incident acoustic beam angle. Cells were also constructed and tested in which an electric field could be applied simultaneously with the acoustic wave in such a way that the sensitivity of the cell to the acoustic field could be adjusted. In this way the acoustic intensity region of interest in the wavefront could be "dialed in".

TABLE OF CONTENTS

		page
INTRODUCTION		1
RESEARCH SUMMARY		1
FUTURE WORK		25
SIGNIFICANCE		27
REFERENCES		28
Appendix I:	"An Ultrasonically Induced Optical Effect in a Nematic Liquid Crystal"	32
Appendix II:	"The Acousto-Optic Effect for a Nematic Liquid Crystal in the Presence of an Applied Electric Field"	54
Appendix III:	"A Study of the Acousto-Optic Effect in Nematics as a Means of Acoustic Field Imaging"	69
Appendix IV:	"The Mathematical Description of a Nematic Liquid Crystal in an Acoustic Field"	99
Appendix V:	"Angular Dependence of Liquid Crystal Based Nematic Acoustic Field Imaging Devices"	119

INTRODUCTION

Although the discovery of the "acousto-optic" effect occurred over forty years ago, only in the last ten years has there been an active research interest with approximately fifty research papers presented in this area. Although a variety of mechanisms to explain the effect had been proposed, only in the last five years has the proper explanation been given. The work performed by the present author was in part responsible for this explanation.

The complete understanding of the acoustic-optic effect should produce a liquid crystal based device which gives a visualization of the acoustic wavefront. Such a tool could be extremely useful for studying the interaction of ultrasonic waves. The author has, in fact, made such a device. Photographs of the resulting acoustic images are included in this proposal. The main task now is to improve the resolution.

RESEARCH SUMMARY

An acousto-optic effect in nematics was noted as early as 1936 by Fredericks and Zolina[4] who observed colors in a homeotropically aligned nematic when it was excited acoustically. Tuning forks with frequencies

from 200 to 600 Hz were used as the acoustic source. They attributed the effect to a rotation of the optic axis in the liquid crystal but gave no details for the mechanism.

In 1969 Fergason[5] proposed from a simplified energy analysis that nematics might be used as detectors of acoustical energy with intensities as low as 10^{-14} W/cm^2. Also in that year Dreyer[6] applied for a patent, later granted, for a liquid crystal optical element composed of a thin (25 μm) aligned nematic sandwiched between either two transparent glass plates or a glass plate and a mirror. The cell was to be observed with crossed polarizers. This device was proposed as a means of detecting electric, magnetic, or acoustic energy. This type of cell has been used to produce the acousto-optic effect which we are considering. The proposed mechanism causing the optical effect was attributed to some sort of physical movement within the liquid crystal.

In 1970 Kessler and Sawyer[7] mounted a 10 MHz ultrasonic transducer on one of the plates of a cell such as Dreyer described with the difference that crossed polarizers were not used. They observed a visual pattern of scattered light above a threshold of 15 mW/cm^2 of acoustic intensity. The pattern had slowly moving domains which traversed the cell and bore similarities to the dynamic scattering mode caused by an electric field. We will refer to this region of acoustic excitation as the "turbulent phase." They attributed the effect to either differential acoustic absorption or acoustic streaming although no detailed theory was given. They measured the on and off response time for the effect to be 0.1 sec and 6 sec respectively. The latter could be reduced, they found, by a factor

of 10 with an applied 20kHz a.c.electric field.

In 1971 Mailer,Likins, Taylor and Fergason[8] used a homeotropically aligned nematic of thickness 25 μm to observe the effects of a 10 MHz bulk acoustic wave. When a threshold intensity of 4 mW/cm^2 was reached,a white light pattern appeared. As the intensity increased,the white light went through all the orders of Newton's colors. We will term this region as that of "tunable birefringence." Above a critical value of acoustic intensity the turbulent region set in as had been found by Kessler and Sawyer. Although no quantitative measurements were given they observed a lowering of the threshold if an electric field were applied. Again no theory was given for the effect.

The first theoretical attempt to explain the effect came in 1972 with Helfrich.[9] For a wave propagating neither parallel nor perpendicular to the optic axis, he calculated the transverse second-order stress which arises since the nematic is anisotropic. He predicted an intensity threshold for which the transverse stress results in a flow and induced tilt in the nematic director. The threshold intensity required by the effect is of the order of 25 W/cm^2 and much higher than that experimentally reported.

Also in 1972 Bertolotti, Martellucci, Scudieri and Sette[10] reported preliminary efforts to obtain the response time for the effect in the region of tunable birefringence. They reported that the response time is less than 12 μsec,their experimental detection limit. Again no theory is proposed for the effect. They did suggest there is a cooperative response of the molecular aggregate rather than a single molecular response.

In 1973 Greguss[11] propagated a 3 MHz ultrasonic wave through water to the nematic cell, after first reflecting the wave from an optically transparent plate. He found the acousto-optic effect occurred at a threshold of

a few mW/cm^2. For the region of tunable birefringence the rise time was in the range of 30 to 50 msec with the fall time less than twice the rise time. For the turbulent phase he obtained a very fast time, faster than the characteristic time of the transducer. If an acoustically opaque object were placed in the path of the wave its quite blurry image appeared on the cell. Also standing acoustic waves in the water were imaged on the cell. Although no theory was proposed, Greguss suggested that the mechanism responsible for the effect may be cybotactic groups which might form in the nematic. He received a patent[12] in 1974 from this work.

In 1974 Dreyer[13] suggested the acoustic pressure in the cell causes an electric potential by means of the piezoelectric properties of the liquid crystal. The resulting potential could then result in a change in the director orientation. More recently, however, he[14] has stated he no longer subscribes to this mechanism, his earlier results being attributed to capacitive effects.

In 1974 Nagai and Iizuka[15] measured the threshold acoustic intensity using a 318 kHz wave for cells of sample thickness ranging from approximately 30 to 100 μm. The values of intensities for the threshold vary from 100 mW/cm^2 to 1 W/cm^2, substantially higher than any other group's findings. They further found the threshold intensity to be proportional to the square of sample thickness. They presented a theory based on the Leslie-Ericksen equations which predicted a threshold that should vary with sample thickness in agreement with their experimental result. The theory was inconsistent, however, with first order equations containing terms of second order and vice versa. Nagai[16] no longer holds to this theory.

In 1974 Kagawa, Hatakeyama and Tanaka[17] measured the threshold of MBBA homeotropically aligned by lecithin treated glass surfaces. They then made comparisons with the threshold for MBBA doped with cetyltrimethylammonium bromide. A frequency of 400 kHz was applied and the sample thickness was 10 μm. Both samples showed a decrease in threshold as the temperature of the sample increased with the doped sample having a lower threshold at all temperatures. They also found an electric field of 66% of the critical electric field increased the acoustic sensitivity by a factor of 50% to 300% depending upon which sample was used. The threshold for the acoustic intensities was of the order of 10 mW/cm^2. They presented no theory for these results.

In 1975 Penz[18] commenting on the work of Kessler and Sawyer[7] suggested that the mechanism for the effect may be a vortex flow due to the anisotropic absorption of the ultrasonic wave.

Also in 1975 Bartolino, Bertolotti, Scudieri, Cette and Sliwinski[19] reported that light passing through a nematic cell of 50 μm thickness could be modulated from low frequencies up to around 1 MHz by acoustic excitation. Both the nematic and smectic phases were investigated. The transducer was attached to one of the plates and was given square wave pulses. They found the threshold acoustic intensity decreases with acoustic frequency, a result they ascribe to an accumulative effect at higher frequencies where the period of oscillation approaches the relaxation time for an elastic deformation. Measuring the intensity of the light as a function of transducer voltage, they found a change of slope in the light intensity versus voltage curve in the region of tunable birefringence. Since their sample, CBOOA, has a smectic

as well as nematic phase they were able to measure the threshold voltage to the transducer as a function of temperature as the nematic phase approached the smectic phase. For this region the threshold voltage has a large increase, a result they attributed to the divergence of K_{33}, the bend elastic constant.

Since this proposal deals with bulk sound waves in nematics we have limited our discussion thus far to this area. However, there have been some studies for surface waves and shear waves as well as bulk waves incident on cholesteric films.

Surface waves were used in 1971 by Davis and Chambers[20] to produce a standing acoustic wave pattern with the nematic in the turbulent phase. The application of an electric field lowered the acoustic power level needed for the effect. No theory was presented to explain the effect. Kapustina et al.[21-25] also using surface waves, produced patterns in the region of tunable birefringence where crossed polarizers are needed to observe the effect. Their analysis is based on a first order velocity gradient effect, the Maxwell effect. They also reported a technique[26] to measure the structural relaxation time of a nematic by measuring the acoustic flow pattern which results from a bulk acoustic wave traveling in a sample whose dimension size is large compared to the acoustic wavelength. In fact some of their work[37] preceded that of Kessler et al.[7] The theory of Kapustina et al. was subsequently criticized by Miyano and Shen[27,32] (Note reference 28 for more detailed information of their experimental technique.) for not correctly explaining the pattern of light that appeared, for not giving the required magnitude of birefringence and for predicting that the transmitted light intensity would oscillate with the imposed frequency, a result which Miyano and Shen report did not occur in their work. Miyano and Shen proposed a simple

quantitative acoustic streaming model to explain their results. They did not observe any threshold for the onset of the effect.

Shear wave excitation of a nematic has been studied by Kagawa, Hatakeyama and Tanaka.[17,29] They found a threshold of oscillation amplitude. As the amplitude increased past the threshold a phase similar to what we have called the turbulent region ultimately set in. They found little effect from changing sample thickness. Their theoretical analysis was based on a simple continuum elastic theory and predicted a threshold which is independent of sample thickness as their experiment indicates. However, their theory also required that the product of frequency and threshold displacement should be a constant, but their experiment did not bear this out.

Cholesteric liquid crystals have also been used[12,30,31] in place of nematics in the acoustic cells. For these cells polarizers are not necessary since the effect is thermal. The acoustic wave heats the cholesteric causing a change in the pitch and hence the color of the cholesteric. Practical application of this technique is difficult due to the relatively high acoustic intensity levels required and the temperature control one must impose.

We may summarize the research prior to 1976 for bulk wave inducement of the acousto-optic effect as follows: As the acoustic intensity increases, a threshold is reached for which white light passes through the cell observed using crossed polarizers. As the intensity continues to increase, Newton's colors appear up to a critical level of intensity where the turbulent phase is established with light scattered, an effect visible without polarizers.

The intensity for the threshold is usually of the order of 10 mW/cm^2 and decreases with an increase in sample thickness, temperature or application of an electric field. The threshold drastically increases near the nematic to smectic phase transition. There have been wide differences reported for the response time for the effect from the μsec to sec range. A wide variety of mechanisms has been reported to explain the effect but only two quantitative theories, both of which predict there should be a threshold for the effect.

In 1976 the author presented a paper (See Appendix 1.) at the Sixth International Liquid Crystal Conference[33] based on research performed here at the University of Hawaii with C. Sripaipan and G.Fang.[34] Since for the previously reported experiments in the last seven years the sample thickness is typically less than one tenth of the acoustic wavelength and there is so large a difference in acoustic impedance at the glass nematic boundaries it seems inappropriate to assume there is a single wave propagated across the nematic perpendicular to the glass plates, as is assumed by the above theories. Rather we assert the acoustic wave causes a lateral flow. If there is a wave at one point in the cell and not in an adjacent point a transverse acoustic wave is induced. It is this transverse wave which causes transverse acoustic streaming resulting in the turning of the director which is responsible for the transmitted light in the region of tunable birefringence. For the case reported in Appendix 1 the difference in pressure was due to the air-nematic boundaries. For most of the cases reported thus far the pressure difference comes from the boundary of the acoustic field or non-uniformity in the intensity across the acoustic

field itself. We further assert that there is no threshold for the effect. What has been previously reported as a threshold results from the transmitted intensity being dependent upon V^4 where V is the transducer voltage.(See Eq. 20 in Appendix I.) The absence of a threshold can be seen from the graph in Fig. 4 of Appendix I. The graph shows the sudden increase in the intensity with voltage is quite a good fit to Eqs. 18 or 20 in Appendix I. which are not threshold equations. The presence of K_{33} in Eq. 18 explains the divergence of the reported threshold as the nematic-smectic transition temperature is approached. The Discussion Section at the end of Appendix I lists our experimental evidence supporting our theory.

Also at the Sixth International Liquid Crystal Conference the work of Candau, Peters and Nagai[35] was presented in which they showed similar conclusions to ours: there is no threshold and the mechanism responsible for the effect is acoustic streaming. However, I believe the details of their theory are in error. Their streaming force is perpendicular to the glass plates even though the spacing between the glass plates is as small as 4% of the acoustic wavelength and the large difference in acoustic impedance between the liquid crystal and the glass gives strong reflections. It is this error in mechanism which forces their assumption that the director must be tilted even when no acoustic field is applied. I believe the mechanism responsible for the effect with their arrangement arises from the boundaries in the cell between where there is an acoustic wave and where there is none. The multiple reflections of the acoustic wave add to give an oscillating pressure, oscillating with the frequency of the acoustic wave. There is little (less than 15%) spacial variation of the pressure along the axis perpendicular to the glass plates due to the multiple reflections of the acoustic wave at the glass-nematic boundaries. The oscillating pressure then causes a lateral oscillating

flow which results in a lateral acoustic streaming force. The same mechanism applies in the acoustic beam where the intensity is not laterally uniform. Less important are the non-insignificant cross terms coupling fluid velocity and director orientation which are omitted from their streaming force. They measure the response time for the effect to be of the order of seconds.

A third paper presented at the same conference by Dion and De Forest[36] also concluded there was no threshold. The mechanism they proposed was based on the anisotropy of acoustic speed in the nematic. The acoustic wave is transmitted to the cell through water at an angle of 45° to the plate normal. The observed pattern indicates the director tilts in one direction, a conclusion which the authors feel implies streaming is not the mechanism. I believe that here also the mechanism is acoustic streaming which occurs as the wave reflects back and forth through the cell. Since the wave comes in at an angle there is a net transverse motion for the reflecting wave in the cell which gives rise to streaming in that direction and hence the tilt in one direction. Their experimental curve is quite similar to our graph, Fig. 4, in the Appendix. If the maxima and minima of the curves are plotted as our Fig.5 in the Appendix their data show a linear fit as well as our data. They reported a very small intensity , $1\ \mu W/cm^2$, is required for the effect. This figure is based, however, on the pressure of an acoustic field with intensities in the mW/cm^2 range which taper off along the edges to the smaller range where the effect is still seen. I feel what is being seen is the result of the lateral acoustic streaming induced by the higher intensity regions.

The author presented an invited paper at the Ordered Fluids and Liquid Crystal Symposium held in conjunction with the 1977 national meeting of the American Chemical Society. See Appendix II. The paper shows that if an electric field is applied to the nematic cell during the simultaneous stimulation of an ultrasonic wave the experimentally determined behavior

agrees with what the author's theoretical model predicts.

In 1977 Dion[38] and Dion and Jacob[39] proposed a new theory where the effect was attributed to anisotropic absorption of the acoustic wave in the nematic giving rise to a torque on the molecules. They reported the power required for the effect was in the microwatt/cm^2 region rather than the milliwatt/cm^2 region reported by other researchers. We feel the new data they report agree with our model and further note that they are using liquid crystal thicknesses of 250 micrometers rather than the 10-100 micrometers used by other researchers. Making such a change for H, the liquid crystal thickness, in our Equation 44 in Appendix III results in a predicted decrease in the level needed for observation of the effect from the milliwatt/cm^2 range to the microwatt/cm^2 range.

In 1977 Hiroshima and Shimizu[40] reported that sound fields could be visualized using a mixture of nematic and cholesteric liquid crystal, where there is a change of texture from planar to focal conic. No polarizer is needed for the observation. They assume the mechanism proposed by Helfrich;[9] however,no detailed comparison is made between the observation and the theory.

In 1978 Nagai and Iizuka[41,42] reported a nematic cell in which the liquid crystal was divided into a series of separated segments. The division was made to confine the flow due to the sound (i.e. the acoustic streaming). With the cell they were able to improve the resolution above what had been previously obtained. This research again implies indirectly the streaming mechanism. In the independent work by Lebrun, Cantau and Letelier[43] in 1979 a similar cell is constructed with similar conclusions. The direction

of the streaming they take to be mainly perpendicular to the glass plates[44] in the area of the incident acoustic beam, rather than the transverse flow model of the present author. This author has consistently insisted the flow is transverse and now has direct evidence that such is the case:

During the initial year this contract with ONR has been in force the present author[45,46,47] has reported the solution to second order of the hydrodynamic equations governing the flow in a system such as the one used in the nematic cell. Experimental confirmation (See Appendix III.) of the direction and magnitude of the flow was made by microscopic observation of fine grains suspended in transparent oil stimulated by an acoustic wave. Various cells have been made for observation of an acoustic wavefront by means of the nematic acousto-optic effect. In Figure 1A a close-up of the cell is shown which allows visualization of the squares of nematic liquid crystal homeotropically aligned with no acoustic wave present. The squares are 0.8 mm on the side and are separated by strips of Riston, a photo-resist. In this way the flow is confined to each nematic square so it should be possible for a square in which there was a flow to have an adjacent square with no flow. The cell appears darkened since it is observed between crossed polarizers. A small amount of light can be seen at the nematic-Riston interface in some of the squares due to alignment of the interface rather than from the glass surfaces which had been treated with lecithin. In Figure 1B the change in transmitted light is shown when an ultrasonic beam is directed to the cell. In Figure 1C the acoustic wave is removed and the cell relaxes back toward the state of Figure 1A. This relaxation process takes place more quickly if an electric field is applied. The dark region on the left of Figure 1D-G is due to the

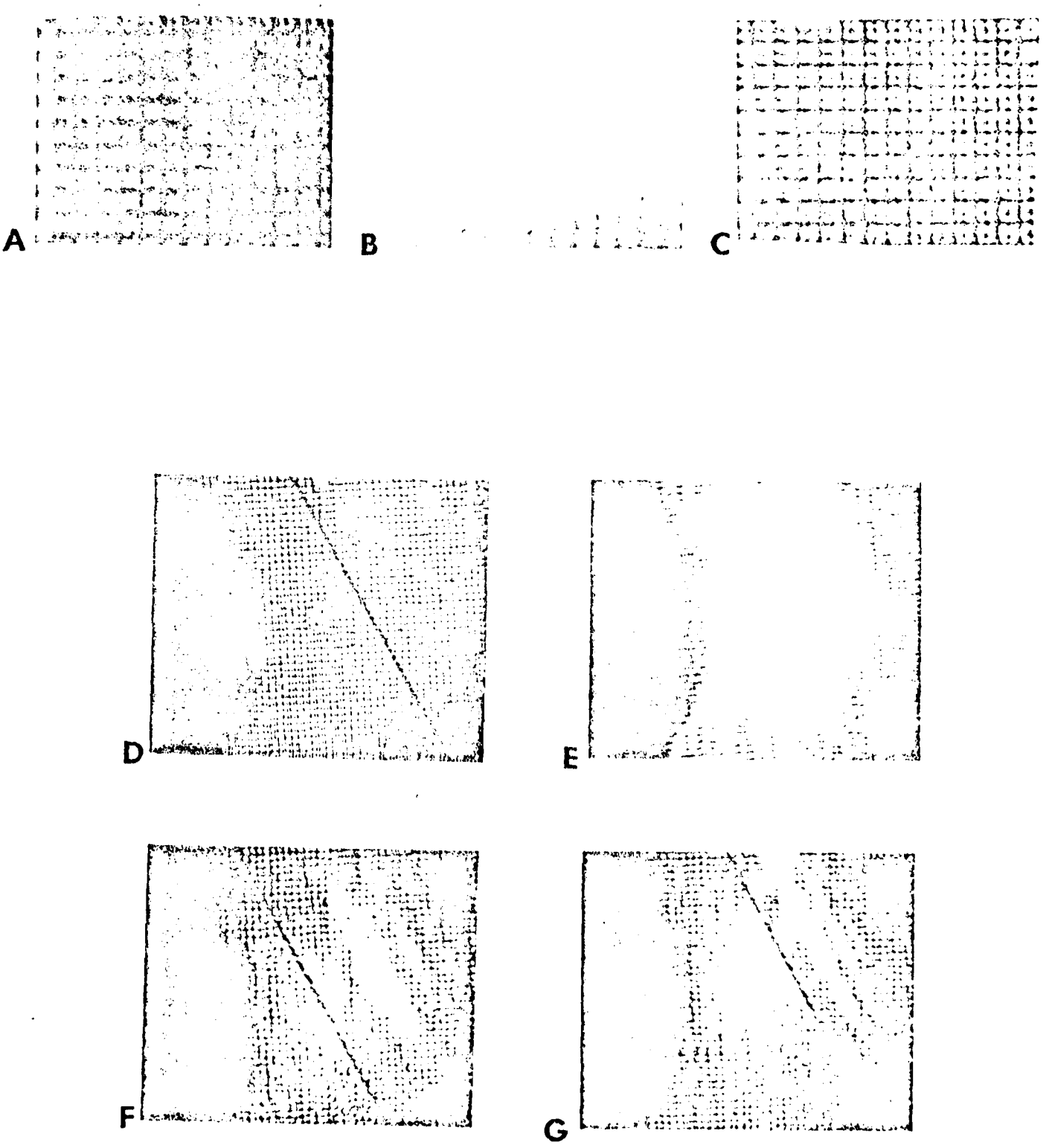

Figure 1

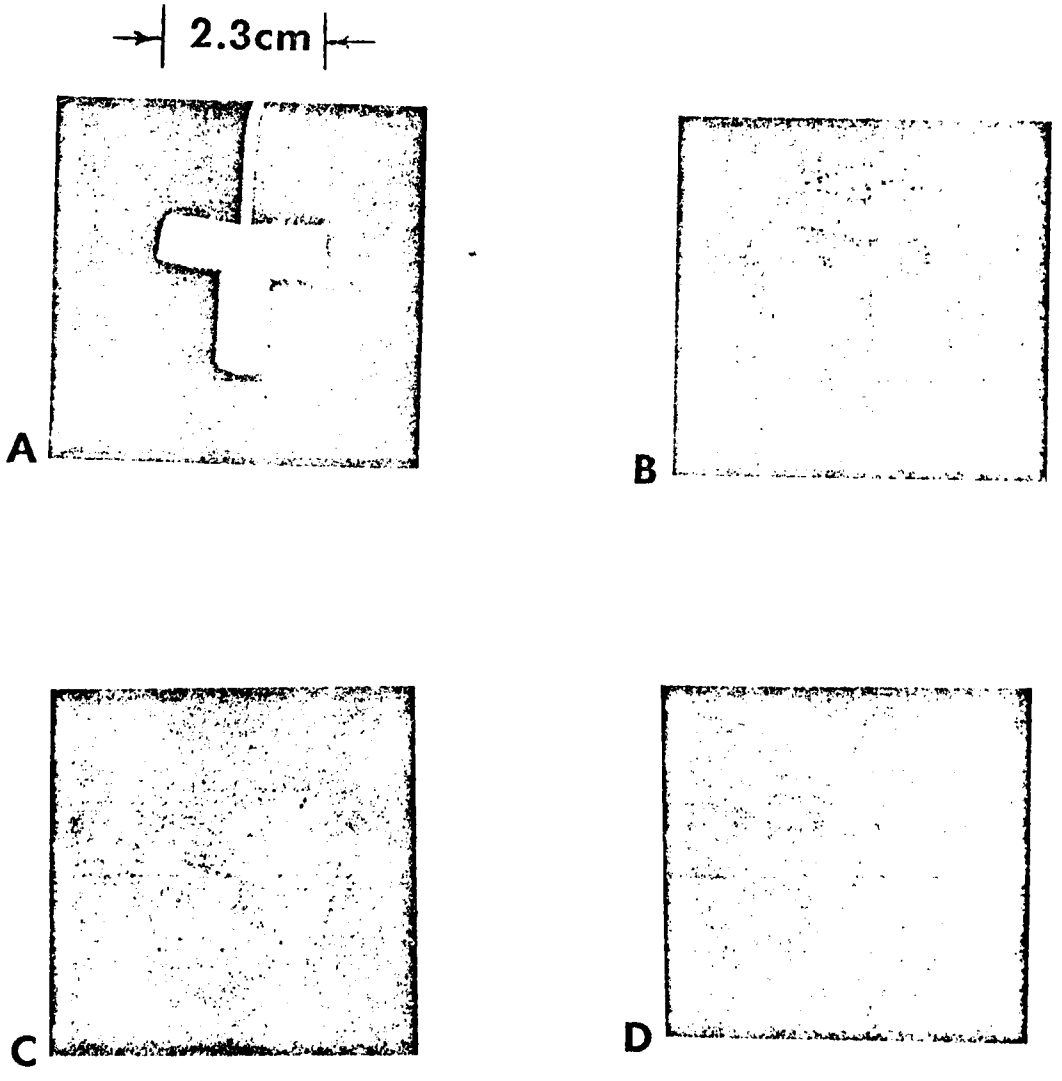

Figure 2

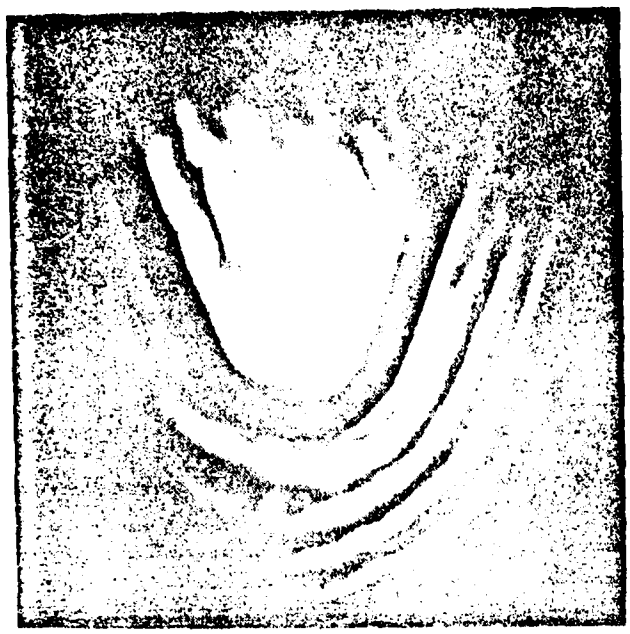

A

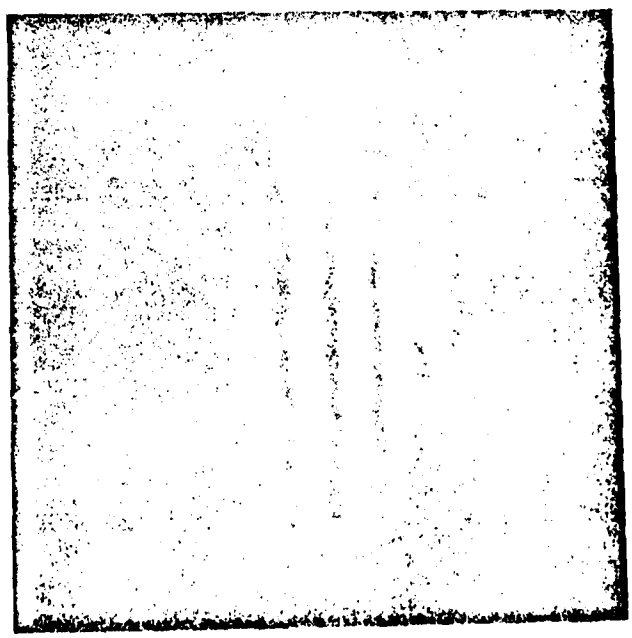

B

STRAIGHT EDGE

Figure 3

A

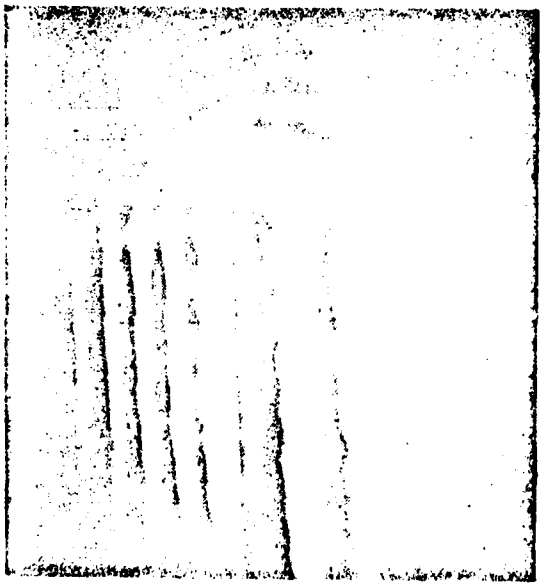

B

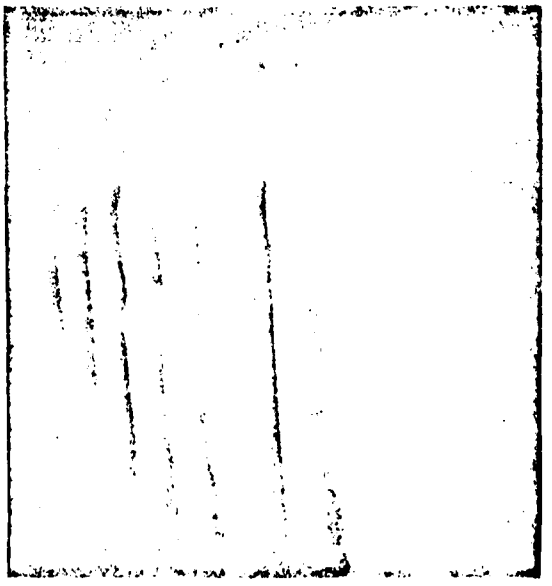

C

Figure 4

transducer blocking the light from the cell. The dark line seen to be almost vertical in Figure 1D,1F and 1G is the edge of a transparent plastic strip which covers the left side of the cell. In D no wave is emitted from the transducer. In F and G the ultrasonic wave is turned on and the diffraction pattern of the acoustic wave is seen as well as a certain amount of the wave which is transmitted through the plastic. The difference between F and G is how far the plastic strip is from the cell. In E the cell is seen with no plastic present. In Figure 2 a cell with no Riston array is compared with the former type of cell. In both of these cells the back glass plate is silvered and therefore observed in reflection. In Figure 2A the optical image of a "T" made of foam is shown with a wire support. The "T" was placed in the acoustic beam giving its acoustic image in B where no Riston array was used. The foam was placed immediately behind the mirrored wall of the cell. Note the wire support which is placed farther from the cell is just barely visible. In C the cell is shown with the "T" removed. In D a cell is shown for which the nematic is confined by a Riston array. Figures 3 and 4 show the acoustic diffraction patterns of various objects placed in the path of the acoustic beam. Cells for these figures are observed in transmission rather than reflection. They do not have a mirrored surface or a Riston array. Figure 3A shows the pattern obtained for a wire bent in a "U" shape. The dark "U" shape is the optical image seen since a transparent cell is utilized. In Figure 3B the pattern is due to the edge of a clear plastic strip. In Figure 4A both the optical image of a straight wire may be seen as well as the acoustic diffraction pattern that is formed. For B the acoustic intensity is increased over that of A and for C the wire is moved farther from the cell. Note the difference in fringe spacing on the left and right sides of the wire. This difference is due to the angle between the incident beam and the nematic cell.

Working with the present author on this project during the first contract year has been W. Laidlaw, a visiting professor from the University of Calgary. Since there is still disagreement in the literature even now[39,40,48] as to whether the acousto-optic effect is due to streaming, Professor Laidlaw has presented an overview which should clear up much of the confusion. See Appendix IV. He also has included time dependence for the onset of the effect which has been omitted theoretically in all previous work.

During the first part of the second contract year we have concentrated on the influence of the incident acoustic angle. One group report[44] that the effect only occurs for their cells at angles from 27 to 31 degrees. We now understand why. For the effect to occur, streaming must occur in the liquid crystal layer. For significant streaming to occur there must be an amplitude maximum in the liquid crystal layer. The incident angle, the impedances of the liquid crystal, cell walls and surrounding fluids, the wall thicknesses and acoustic frequency which result in the large amplitudes are those which allow maximum acoustic transmission. Therefore a theoretical model has been developed which prescribes how these parameters may be optimized for maximization of the effect. The details of this work is in Appendix V. This report, therefore, should prove most useful since it directs how a cell should be constructed for a given acoustic frequency. Cells were constructed which verified our model.

Also during the second year of the contract the effect of an applied electric field upon the visual pattern was investigated. The author had developed an equation (Appendix II) which shows how the sensitivity of the acousto-optic effect depends upon a simultaneously applied electric field. Although previous authors have referred to the change in the time response due to an electric field the pattern sensitivity to the electric field has

not been investigated. For a nematic liquid crystal with positive (negative) dielectric anisotropy an increase in the electric field causes a decrease (increase) in the sensitivity of the cell to the acoustic field. Therefore, it would appear the acoustic intensity region of interest could be "dialed in" by an electric field. For Figure 5 the ultrasonic beam was incident upon a thin lucite sheet in which a one-quarter inch circle has been cut. Part of the sound was transmitted through the lucite and superimposed upon this intensity was the diffraction pattern from the hole. The intensity is of form:

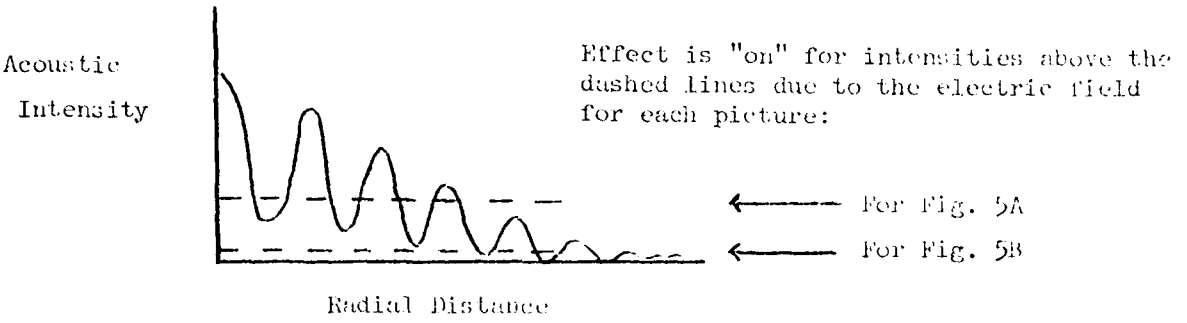

The electric field for Figure 5 part A was adjusted to reveal the diffraction pattern and for Figure 5 part B for a more sensitive acoustic detector. Since the nematic used for this cell has positive dielectric anisotropy the electric field was reduced in going from Figure 5A to 5B. For an increase in electric field the entire field of view would go dark.

In Figure 6 a transparent cell covers the field of view for each picture. The solid circle in the left of each picture is the transducer operating at 1 Mhz. The open circle centered in each picture is the mount for the initial light polarizer. At approximately 45 degrees to the horizontal is an aluminum rod located just on the transducer side of the cell. In Figure 6A the acoustic diffraction pattern of the rod is visualized. The electric field is approximately 10 v rms at 100 Hz. For Figure 6B the applied electric

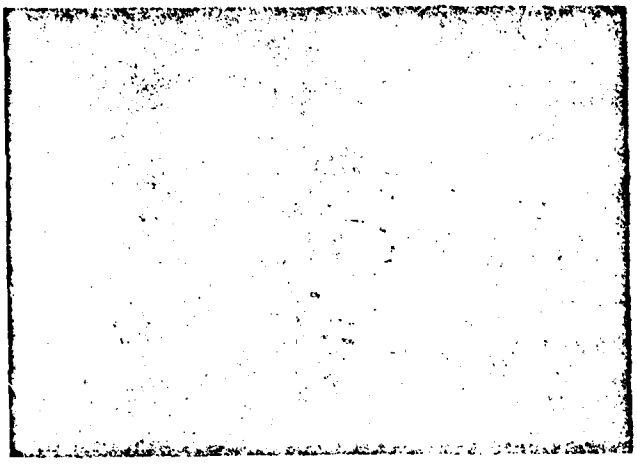

A

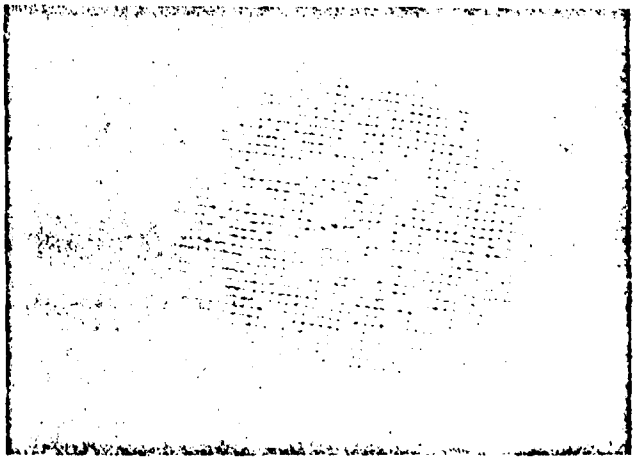

B

Figure 5

A

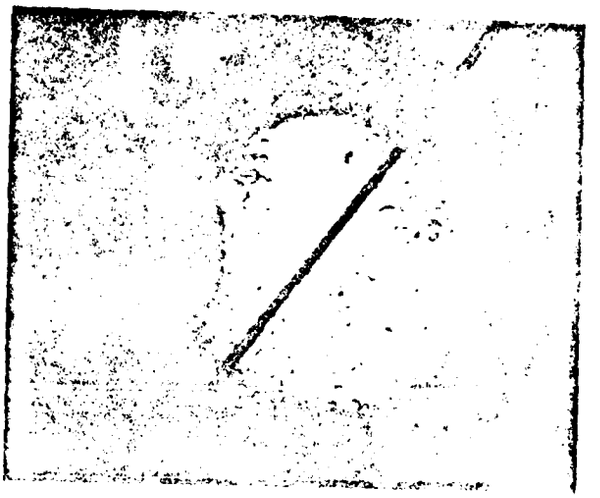

B

C

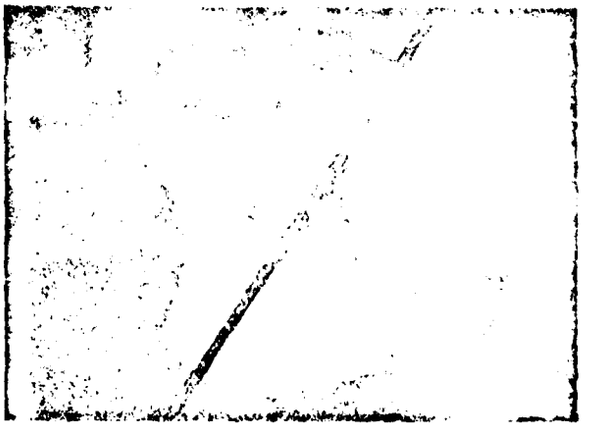

D

Figure 6

A

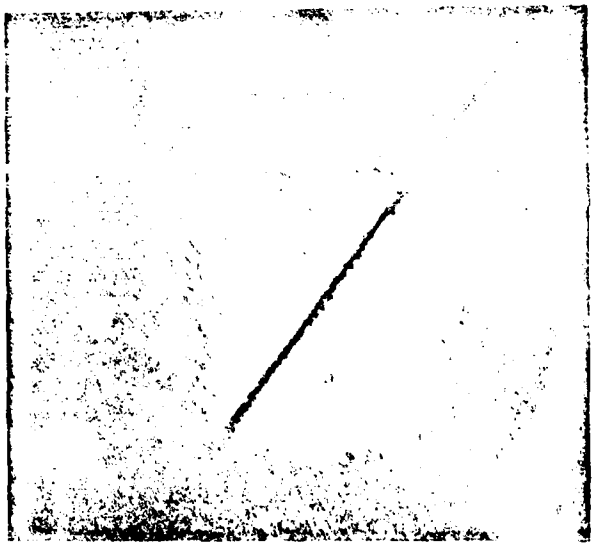

B

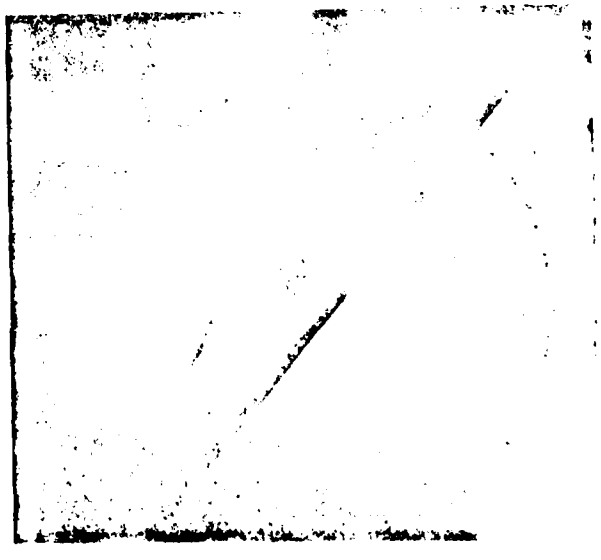

C

Figure 7

A

B

Figure 8

field is reduced to zero and the turbulent mode appears, all but destroying the observation of the acoustic diffraction pattern. By increasing the electric field above the value in Figure 6A order may be restored and the cell is sensitive to only the first few fringes, Figure 6C. However, even with the high electric field more fringes may be seen by merely increasing the sound intensity, Figure 6D. The picture in Figure 6 were all taken for sound intensities in the range of 0.02 to 0.10 W/cm^2. This same cell can be used for visualization of intensities over an order of magnitude larger, by merely using a larger electric field. In Figure 7 the acoustic intensity is 1.5 W/cm^2. In Figure 7A a series of concentric circles is shown as well as the pattern from the aluminum rod. The circles are the acoustic diffraction from an air bubble formed on the cell wall by cavitation which occurs for an acoustic wave of such intensity. Again in Figure 7B the turbulent mode is seen when the field is reduced. In Figure 7C the acoustic wave is removed and the field restored but still one minute later some regions of non-alignment persist along the fringe lines where the turbulence was more pronounced.

In Figure 8A the acoustic diffraction pattern from a straight edge is shown. The transparent plastic strip blocks the beam from the left portion of the pictures. For Figure 8B a red filter is placed in front of the camera. In this case it is shown that the contrast of the pattern may be improved for the cell by yet another method, a light filter.

FUTURE WORK

We now understand the mechanism (acoustic streaming) which causes the acousto-optic effect; the simultaneous effect of an applied electric field; the role of cell wall thickness, density, and wave speeds; the role of the liquid crystal layer thickness and wave speed; the role of the density and wave speed of the surrounding fluids; and the effect of changing the incident acoustic angle. We have succeeded in making a variety of cells to visualize acoustic shadows from objects as well as acoustic diffraction patterns.

However, a number of areas need to be investigated. The most important of these is the resolution of the acoustic image. There are a variety of cell designs which we now have in mind utilizing the insights obtained from the study completed thus far. One of these designs encapsulates the nematic in thin, flexible, transparent plastic. The plastic should be coated to make it electrically conductive so an electric field may be maintained for proper alignment of the liquid crystal. The technology of encapsulating liquid crystals is well established as evidenced by the liquid crystal thermometers and "mood" rings now on the market. We merely used to have a nematic liquid crystal encapsulated rather than the cholesteric liquid crystal presently used. There are companies which make electrically coated thin plastic and we have received a sample from one such company. By matching the impedance of the plastic to that of water the cell should be quite transparent to the sound and therefore distort the field being studied as little as possible. The flexible plastic is less fragile than the thin glass presently used and yet thin enough to prevent multiple reflections in the cell walls thereby increasing the resolution. Encapsulating the liquid crystal should also improve the resolution since the acoustic streaming

which causes the effect will be confined.

It is also advisable to use higher frequencies than we have used thus far. As the frequency increases the wavelength decreases thereby improving the present diffraction limited resolution. We have been working with a 1.5 mm wavelength acoustic wave, so naturally it is not surprising that the resolution in our present cells are about this length.

Although the mathematical groundwork has been laid, we still need to study quantitatively the time response of the cell. The response will be measured as a function of acoustic intensity, frequency, liquid crystal layer thickness and viscosity.

Finally, there are important temperature effects which should be investigated. If the liquid crystal has a smectic as well as a nematic phase, as the temperature is lowered through the nematic phase, the K33 elastic constant will diverge causing a striking change in the acousto-optic effect which is governed by this constant.

SIGNIFICANCE

There is widespread technological importance to the research which we are proposing. We feel we understand the basic mechanism responsible for the acousto-optic effect in the birefringent region and wish to extend and further test our formulation. The result will have immediate implications for application. An adequate understanding of the mechanism is necessary before one can successfully use the effect, for instance, in amplitude-phase data converters, detection of acoustic signals and acoustic field imaging. We feel the poor results obtained thus far in attempted applications are the result of the lack of understanding of the underlying mechanism. The success of the technique would be important in acoustic holography, medical diagnosis, and naval underwater visualization.

Finally, the widespread current interest in the field of liquid crystals among scientists from a wide variety of disciplines is indicative of its perceived importance in the pursuit of understanding of condensed matter. These mesophases are particularly important in areas of statistical mechanics, phase transitions and the many body approach to condensed matter. Acoustic excitation of liquid crystals both near and removed from regions of phase transitions is an important tool in this pursuit. Although much work has been done on first order interactions of an acoustic field with a liquid crystal, our proposal would substantially increase the knowledge of second order effects on liquid crystals for which so little is known.

References

1. J.D. Parsons and C.F. Hayes, Solid State Commun. 15, 429 (1974).
2. I. Muscutariu, S. Bhattacharya, J.B. Ketterson, Phys. Rev. Lett. 35, 1584 (1975).
3. S. Bhattacharya, I. Muscutariu and J.B. Ketterson, Sixth International Liquid Crystal Conference, J-17 (1976).
4. V.V. Zolina, Trudy Lomonosov Inst. Akad. Nauk SSSR 8, 11 (1936).
5. J.L. Ferguson, Proc. Second International Symposium on Acoustic Holography, 2, 53 (1970).
6. J.F. Dreyer, U.S. Patent No. 3,597,043 (1971).
7. L.W. Kessler and S.P. Sawyer, Appl. Phys. Lett. 17, 440 (1970).
8. H. Mailer, K.L. Liking, T.R. Taylor and J.L. Ferguson, Appl. Phys. Lett. 18, 105 (1971).
9. W. Helfrich, Phys. Rev. Lett. 29, 1583 (1972).
10. M. Bertolotti, S. Portelluccci, F. Scudieri and D. Sette, Appl. Phys. Lett. 21, 74 (1972).
11. P. Greguss, Acustica 29, 52 (1973).
12. P. Greguss, U.S. Patent No. 3,831,434 (1974).
13. J.F. Dreyer, J. Acoust. Soc. Am. 55, 407 (1974).
14. J.F. Dreyer, Private Communication.
15. S. Nagai and K. Iizuka, Japan J. Appl. Phys. 13, 189 (1974).
16. S. Nagai, Private Communication.
17. Y. Kagawa, T. Hatakeyama and Y. Tanaka, J. Sound Vibration 36, 407 (1974).
18. P.A. Fox, Physics Teacher, 199 (April, 1975).
19. R. Bartolino, M. Bertolotti, F. Scudieri, D. Sette and A. Sliwinski, J. Appl. Phys. 46, 1928 (1975).
20. L.E. Davis and J. Crowbers, El. Lett. 7, 297 (1971).
21. O.A. Karnaukina and Y.G. Stathnikov, Sov. Phys. JETP 37, 117 (1973).

References (continued)

22. O.A. Kapustina and Y.G. Statnikov, Sov. Phys. Acoust. 20, 154 (1974).

23. O.A. Kapustina and A.A. Talashev, Sov. Phys. Acoust. 19, 397 (1974).

24. O.A. Kapustina, Sov. Phys. Acoust. 20, 291 (1974).

25. O.A. Kapustina, Sov. Phys. Acoust. 20, 1 (1974).

26. O.A. Kapustina and Y.G. Statnikov, Sov. Phys. JETP 39, 306 (1974).

27. K. Miyano and Y.R. Shen, Appl. Phys. Lett. 28, 473 (1976).

28. K. Miyano and Y.R. Shen, Appl. Phys. Lett. 28 699 (1976).

29. Y. Kagawa, T. Hatakeyama and Y. Tanaka, J. Sound Vib. 41, 1 (1975).

30. J.F. Havlice, Electron. Lett. 5, 477 (1969).

31. B.D. Cook and R. Werchan, Ultrasonics 9, 101 (1971).

32. K. Miyano and Y.R. Shen, Sixth International Liquid Crystal Conference, J-31 (1976).

33. C. Sripaipan, C. Hayes and G.T. Fang, Sixth International Liquid Crystal Conference, J-29 (1976).

34. C. Sripaipan, C. Hayes and G.T. Fang, "Ultrasonically Induced Optical Effect in a Nematic Liquid Crystal," 15A , 1297 (1977).

35. S. Candau, A. Peters and S. Nagai, Sixth International Liquid Crystal Conference J-30 (1976).

36. S. Nagai, A. Peters and S. Candau, Rev. Phys. Appl. 12, 21 (1977).

37. J.L. Dion and F. DeForest, Sixth International Liquid Crystal Conference, K-18 (1976).

38. A. Kapustina and L. Dmitriev, Kristallogr. 7, 332 (1962).

39. J. L. Dion, C.R. Acad. Sc. Paris 284, 219 (1977).

40. J.L. Dion and A.D. Jacob, Applied Physics Letters 31, 490 (1977).

41. K. Hiroshima and H. Shimizu, Japan, J. Appl. Phys. 16, 1889 (1977).

42. S. Nagai and K. Iizuka, Japan. J. Appl. Phys. 17, 723 (1978).

43. S. Nagai and K. Iizuka, Mol. Cryst. Liq. Cryst. 45, 83 (1978).

44. J. Lebrun, S. Candau, S.V. Letcher, Journal de Physique C3, 293 (1979).

45. S. Letcher, J. Lebrun and S. Candau, J. Acoust. Soc. Am. 63, 55 (1978).

46. C. Hayes, J. Acoust. Soc. Am. 64, 561 (1978).

References (continued)

47. C. Hayes, Symposium of the Physics and Chemistry of Liquid Crystal Devices, 19 (1979).

48. C. Hayes, "A Study of the Acousto-Optic Effect in Nematics as a Means of Acoustic Field Imaging," Technical Report, ONR Contract N00014-78-C-0417 (March, 1979).

49. I.A. Chaban, Sov. Phys. Acoust. 24, 145 (1978).

50. J.N. Perbet, M. Hareng and S. Le Berre, Rev. Phys. Appl. 14, 569(1979).

APPENDIX I TO APPENDIX V

The following papers are included in the Appendix:

I. "An Ultrasonically Induced Optical Effect in a Nematic Liquid Crystal." Phys. Rev. 15A, 1297 (1977).

II. "The Acousto-Optic Effect For a Nematic Liquid Crystal in the Presence of an Applied Electric Field," Liquid Crystals and Ordered Fluids, 3, 287 (1978).

III. "A Study of the Acousto-Optic Effect in Nematics as a Means of Acoustic Field Imaging," Technical Report, ONR Contract N0001h-78-C-0h17 (March, 1979).

IV. "The Mathematical Description of a Nematic Liquid Crystal in an Acoustic Field,"Mol.Cryst.Liq.Cryst. 59, p.13 by W.C.Laidlaw,1980.

V. "Angular Dependence of Liquid Crystal Based Nematic Acoustic Field Imaging Devices," Technical Report, ONR Contract N0001h-78-C-0h17 (April, 1980).

AN ULTRASONICALLY INDUCED OPTICAL EFFECT IN A NEMATIC LIQUID CRYSTAL

Chatri Sripaipan

Department of Electrical Engineering, University of Hawaii

Charles F. Hayes

Department of Physics and Astronomy, University of Hawaii

and

Gautier T. Fang

Department of Electrical Engineering, University of Hawaii

Honolulu, Hawaii 96822, U.S.A.

ABSTRACT

A series of lines parallel to the liquid crystal boundary have been observed using crossed polarizers on a homeotropically aligned nematic liquid crystal cell excited by ultrasonic bulk waves of about 1 MHz. We propose that the physical mechanism responsible for the rotation of the molecules of the liquid crystal from their perpendicular position is the acoustic streaming which occurs in any viscous liquid. Theoretical analysis of the model shows that the lines should be separated by one quarter of the acoustic wavelength and the intensity of the light reflected from the cell through crossed polarizers should be proportional to $\sin^2(BV^4)$, where V is the excitation voltage applied to the transducer and B is a constant. Both predictions are supported by our experimental results.

I. Introduction

It has recently been found [1-4] that when the intensity of an ultrasonic bulk wave, incident normally on a homeotropically aligned nematic liquid cell, exceeded a certain threshold, the cell became birefringent. The birefringence was attributed to the tilt of the liquid crystal director from its perpendicular position with the tilt caused by some sort of hydrodynamic flow. But the physical mechanism of the flow has been unclear.

In order to explain this phenomenon, some mechanisms such as cybotactic nematic phase [2], and anisotropic absorption [5] have been suggested, but they are neither supported by quantitative theories nor verified by experimental results. The first quantitative theory was proposed by Helfrich [6]. He considers the transverse component of the radiation pressure generated by the anisotropy in the visco-elastic properties of the liquid crystal to be responsible for the acousto-optic effect. The threshold acoustic intensity for hydrodynamic instability is estimated by his theory to be 25 W/cm^2, which is much higher than the experimental results found by others [1,2,4] to be only a few milliwatts per square centimeter. Nagai and Iizuka [3] have obtained, from the Leslie-Ericksen hydrodynamic equations, a threshold intensity for hydrodynamic instability of 0.2 W/cm^2 but recently Nagai [7] expressed doubts about the existence of such a threshold.

In this paper, we report the results of an investigation of the acousto-optic effect in a homeotropically aligned nematic liquid crystal cell. We observe a series of lines parallel to the free edges of the liquid crystal cell and have made quantitative measurements of the reflected light intensity through crossed polarizers as a function of

the excitation voltage to the piezoelectric transducer. A physical model based on acoustic streaming is proposed to explain the observed phenomena and a quantitative relationship between the reflected light intensity and the excitation voltage is derived from the Leslie-Ericksen hydrodynamic equations using the acoustic streaming theory. Finally, we list the evidence supporting our model and compare it with other models.

2. Experiment

2.1 Experimental Set-up

The test cell consisted of a thin layer of N-(p-Methoxybenzylidene)-p-n-butylaniline (MBBA) (Eastman Chemical No. X11246) sandwiched between a glass plate and a mirror (Fig. 1) at a room temperature of 21°C. Homeotropic alignment was achieved by a thin coating of lecithin on the two inner surfaces which were separated by two narrow strips of mylar spacers. The glass plate and the mirror were glued together on the two edges along the spacers; the other two edges were left open. The cell was coupled to a thickness mode piezoelectric transducer through a thin layer of vacuum grease.

Optical observations were made using a reflected-light polarizing microscope (Nikon S-KE). For a larger field of view (2.5 cm diameter), a Bausch and Lomb Stereozoom microscope converted into a reflected-light polarizing microscope was used.

For quantitative measurements of reflected-light intensity from the test cell, the system of Fig. 2 was used. The light source of the microscope was a 3-mW He-Ne laser. A 20X objective was used with the field aperture fully closed so that the area investigated was small (0.2 mm diameter) and therefore more uniform. The image projected on the front

end of the photomultiplier without the eye piece was a uniaxial cross when the liquid crystal was in its unexcited state. The pin hole aperture of the photomultiplier was placed at the center of the cross. As the signal applied to the transducer was linearly increased, the light intensity was plotted as a function of excitation voltage on the XY plotter.

2.2 Experimental Results

a) Optical observation of a small area (2.5 mm diameter)

As the voltage applied to the transducer at about 1 MHz was slowly increased, the liquid crystal changed from a dark appearance to one having a pattern of white areas. Then colors started to appear at the center of the white areas in the sequence of increasing phase difference while the preceding color moved to the perimeter. After several orders of color change, the centers became light brown. This we identified as the end of the region of tunable birefringence and the start of the turbulent region where the liquid crystal strongly scattered light. The light brown areas replaced the colored pattern. Continuing to increase the voltage disinclination lines and wave-like patterns (period ≈ 100μm) appeared. They moved in a vortex motion (Fig. 3a) with their speed increasing with voltage. Finally, totally dark areas appeared as the liquid crystal went into its isotropic phase. A thermistor attached to the bottom glass plate of the liquid crystal cell registered a significant temperature increase during the turbulent phase.

When a voltage ($350V_{p-p}$ at 1 MHz) larger than that needed for the turbulent region was suddenly applied to the transducer with the cell at room temperature, the liquid crystal cell went immediately to the end of the region of tunable birefringence, then moved through the

turbulent region and into the isotropic phase in about one minute.

b) Pattern on the whole liquid crystal cell in the region of tunable birefringence

Looking over the whole cell, we saw that the white areas formed lines parallel to the two free edges (Fig 3b). This pattern was best seen when these lines were making 45° to the polarizer and the analyzer.

The distance between the lighted lines decreased as the ultrasonic frequency increased. Pictures of the liquid crystal cells (25 μm and 70 μm thick) were taken at different frequencies from 640 kHz to 1.33 MHz. The distances between lighted lines were measured at 17 places on these photographs and found to be $(0.29 \pm 0.08)\lambda$ where λ is the wavelength of acoustic bulk waves.

When the liquid crystal cell was placed directly above the transducer, two dark lines, one parallel to the polarizer and the other to the analyzer, formed a cross at the center of the cell. As the stage was rotated, the cross remained basically intact. When a small air bubble was introduced into the liquid crystal, concentric rings of lighted lines were seen surrounding it (Fig. 3c).

c) Light detection using a photomultiplier

The set-up of Fig. 2 was used to find and plot the reflected light intensity at the center of a lighted area as a function of the excitation voltage to the transducer. The orientation of the microscope stage was set for maximum birefringence, at which the lighted lines made 45° to the polarizer and the analyzer. The result for a 60 μm cell at 0.669 MHz is presented in Fig. 4.

When the signal from the photomultiplier amplifier was observed directly on an oscilloscope, it did not contain the ultrasound frequency

when the liquid crystal was in the tunable birefringence region. However, in the turbulent region, the light was seen to be modulated by the ultrasound frequency.

3. Theory

3.1 Description of the Physical Model

Our physical model is as follows: As the bottom glass plate of the liquid crystal cell moves vertically upward the pressure in the MBBA is increased. A horizontal pressure gradient will be induced at the two free edges of the cell, the air-MBBA boundaries. As the bottom glass plate moves downward the gradient is reduced and then reversed. The oscillating gradient induces an oscillation in the positions of the boundaries which cause waves to travel horizontally through the cell. Consequently a standing wave may be set up between the air-MBBA boundaries with nodes and antinodes in lines parallel to the boundaries. The standing wave sets up acoustic streaming [8] between the nodes and antinodes which turns the liquid crystal molecules in the plane perpendicular to the free boundaries and the glass plates. The areas between the nodes and antinodes appear as lighted lines under a polarizing microscope with dark lines indicating the nodes and antinodes.

3.2 Theoretical Analysis

In the hydrodynamic formulation of Stephen [9] based on the Oseen, Frank, Ericksen and Leslie theories, the director, velocity, pressure and density are all coupled. We expand the variables in the coupled

equations around their equilibrium values assuming a standing compression wave. Taking u to be any of these variables,

$$u = u_c + \varepsilon u_1 + \varepsilon^2 u_2$$

where u_o is the equilibrium value and ε a parameter to indicate the degree of approximation we are using. Each equation is valid to each power of ε. The equilibrium value of the director is taken in the z direction. The pressure and density equilibrium values are constant and the velocity equilibrium value is zero. For each variable, u_1 is a sinusoidal function of time. Therefore, u_2 consists of a sinusoidal function of time with twice the frequency of u_1 and a static part coming from the time average of the u_1^2 terms. We take the time average of the equations to order ε^2 so only the static part of u_2 is of interest.

We consider a homeotropically aligned nematic sandwiched between two glass plates at $z = 0$ and $z = h$. Assuming the director may turn from the z direction, we may take the x-z plane to always contain the director and solve the equations in two dimensions without loss of generality. Later we will identify the x axis as the direction of second-order hydrodynamic flow.

To first order we have five variables: the two components of velocity, the director, pressure and density. We have the four hydrodynamic equations of Stephen and we take the first-order pressure

$$P_1 = c^2 \rho_1 \qquad (1)$$

where c is the velocity of sound and ρ_1 the first-order density of the fluid. A term proportional to the partial time derivative of ρ_1 could be added but the net effect may be absorbed by a change in the bulk viscosity [8].

To first order in ϵ the hydrodynamic equations are

$$0 = \frac{\partial n_{x1}}{\partial t} - \frac{\partial v_{x1}}{\partial z} \tag{2}$$

$$0 = \rho_o \frac{\partial v_{x1}}{\partial t} + c^2 \frac{\partial \rho_1}{\partial x} - (\mu_2 + \mu_9) \frac{\partial^2 v_{x1}}{\partial x^2} - \mu_8 \frac{\partial^2 n_x}{\partial t \partial z}$$
$$- (\mu_2 + \mu_3 + \frac{\mu_8 + \mu_9 + \mu_{11}}{2}) \frac{\partial^2 v_{z1}}{\partial x \partial z} - (\frac{-\mu_8 + \mu_9 + \mu_{11}}{2}) \frac{\partial^2 v_{x1}}{\partial z^2} \tag{3}$$

$$0 = \rho_o \frac{\partial v_{z1}}{\partial t} + c^2 \frac{\partial \rho_1}{\partial z} - (\mu_2 + \mu_3 + \mu_5 + \mu_6 + \mu_9 + \mu_{10} + \mu_{11}) \frac{\partial^2 v_{z1}}{\partial z^2}$$
$$- (\mu_2 + \mu_5 + \frac{\mu_9 + \mu_{10}}{2}) \frac{\partial^2 v_{x1}}{\partial z \partial x} - (\frac{\mu_9 + \mu_{10}}{2}) \frac{\partial^2 v_{z1}}{\partial x^2} \tag{4}$$

$$0 = \frac{\partial \rho_1}{\partial t} + \rho_o \frac{\partial v_{x1}}{\partial x} + \rho_o \frac{\partial v_{z1}}{\partial z} \tag{5}$$

We are using Stephen's [9] notation for the viscosity coefficients, μ_i. We have omitted the small elastic terms from Eq. 2 and have taken μ_7 to be zero since experimentally [11] its value is much smaller than the other coefficients. (Care must be taken in identifying the proper viscosity since Stephen takes the viscous force as $\partial t_{ij}/\partial x_j$ and many others as $\partial t_{ij}/\partial x_i$)

We seek solutions of Eq's. 2 - 5 near the lower nematic boundary, $z = 0$, which become standing waves in the bulk of the nematic. Using the approximation $k^2 \ll \omega \rho_o / \mu_i$ we obtain

$$n_{x1} = \frac{A \cos kx}{\omega} \left\{ e^{-\alpha_2 z} [\alpha_2 \sin(\omega t - \gamma_2 z) + \gamma_2 \cos(\omega t - \gamma_2 z)] - e^{-\alpha_1 z} [\alpha_1 \sin(\omega t - \gamma_1 z) + \gamma_1 \cos(\omega t - \gamma_1 z)] \right. \tag{6}$$

$$v_{x1} = A \cos kx \left\{ - e^{-\alpha_2 z} \cos(\omega t - \gamma_2 z) + e^{-\alpha_1 z} \cos(\omega t - \gamma_1 z) \right. \tag{7}$$

$$v_{z1} = \frac{- k A \sin kx}{\alpha_1 (1 + \gamma_1^2/\alpha_1^2)} \left\{ - e^{-\alpha_2 z} [\cos(\omega t - \gamma_2 z) + \frac{\gamma_1}{\alpha_1} \sin(\omega t - \gamma_2 z)] + e^{-\alpha_1 z} [\cos(\omega t - \gamma_1 z) + \frac{\gamma_1}{\alpha_1} \sin(\omega t - \gamma_1 z)] \right. \tag{8}$$

where

$$\alpha_1 + i\gamma_1 = \sqrt{\frac{\omega \rho_o}{(\mu_8 + \mu_9 + \mu_{11})}} \left\{ [1 + \frac{(2\mu_6 - 2\mu_8 + \mu_9 + \mu_{10}) k^2}{2\omega\rho_o}] + i [1 - \frac{(2\mu_6 - 2\mu_8 + \mu_9 + \mu_{10}) k^2}{2\omega\rho_o}] \right\} \tag{9}$$

and

$$\alpha_2 + i\gamma_2 = \sqrt{\frac{\omega(\mu_2 + \mu_9) k^2}{2\rho_o c^2}} (1 + i) \tag{10}$$

If we expand α_i and γ_i in terms of $\mu_i k^2/\omega\rho_o$ we have $\alpha_2 = \gamma_2 = 0$ and $\alpha_i = \gamma_i = \sqrt{\omega\rho_o/(\mu_8 + \mu_9 + \mu_{11})} \equiv \beta$. In the normal fluid case [12] we have $\beta_o = \sqrt{\omega\rho_o/2\eta}$ where η is the shear viscosity. For the nematic we have as one may expect $\beta = \sqrt{\omega\rho_o/2\eta_2}$ where η_2 is the shear viscosity in the direction of the director, the z direction.

Taking the time average of Eq. 3 to second order in ε we have

$$0 = \left\langle -2\rho_o v_{x1}\frac{\partial v_{x1}}{\partial x} - \rho_o v_{z1}\frac{\partial v_{x1}}{\partial z} - \rho_o v_{x1}\frac{\partial v_{z1}}{\partial z}\right\rangle - \frac{\partial P_2}{\partial x}$$

$$+\left\langle (\mu_5 + \mu_{11})\frac{\partial}{\partial z}\left(n_{x1}\frac{\partial v_{x1}}{\partial x}\right)\right\rangle + \left\langle (\mu_5 + \mu_6 + \mu_{10})\frac{\partial}{\partial z}\left(n_{x1}\frac{\partial v_{z1}}{\partial z}\right)\right\rangle$$

$$+\left\langle \mu_8\frac{\partial}{\partial z}\left(v_{x2}\frac{\partial n_{x1}}{\partial x} + v_{z1}\frac{\partial n_{x1}}{\partial z}\right)\right\rangle - \left(\frac{\mu_8 - \mu_{11} - \mu_9}{2}\right)\frac{\partial^2 v_{x2}}{\partial z^2} \qquad (11)$$

where the bracket, $\langle\ \rangle$, denotes the time average. We have omitted terms whose time average is found to be zero and have again assumed $k^2 \ll \omega\rho_o/\mu_i$. We have only included the viscosity coefficients of Leslie. For example products of the director gradients with velocity gradients are omitted from the viscosity tensor. For first order such terms will not appear. However, they can appear in second order. Nevertheless since each term would involve an n_{x1} and hence a factor of $e^{-\beta z}$ only the boundary region will be affected. We will assume $\beta h >> 1$ where h is the thickness of the nematic in the z direction. Therefore in calculating the light transmitted through the nematic we find the omitted terms do not affect the answer.

The director equation becomes, to second order in ε, after a time

average,

$$0 = -k_{33}\frac{\partial^2 n_{x2}}{\partial z^2} + (\lambda_2+\mu_8)\left\langle n_{x1}\frac{\partial v_{x1}}{\partial x}\right\rangle + (\lambda_2+\lambda_3)\left\langle n_{x1}\frac{\partial v_{z1}}{\partial z}\right\rangle$$
$$-\mu_8\left\langle v_{x1}\frac{\partial n_{x1}}{\partial x}\right\rangle - \mu_8\left\langle v_{z1}\frac{\partial n_{x1}}{\partial z}\right\rangle + \mu_8\frac{\partial v_{x2}}{\partial z} \qquad (12)$$

where the λ_i are viscoelastic coefficients and k_{33} is the Frank bend elastic constant. Using the previous solutions Eq's. 6 - 8 we may solve Eq's. 11 and 12. Assuming a solid immovable plane at $z = 0$, we take: $v_{x2} = v_{z2} = 0$ at $z = 0$. Assuming the nematic is sandwiched between two planes the second at $z = h$ from symmetry we take $\partial v_{2x}/\partial z = v_{z2} = 0$ at $z = h/2$. For homeotropic alignment we take $n_{x2} = 0$ at $z = 0$ and from vertical symmetry we take $n_{x2} = 0$ at $z = h/2$. We obtain assuming $\beta h >> 1$

$$v_{x2} = \frac{3kA^2 \sin 2kx\,(2\mu_6-\mu_8+3\mu_9+2\mu_{10}+\mu_{11})}{4\omega(-\mu_8+\mu_9+\mu_{11})}\left[C_1 - \frac{z}{h} + \frac{z^2}{h^2}\right] \qquad (13)$$

The bracketed term on the right of Eq. 13 would also contain three additional terms involving factors: $e^{-2\beta z}$, $\cos\beta z\, e^{-\beta z}$ and $\sin\beta z\, e^{-\beta z}$ each of which is only significant near the boundary. The constant, C_1, is the sum of the coefficients of the first two of the three omitted terms. It is a function of μ_6, μ_8, μ_9, μ_{10}, and μ_{11}. However, since in Eq. 12 we take $\partial v_{x2}/\partial z$ its value is not important in the determination of n_{x2}. We find v_{z2} is smaller than v_{x2} by the factor k/β. By letting $\mu_i = 0$, $i \neq 9$ and $\mu_9 = 2\eta$, Eq. 13 reduces [8] to the normal fluid streaming velocity

For the static change in the director we find

$$n_{x2} = \frac{3kA^2 \sin 2kx \quad \mu_8(2\mu_6 - \mu_8 + 3\mu_9 + 2\mu_{10} + \mu_{11})}{h\omega k_{33}(-\mu_8 + \mu_9 + \mu_{11})}\left[\frac{z}{6} - \frac{z^2}{2h} + \frac{z^3}{3h^2}\right] \qquad (14)$$

The bracketed term on the right in Eq. (14) should also contain five additional terms. Three terms involve $e^{-2\beta z}$, $\cos \beta z e^{-\beta z}$ and $\sin \beta z e^{-\beta z}$ as we found in v_{x2}. There is a constant term arising from the boundary condition $n_{x2}(0) = 0$ and a term linear in z arising from the boundary condition $n_{x2}(h/2) = 0$. In the bulk these last two terms are smaller than other included terms by $1/\beta h$. Therefore omitting the region near $z = 0$ we have the form given in Eq. 14.

The light intensity through crossed polarizers is given by [10]

$$I = I_o \sin^2(2\phi) \sin^2(\delta/2) \qquad (15)$$

where ϕ is the angle between the polarization of the incident beam and the projection of the optic axis of the material, δ is the phase difference between the ordinary ray and the extraordinary ray:

$$\delta = \frac{2\pi d (n_e - n_o) \sin^2 \theta}{\lambda_o}$$

Here d is the thickness of the material, n_e and n_o are the refractive indices of the extraordinary ray and ordinary ray respectively, λ_o is

the wavelength of light, and θ is the angle between the optic axis of the material and the direction of light propagation.

In our case, ϕ has been chosen to 45°, d = 2h because we detect the light reflected by the mirror, the tilt angle of the liquid crystal molecule θ varies with z and

$$\sin\theta = n_{x1} + n_{x2} \tag{16}$$

From Eq. 6, we see that $n_{x1} \to 0$ for $\beta z \gg 1$. That is, n_{x1} is zero in the bulk of the liquid. Also, since we do not observe any ultrasound frequencies from the reflected light, n_{x1} can be neglected. We take the approximation

$$d\sin^2\theta \sim 4\int_0^{h/2} n_{x2}^2\, dz \tag{17}$$

and again assume $h\beta \gg 1$ to obtain

$$I=I_o\sin^2(2\phi)\sin^2\left\{\frac{\pi(n_e-n_o)h^3A^4\sin^2 2kx}{2^6\cdot 3\cdot 5\cdot 7\ \lambda_o\ k_{33}^2\ c^2}\left[\frac{\beta(2\mu_6+3\mu_9+2\mu_{10}+\mu_{11}-\mu_8)}{(-\mu_8+\mu_9+\mu_{11})}\right]^2\right\} \tag{18}$$

For the piezoelectric transducer, A is proportional to the excitation voltage V, thus we obtain the reflected light intensity

$$I \alpha \sin^2\left[BV^4(1-\cos(4kx))/2\right] \tag{19}$$

where B is a constant. At the center of the lighted area, cos (4kx) = -1, hence

$$I \alpha \sin^2(BV^4) \tag{20}$$

Eqs. 19 and 20 show that the periodicity of I in the x direction is 0.25 λ and the phase difference is proportional to V^4. The light intensity has a maximum or minimum whenever

$$BV^4 = N\pi/2 \qquad (21)$$

where $N = \delta/\pi = 0, 1, 2, \ldots$

4. Discussion

Our theoretical model proposes that the change in the optical properties of the liquid crystal is the result of acoustic streaming. Experimental evidence supporting this model are

1. A series of lighted lines parallel to the liquid-to-air boundaries are observed. Those lines are clearest when the boundaries are making 45° angle with the polarizer and the analyzer. Therefore, the molecules tilt in planes perpendicular to the boundaries and the glass plates as we assume in our theory.

2. We see concentric rings of lighted lines around an air bubble with circular liquid-to-air boundary which shows the existence of waves reflecting from the boundary.

3. These lighted lines are separated by distances of $(0.29 \pm 0.08)\lambda$ compared to the theoretical value of 0.25λ.

4. The reflected light from the liquid crystal is not modulated by the frequency of the ultrasound in the region of tunable birefringence. Therefore, the observed acousto-optic effect is not due to the first order effect which is shown to be negligible in the theory.

5. The plot of reflected light intensity versus excitation voltage agrees reasonably well with the theoretical prediction of Eq. 20 (plotted as a broken line) up to excitation voltage $\simeq$ 40 V. The phase difference obtained from Fig. 4 at the maxima and minima of the light intensity is plotted in Fig. 5 against V^4. It shows good linear dependence of V in agreement with the theory up to $N = \delta/\pi \simeq 6$. Since we have made the

assumption that $n_x \ll 1$ in the derivation of our theory, we do not expect the experimental results to agree with the theory for large values of phase difference.

6. The first peak in the transmitted intensity curve, Fig. 4, occurs for an applied rms voltage of 24v. Measuring the electrical power to the transducer at this voltage and taking into account the change of acoustic impedance from transducer to liquid crystal gives an intensity of approximately 20 mwatt/cm^2 to the liquid crystal at this voltage. We may compare this experimentally determined acoustic intensity with the theoretical value using Eq's. (15) and (18) with $\delta/2$ equal to $\pi/2$. We assume a standing wave between the free boundaries which are separated by $4\lambda_s$ where λ_s equals the acoustic wavelength in the MBBA and take the acoustic damping constant[13] to be $.01/\lambda_s$. The resulting theoretically required intensity is approximately 10 mwatt/cm^2 in order of magnitude agreement with the above value and much lower than previous theoretical values.[3,6]

In contrast with other models [3,6] which considered the anisotropy of the visco-elastic properties of the nematic liquid crystal to be responsible for the hydrodynamic flows, our model proposes that the rotation of the liquid crystal molecules is due to acoustic streaming which occurs for any viscous liquid. Instead of predicting a threshold of instability, our theory predicts a V^4 dependence in closer agreement to our experimental results. Furthermore, other models assuming no transverse dependence could not predict any variation in the transverse directions while our model can explain the pattern of parallel lines on the liquid crystal cell.

References (For Appendix I)

1. H. Hailer, K.L. Likins, T.R. Taylor and J.L. Fergason, Appl. Phys. Lett., 18, 105 (1971)

2. P. Greguss, Acustica, 29, 52 (1973)

3. S. Nagai and K. Iizuka, Japan J. Appl. Phys., 13, 189 (1974)

4. Y. Kagawa, T. Hatakeyama and Y. Tanaka, J. of Sound and Vib., 36, 407 (1974)

5. P.A. Penz, Phys. Teach., Apr., 199 (1975)

6. W. Helfrich, Phys. Rev. Lett., 29, 1583 (1972)

7. S. Nagai, Private communication

8. W.L. Nyborg, in Physical Acoustics, vol. 2, pt. B, edited by W.B. Mason, Academic Press, New York & London (1965)

9. M.J. Stephen, Phys. Rev. A, 2, 1558 (1970)

10. M. Born and E. Wolf, Principles of Optics, Pergamon Press, 1970, p. 692

11. C. Cahwiller, Phys. Lett., 36A, 311 (1971)

12. J.W. Strutt, Baron Rayleigh, Theory of Sound, Vol. II Dover Publications, New York, 1945, p. 337.

13. D.Eden, C.W. Garland and R.C.Williamson, J.Chem.Phys.,58, 1861 (1973).

Figure Captions

Figure 1 Test Cell

Figure 2 Block diagram of the system for plotting reflected light intensity versus excitation voltage

Figure 3a Liquid crystal in the turbulent region showing disinclination lines and wave-like pattern without the polarizer (excitation voltage = $120V_{rms}$ at 0.669 MHz, cell thickness = 70 μm)

Figure 3b The liquid crystal cell in the region of tunable birefringence showing a series of white lines parallel to the two free boundaries (excitation voltage = $36V_{rms}$ at 0.669 MHz, cell thickness = 70 μm)

Figure 3c Concentric rings of white lines surrounding an air bubble (excitation voltage = $12V_{rms}$ at 0.84 MHz, cell thickness = 70 μm)

Figure 4 Plot of relfected light intensity through crossed polarizers versus excitation voltage to the transducer using the system of Fig. 2 (frequency = 0.669 MHz, cell thickness = 70 μm, time taken to plot = 1 hour). Eq. 24 is plotted as a broken line for comparison

Figure 5 Plot of phase difference versus (excitation voltage)^4 using the data from Fig. 4

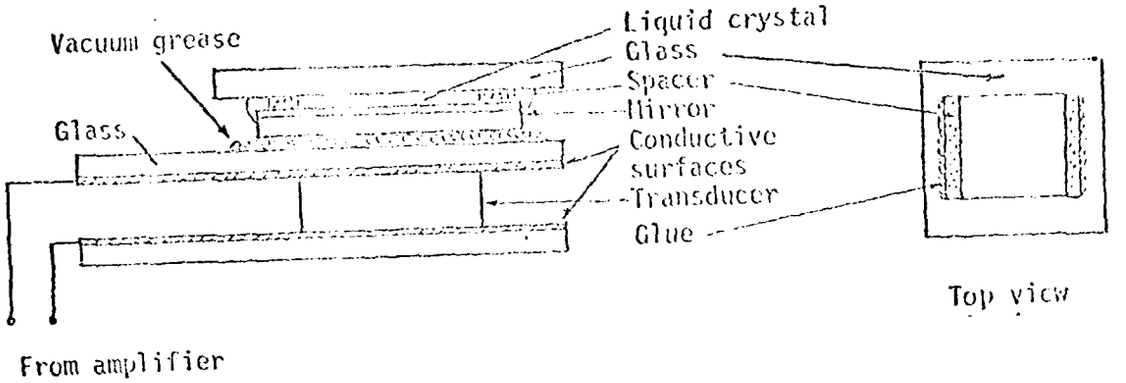
Vacuum grease
Glass
Liquid crystal
Glass
Spacer
Mirror
Conductive
surfaces
Transducer
Glue
Top view
From amplifier

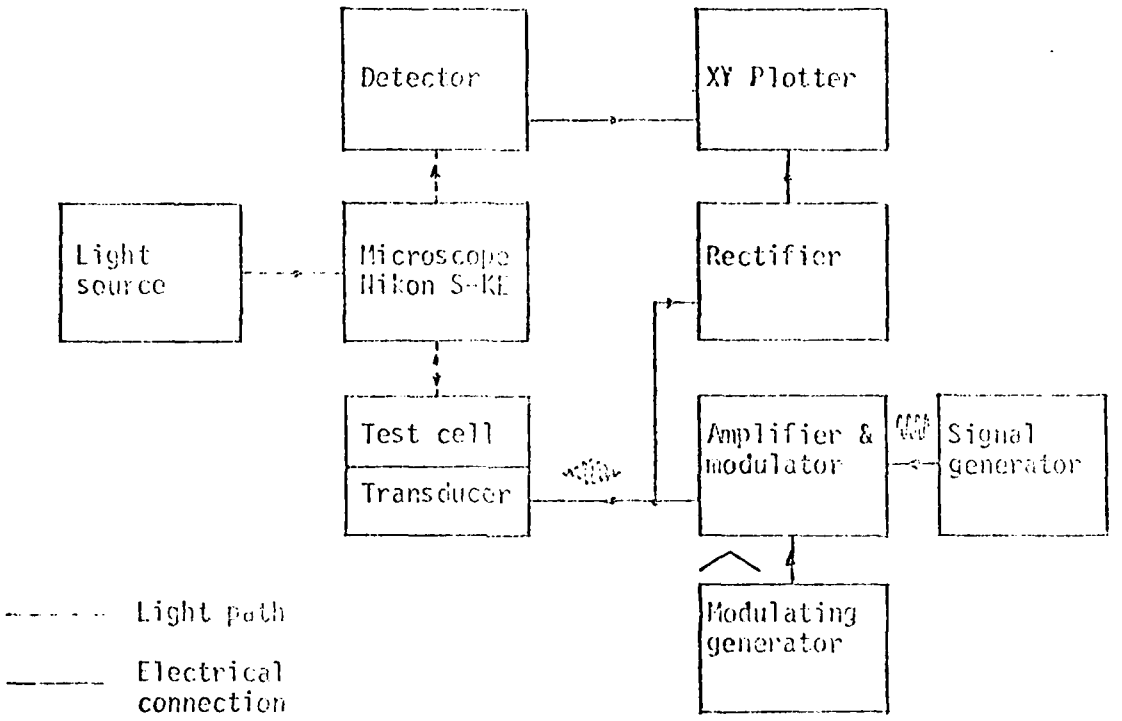

Fig. 3 Block diagram of the system for plotting reflected light intensity versus excitation voltage.

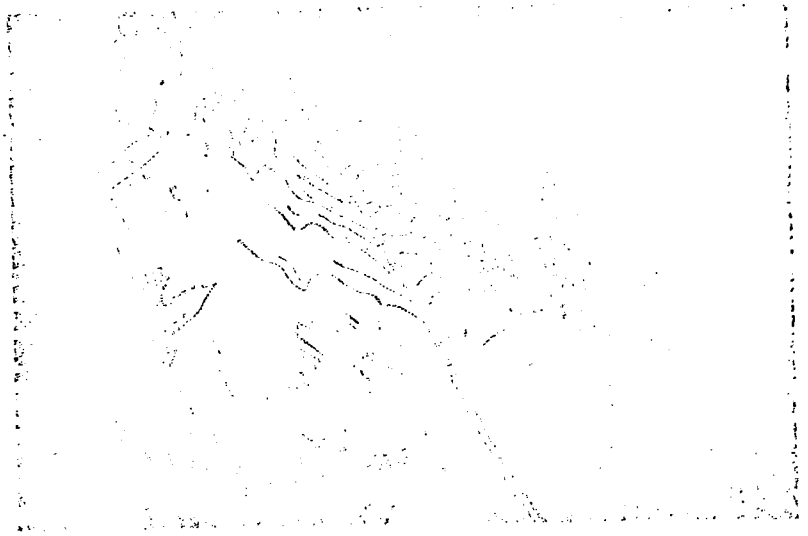

A

0,5 MM

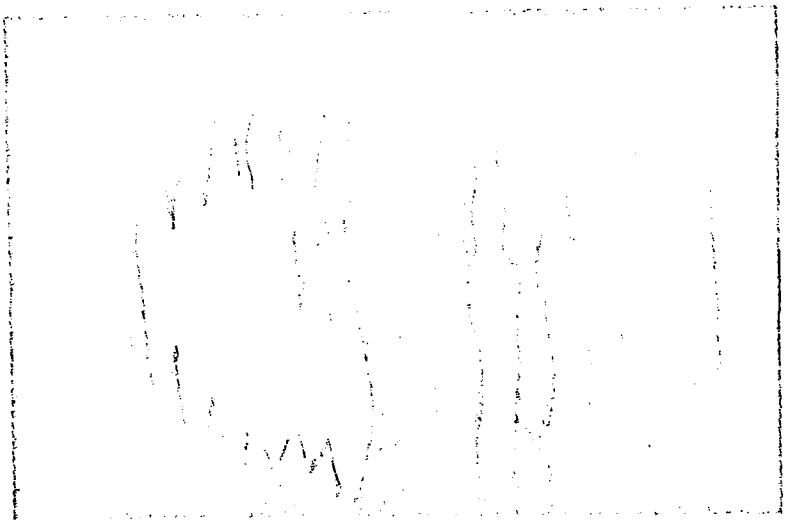

B

2 MM

C

2 MM

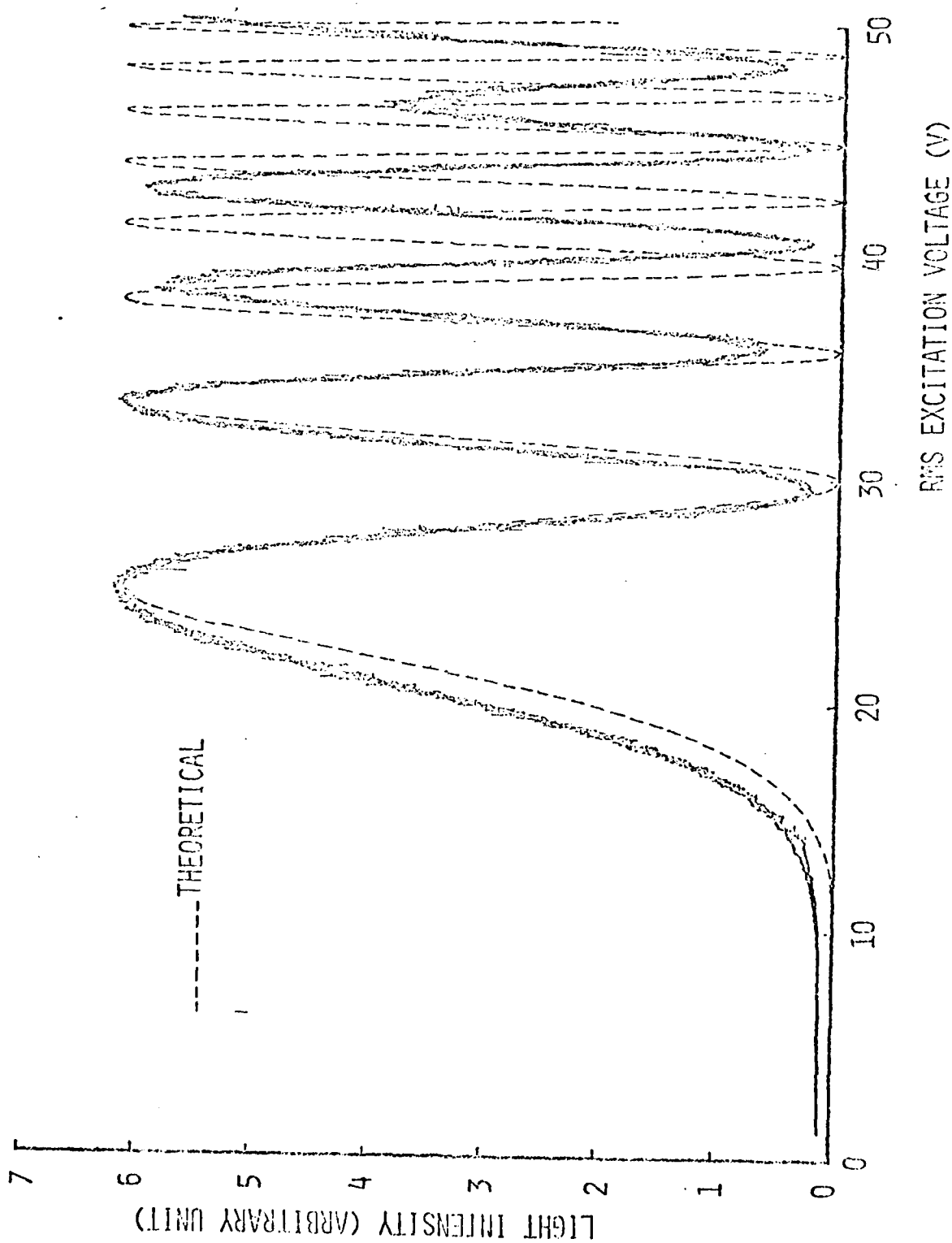
LIGHT INTENSITY (ARBITRARY UNIT)
0
1
2
3
4
5
6
7
RMS EXCITATION VOLTAGE (V)
0
10
20
30
40
50
THEORETICAL

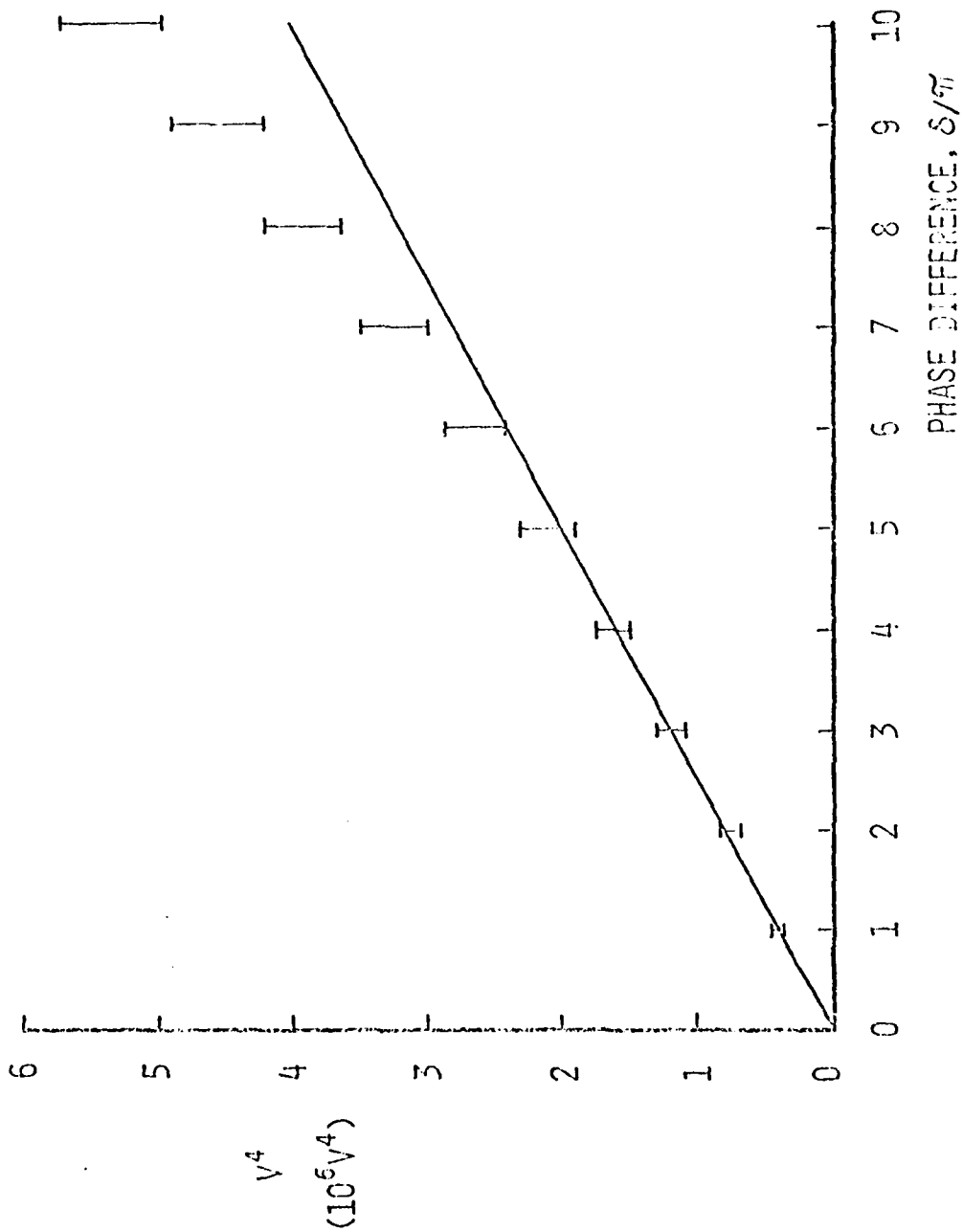
V^4
$(10^6 V^4)$
0
1
2
3
4
5
6
0
1
2
3
4
5
6
7
8
9
10
PHASE DIFFERENCE, δ/π

The Acousto-Optic Effect For a Nematic Liquid Crystal in the Presence of an Applied Electric Field

By C.F.Hayes

Department of Physics and Astronomy

University of Hawaii

Honolulu, Hawaii 96822

A homeotropically aligned nematic liquid crystal cell, N-P-Methoxybenzylidene-P-N-Butylaniline (MBBA) was excited by ultrasonic bulk waves of 270 kHz. A d.c. electric field was simultaneously applied parallel to the optic axis of the liquid crystal. The cell was observed with a polarizing microscope in the reflecting mode. Detection of the transmitted light shows successive maxima and minima as the ultrasonic intensity increases. These maxima and minima occur at lower acoustic intensities as the electric field is increased. A theory is proposed based on acoustic streaming in the presence of an electric field to explain these results.

I. Introduction

It has been over forty years since Frederiks and Zolin[1] observed the acousto-optic effect. They took tuning forks from 200 to 600 Hz and acoustically excited a nematic. The cause of the effect was attributed to a rotation of the optic axis although no details for the mechanism were given. In the last eight years there has been a renewed interest in the effect with a number of quantitative studies performed.[1-8] Most of the experimental reports refer to a threshold of acoustic intensity required before the effect occurs. The first two theoretical explanations for the effect also predict such a threshold.[9,6] In 1976 experimental results were presented which indicated there was no threshold for the effect.[10-12] Two of these reports[10,11] indicate the mechanism responsible for the effect is acoustic streaming, although the formulation in each case is quite different.

In this paper we will extend one of these formulations[10] to include the effects of an applied electric field. In the next section the theory is presented which shows how the previously derived equations need to be modified for inclusion of the field. Although our results are for an electric field they are equally valid for a magnetic field as well. In the last section the results of experimental evaluation of Section II are presented.

II. Theory

In our sample the nematic is sandwiched between two glass plates. The lateral edges of the nematic are open to a free air boundary. As the ultrasonic wave passes from one glass plate to the nematic to the other glass plate it produces a lateral wave. This lateral wave must be produced since in the nematic there is an ultrasonic wave and hence a pressure and in the adjacent air there is much less intensity for the ultrasonic wave and hence less pressure. The difference in acoustic intensity is the result of the difference in acoustic impedence change for the wave traveling from glass to nematic compared with from glass to air. The difference in pressure in these laterally adjacent regions oscillates with the frequency of the applied wave causing a lateral wave which reflects back and forth from free edge to free edge.

We will use the hydrodynamic formulation of Stephen[13] to describe the subsequent motion of the nematic including the director's resulting orientation. With the exception of the electric field terms our equations will be the same as we have previously reported.[10] To first order we have:

$$0 = \frac{\partial n_{x1}}{\partial t} - \frac{\partial v_{x1}}{\partial z} \tag{1}$$

$$0 = \rho_0 \frac{\partial v_{x1}}{\partial t} + c^2 \frac{\partial \rho_1}{\partial x} - (\mu_2 + \mu_4) \frac{\partial^2 v_{x1}}{\partial x^2} - \mu_8 \frac{\partial^2 n_x}{\partial t \partial z} - \left(\mu_2 + \mu_3 + \frac{\mu_8 + \mu_4 + \mu_{11}}{2}\right) \frac{\partial^2 v_{z1}}{\partial x \partial z} - \left(\frac{-\mu_8 + \mu_4 + \mu_{11}}{2}\right) \frac{\partial^2 v_{x1}}{\partial z^2} \tag{2}$$

$$0 = \rho_0 \frac{\partial v_{z1}}{\partial t} + c^2 \frac{\partial \rho_1}{\partial z}$$

$$- \left(\mu_2 + \mu_3 + \mu_5 + \mu_6 + \mu_9 + \mu_{10} + \mu_{11} \right) \frac{\partial^2 v_{z1}}{\partial z^2}$$

$$- \left(\mu_2 + \mu_5 + \frac{\mu_9 + \mu_{10}}{2} \right) \frac{\partial^2 v_{x1}}{\partial z \partial x} \qquad (3)$$

$$- \left(\frac{\mu_9 + \mu_{10}}{2} \right) \frac{\partial^2 v_{z1}}{\partial x^2}$$

$$0 = \frac{\partial \rho_1}{\partial t} + \rho_0 \frac{\partial v_{x1}}{\partial x} + \rho_0 \frac{\partial v_{z1}}{\partial z} \qquad (4)$$

We are assuming the z direction to be perpendicular to the glass boundaries and the lateral wave to travel along the x axis. The equilibrium orientation of the director we have taken to be along the z axis. We use the subscript 1 to refer to variables oscillating with the frequency of the acoustic wave, and the subscript 2 to refer to the second order solutions for the variables. Then t is the time; ρ, the density; v, the fluid speed; μ_i, the i th Leslie viscosity and c, the wave speed. We omit the elastic and electric field terms from Eq. 1 since they may be shown to be small. Taking the approximation $k^2 \ll \omega \rho_0 / \mu_i$ we obtain the following solutions to Eq's. 1 - 4:

$$n_{x1} = \frac{A \cos kx}{\omega} \left\{ e^{-\alpha_2 z} [\alpha_2 \sin(\omega t - \gamma_2 z) + \gamma_2 \cos(\omega t - \gamma_2 z)] \right. \quad (5)$$
$$\left. - e^{-\alpha_1 z} [\alpha_1 \sin(\omega t - \gamma_1 z) + \gamma_1 \cos(\omega t - \gamma_1 z)] \right.$$

$$v_{x1} = A \cos kx \left\{ - e^{-\alpha_2 z} \cos(\omega t - \gamma_2 z) + e^{-\alpha_1 z} \cos(\omega t - \gamma_1 z) \right. \quad (6)$$

$$v_{z1} = \frac{-kA \sin kx}{\alpha_1 (1 + \gamma_1^2/\alpha_1^2)} \left\{ - e^{-\alpha_2 z} [\cos(\omega t - \gamma_2 z) + \frac{\gamma_1}{\alpha_1} \sin(\omega t - \gamma_2 z)] \right.$$
$$\left. + e^{-\alpha_1 z} [\cos(\omega t - \gamma_1 z) + \frac{\gamma_1}{\alpha_1} \sin(\omega t - \gamma_1 z)] \right. \quad (7)$$

where

$$\alpha_1 + i\gamma_1 = \sqrt{\frac{\omega \rho_o}{(\mu_8 + \mu_9 + \mu_{11})}} \left\{ [1 + \frac{(2\mu_6 - 2\mu_8 + \mu_9 + \mu_{10}) k^2}{2\omega\rho_o}] \right. \quad (8)$$
$$\left. + i [1 - \frac{(2\mu_6 - 2\mu_8 + \mu_9 + \mu_{10}) k^2}{2\omega\rho_o}] \right\}$$

and

$$\alpha_2 + i\gamma_2 = \sqrt{\frac{\omega(\mu_2 + \mu_3) k^2}{2\rho_o c^2}} (1 + i) \quad (9)$$

We expand α_i and γ_i to powers of $\mu_i k^2/\omega\rho_o$ to lowest order we have $\alpha_2 = \gamma_2 = 0$ and

$$\alpha_i = \gamma_i = \sqrt{\omega\rho_o/(\mu_3 + \mu_9 + \mu_{11})} \equiv \beta$$

In taking the hydrodynamic equations to first order we have omitted terms involving products of the variables which are oscillating with the frequency of the imposed acoustic wave. If we take the equations to second order we must take these terms into account. Since the variation is sinusoidal these terms involve a constant term plus one which varies with twice the acoustic frequency. We will be interested only in the former type and therefore take a time average of our equations to second order to eliminate terms having twice the imposed frequency. Eq. 2 to second order is then:

$$
\begin{aligned}
0 = \Big\langle & -2\rho_0 v_{x1}\frac{\partial v_{x1}}{\partial x} - \rho_0 v_{z1}\frac{\partial v_{x1}}{\partial z} - \rho_0 v_{x1}\frac{\partial v_{z1}}{\partial z} \\
& - \frac{\partial p_2}{\partial x} + \Big\langle (\mu_5 + \mu_{11})\frac{\partial}{\partial z}\left(n_{x1}\frac{\partial v_{x1}}{\partial x}\right)\Big\rangle \\
& + (\mu_5 + \mu_6 + \mu_{10})\Big\langle \frac{\partial}{\partial z}\left(n_{x1}\frac{\partial v_{z1}}{\partial z}\right)\Big\rangle \\
& + \Big\langle \mu_8 \frac{\partial}{\partial z}\left(v_{x1}\frac{\partial n_{x1}}{\partial x} + v_{z1}\frac{\partial n_{x1}}{\partial z}\right)\Big\rangle \\
& - \frac{(\mu_8 - \mu_{11} - \mu_4)}{2}\frac{\partial^2 v_{x2}}{\partial z^2}
\end{aligned}
$$

where the bracket, $\langle\ \rangle$, represents the time average.

In a similar manner we may find an equation for the director neglecting those terms which are zero in the nematic bulk:

$$0 = K_{33}\frac{\partial^2 n_{x2}}{\partial z^2} + \frac{\epsilon_a E^2}{4\pi} n_{x2} - \mu_8 \frac{\partial v_{x2}}{\partial z} \qquad (11)$$

We are here assuming that the nematic is a perfect insulator and also omitting any piezoelectric effects.

We assume the glass boundaries are at z = 0 and z = h which results in the boundary conditions: $v_{x2} = v_{z2} = 0$ at z = 0 and $\partial v_{2x}/\partial z = v_{z2} = 0$ at z = h/2. We obtain:

$$v_{x2} = \frac{3hA^2 \sin 2hx\,(2\mu_6 - \mu_8 + 3\mu_9 + 2\mu_{10} + \mu_{11})}{4\omega(-\mu_8 + \mu_9 + \mu_{11})}\left[C_1 - \frac{z}{h} + \frac{z^2}{h^2}\right] \qquad (12)$$

For the director we assume $n_{x2} = 0$ both at z = 0 and z = h. We obtain:

$$n_{x2} = \frac{9hA^2 \sin(2hx)\,\mu_8(\mu_8 + \mu_9 + \mu_{11})}{4\omega K_{33}(-\mu_8 + \mu_9 + \mu_{11})a^2 h}\left\{-1 + \frac{2z}{h}\right.$$

$$\left. + \cos(az) - [\operatorname{ctn}(ah) + \csc(ah)]\sin(az)\right\} \qquad (13)$$

where

$$a = \sqrt{\epsilon_a E^2 / 4\pi K_{33}} \qquad (14)$$

There are also terms in Eq. 11 involving $e^{-\beta z}$ which we have omitted since they contribute nothing to the equation in the bulk of the nematic. This assumption may be stated as $h >> 1/\beta$ where for our experiment the ratio of these quantities is of the order of 10 to 1.

If light is now passed through the sample in a direction perpendicular to the glass plates the intensity of the light which is transmitted if the sample is placed between crossed polarizers is

$$I = I_o \sin^2(2\phi) \sin^2(\delta/2) \tag{15}$$

where ϕ is the angle between the plane formed by the optic axis and the direction of light propagation and the axis of polarization and δ is the phase difference between the ordinary ray and the extraordinary ray

$$\delta = \frac{2\pi h (n_e - n_o) \sin^2\theta}{\lambda_o} \tag{16}$$

where n_e and n_o are the refractive indicies for the extraordinary and ordinary rays respectively, θ is the angle the direction of light makes with the optic axis and λ_o is the wavelength of light. We have

$$\sin\theta = n_{x1} + n_{x2} \tag{17}$$

However, since n_{x1} is zero in the bulk of the nematic we will make the approximation that

$$h \sin^2\theta = \int_0^h n_{x2}^2 \, dz \tag{18}$$

We are also again assuming $\beta >> 1/h$.

Combining Eq's. 13 - 18 we find

$$I = I_o \sin^2(2\phi) \sin^2 \left[\frac{3(n_e - n_o) h_1^3 k^2 A^4 \sin^2(2kx) \mu_x^2 (\mu_s + \mu_q + \mu_n)^2 F}{2^4 \lambda_o \omega^2 K_{33}^2 \pi^5 (-\mu_s + \mu_q + \mu_n)^2} \right] \tag{19}$$

where

$$F = \frac{1}{S^6 \sin^2(\pi S)} \left[3\pi^2 S^2 \cos(\pi S) + \pi^2 S^2 \sin^2(\pi S) \right.$$

$$+ 3\pi^2 S^2 + 3^2 \pi S \sin(\pi S) \qquad (20)$$

$$\left. + 3^2 \pi S \sin(\pi S) \cos(\pi S) - 2^3 \cdot 3 \sin^2(\pi S) \right]$$

where s is the ratio of the electric field applied perpendicular to the glass plates to the critical value of electric field for a Frederiks transition:

$$S = E / E_c \qquad (21)$$

At a lateral position where $2kx = \pi/2$ we would expect the light intensity to vary as $\sin^2(BFV^4)$ where B is a constant, since V the voltage applied to the transducer, is proportional to A. This dependence has been tested experimentally[10] for the case where no electric field was applied. As V was increased a series of maxima and minima occurred just as the $\sin^2(BFV^4)$ function predicts. However, the purpose of this present study is to examine how the light intensity changes with electric field. As the field increases so does F thereby moving the maxima and minima so they occur at lower values of V. One way to examine the field dependence is to measure the shift in the maxima and minima as a function of electric field. However, the equations involved would still include several unknown constants. One way of eliminating these constants is by setting V and hence A for the first maxima for no applied field and then measuring the intensity as the electric field is increased.

For A fixed so the light intensity is at the first maximum with s = 0 we have:

$$\frac{I}{I_o} = \sin^2 \left[2^2 \times 3^2 \times 5 \times 7 \, F / \pi^5 \right] \qquad (22)$$

The only unknown in Eq. 22 is s the ratio of applied electric field to critical electric field. This equation will be the basis for comparison with experimental results.

III. Experiment

The sample cells were made of a thin layer of N-P-Methoxbenzylidene-P-N-Butylaniline (MBBA) sandwiched between either a conducting glass plate and a front surface mirror or two glass plates. The experiment was performed at room temperature , 24°C. The plates were held apart by two thin spacers making the MBBA thickness 80 μm. The cross section of the MBBA was circular in shape with a diameter of about 2 mm. The sample being studied was disk shaped with the flat sides in contact with the glass plates and the circular edges open to the air.

The cell was mounted with vacuum grease to a piezoelectric transducer oscillating in the thickness mode causing a continuous compression wave to be propagated through the sample having a frequency of 270.9 kHz. Therefore, the acoustic wavelength in the MBBA was about 5.5 mm, a value much larger than the thickness of the MBBA disk . The value of wavelength is close to the value for a standing wave laterally across the MBBA with the center of the disk a node and the edges antinodes. It would be worthwhile to test the theory we are proposing by studying the effects of variation of the radius of the MBBA disk. We have not as yet made such a study. The pattern which appears in the microscope when the cell is acoustically excited is a dark cross centered about the middle of the sample extending to the edges with an orientation parallel to that of the polarizer and analyzer. Both the center and edges of the sample are dark. Between them is a ring of light which appears white at lower transducer voltages and then colored as the voltage is increased. These observations are in keeping with the physical model presented in the previous section. For higher frequencies more complicated patterns appear.

Since the effect of acoustic excitation which we are considering is not sensitive to impurities the MBBA as supplied by the manufacturer was used without further purification. A thin coating of lecithin on the inner glass surfaces was used to achieve homeotropic alignment. The electric field was maintained across the sample by connecting electrodes to the inner conducting surfaces of the sample cell.

A polarizing microscope in the reflecting mode held the sample cell for study. The white light source of the microscope was used with a filter to allow light of wavelength 0.63 ± 0.04 μm to pass through the sample to the bottom plate or mirror and on to the photomultiplier. The method of detection is described in more detail elsewhere.[10] A x20 objective was used to limit the field of view to a small region (0.2 mm diameter), thereby giving more uniformity.

The procedure was to increase the voltage to the transducer until the first maxima in light intensity was reached while holding the applied electric field to zero. The voltage applied to the transducer for this point was 13.2 Volts. Calling the light intensity, I, for this point I_o measurements were taken for I as a function of applied electric field. The results are shown in Fig. 1 where the solid line is a graph of Eq. 22. Within the accuracy of the experiment the data and theory agree.

The agreement strengthens the validity of the physical model we are proposing. However, it would appear that as far as practical applications are concerned the sensitivity of the acousto-optic effect in nematics can not be greatly increased by the application of an applied field. It should be noted finally that whereas we have been concerned with an electric field Eq. 22 is equally valid for a magnetic field where $s = H/H_c$ with H_c the critical magnetic field for a Frederiks transition.

References (For Appendix II)

1. V.V.Zolina,Trudy Lomonosov Inst.Akad.Nauk SSSR 8,11 (1936).

2. L.W.Kessler and S.P.Sawyer, Appl.Phys.Lett. 17,440 (1970).

3. H.Mailer,K.L.Likins,T.R.Taylor and J.L.Fergason,Appl.Phys.Lett. 18, 105 (1971).

4. M.Bertolotti,S.Martellucci,F.Scudieri and D.Sette,Appl.Phys.Lett. 21, 74 (1972).

5. P.Greguss, Acustica 29, 52 (1973).

6. S.Nagai and K.Iizuka, Japan J.Appl.Phys. 13, 189 (1974).

7. Y.Kagawa,T.Hatakeyama and Y.Tanaka, J.Sound Vibration 36, 407 (1974).

8. R.Bartolino,M.Bertolotti,F.Scudieri,D.Sette and A.Sliwinski, J.Appl. Phys. 46, 1928 (1975).

9. W.Helfrich, Phys.Rev.Lett. 29, 1583 (1972).

10. C.Sripaipan, C.Hayes and G.T.Fang, Phys.Rev. 15A, 1297 (1977).

11. S.Candau,A.Peters and S.Nagai, Sixth International Liquid Crystal Conference J-30 (1976).

12. J.L.Dion and F.DeForest, Sixth International Liquid Crystal Conference K-18 (1976).

13. M.J.Stephen, Phys.Rev.A,2 1558 (1970).

Figure 1. A graph of the ratio of the light intensity transmitted through the cell with and without an applied electric field while the cell was being excited acoustically by an ultrasonic wave of magnitude equal to that required for the first light intensity maxima in the absence of an electric field versus the ratio of the applied electric field to the electric field required for a Frederiks transition. The solid line is for Equation 22.

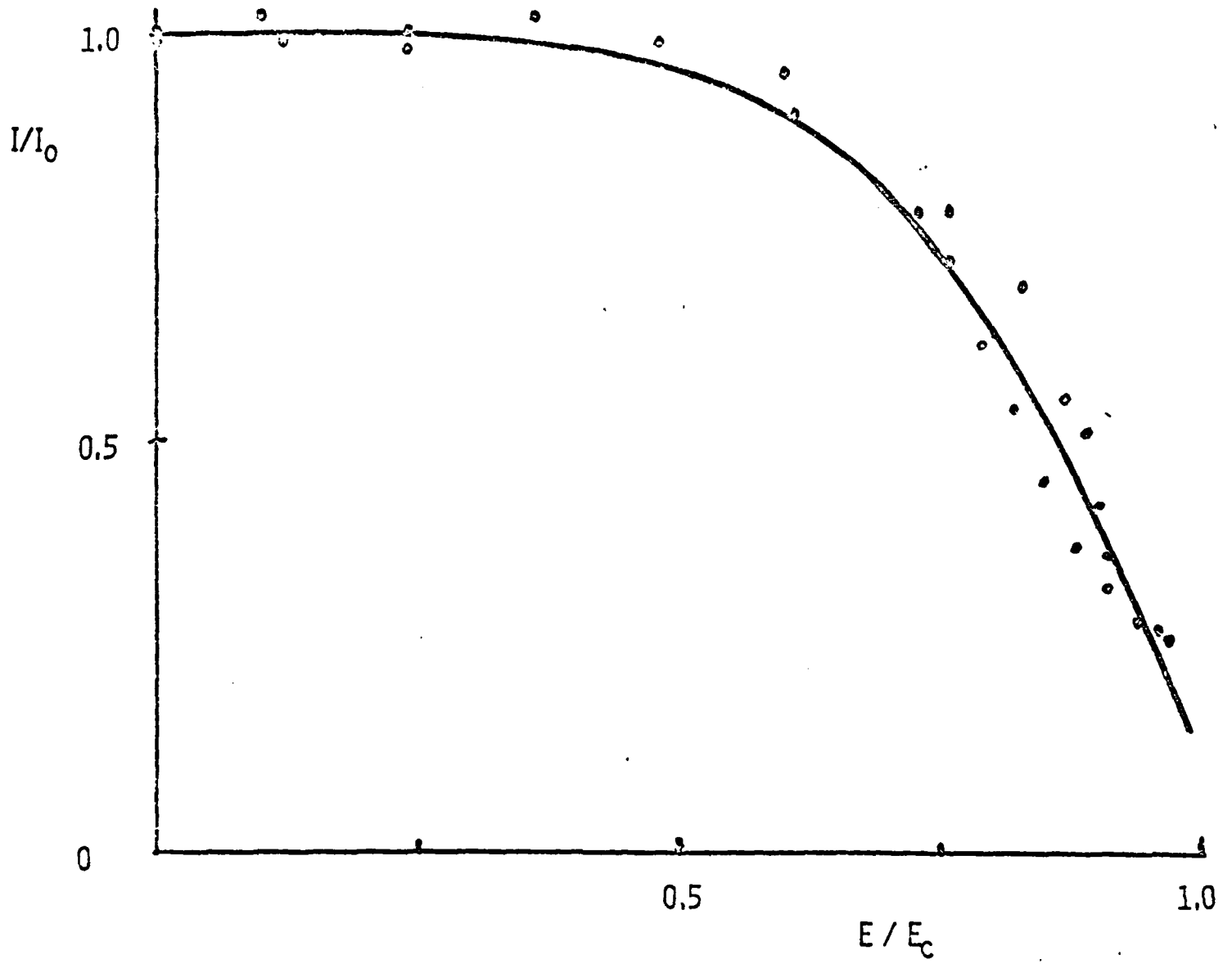
1.0
I/I0
0.5
0
0.5
1.0
E / Ec

Technical Report: 002

A Study of the Acousto-Optic Effect in Nematics as a Means of Acoustic Field Imaging

C. F. Hayes

Department of Physics and Astronomy

University of Hawaii

Honolulu, Hawaii 96822

March 1979

I. INTRODUCTION

The fact that acoustic waves could give optical effects in nematic liquid crystals has been known since 1936. In that year Fredericks and Zolin[1] excited a nematic liquid crystal by tuning forks of 200 to 600 Hz while making optical observations with crossed polarizers. It was not until 1969 that Fergason[2] suggested that a liquid crystal device may be made for detecting acoustic intensity. Since 1970 there have been approximately forty research articles published in this area. However, the basic mechanism causing the effect was not understood until the last three years. Differential acoustic absorption,[3] transverse second-order stress,[4] cybotactic groups,[5] the piezoelectric effect[6] and anisotropy of acoustic speed have all been proposed to be the mechanism for the effect. In the early work, both experimental and theoretical, a threshold of acoustic intensity was reported to be required. In 1976, three groups: Sripaipan, Hayes, Fang;[7] Candau, Peters, Nagai;[8] and Dion, DeForest;[9] reported that there is in fact no threshold for the effect. The former two groups attributed the effect to acoustic streaming. Further, whereas all of the previous work had required some special property of a liquid crystal for the effect acoustic streaming would result in any viscous liquid. It is simply that acoustic streaming or any flow in a liquid crystal results in optical effects. The streaming theory has been extended to include the simultaneous effect of an electric field by Hayes[10] in 1978. Again the streaming model successfully explained the experimental results. The logical result of the streaming explanation is that a cell to visualize an acoustic field could be made by separating the liquid crystal into distinct regions to confine the flow. Nagai and Iizuka[11,12] have made such a device. However, there has not been a direct observation of the flows induced in these cells nor quantitative

theoretical work performed giving the speeds of flow or the flow patterns in the cell. It is the goal of this report to provide direct evidence for the flows. In Section II a theory is presented which predicts the magnitude of the flow speed and the form of the flow pattern one would expect in a viscous fluid. In Section III results are presented for observations of these fluid flows.

II. THEORY OF FLUID MOTION

A. Non-viscous Limit

We will develop equations describing the motion induced in a disc shaped liquid bound between two solids. The solid surfaces are assumed planar with an ultrasonic wave traveling from one solid, through the fluid and on through the second solid. We will take the cylindrical boundary of the disc to be open to a gas of negligible density. Such a system could be made by placing a drop of water between two glass microscope slides. We will further take the distance between the planes, the height of the disc, to be smaller than the wavelength of the ultrasonic wave. The oscillatory motion of the wave will produce a static flow in the fluid, acoustic streaming. We will find the form of the resulting flow patterns and the magnitude of the fluid speed.

In order to understand the approximations which must be made to obtain a tractable solution we will first investigate a simpler problem where viscosity is omitted and the disc is assumed of infinite height.

Consider a column of non-viscous fluid with equilibrium density ρ_0 supported by a piston. See Figure 1. We assume the piston-fluid interface is located at $z = 0$ and take the radius of the fluid to be R. The result of the piston's velocity, $Ae^{-i\omega t}$, is a compression wave which propagates along the cylindrical axis of the column, the positive z axis. Because of the boundary at $r = R$ there will also be laterally induced waves as well. The equation describing the pressure, P, in the column is

$$\nabla^2 P = \frac{1}{C^2} \frac{\partial^2 P}{\partial t^2} \tag{1}$$

where C is the speed of the wave in the fluid. At $r = R$ we must have $P = 0$. The solution to Eq. 1 satisfying this boundary condition is

$$P = \sum_n A_n J_o (k_n r)\, e^{i k_n'' z - i\omega t} \tag{2}$$

where $J_o(\ )$ is the Bessel function of order zero,

$$k_n^2 = \frac{\omega^2}{C^2} - k_n''^2 \tag{3}$$

and

$$\alpha_n = k_n R = 2.405,\ 5.520,\ 8.654,\ 11.792,\ \ldots \tag{4}$$

where

$$J_o(\alpha_n) = 0 \qquad n = 0,\ 1,\ 2,\ \ldots \tag{5}$$

The partial differential equation relating the pressure to $\vec{v}$, the fluid velocity is given by

$$\rho_o \frac{\partial \vec{v}}{\partial t} = -\nabla P \tag{6}$$

We have at $z = 0$ the further boundary condition:

$$v_z = A\, e^{-i\omega t} \tag{7}$$

Combining Eq's. 2, 6, and 7 we have

$$\rho_o \omega A = \sum_n A_n k_n'' J_o (k_n r) \tag{8}$$

Operating on both sides of Eq. 8 with $\int_o^1 \frac{r}{R} J_o\left(\alpha_m \frac{r}{R}\right) d\left(\frac{r}{R}\right)$ we obtain

$$A_n = \frac{2\rho_o \omega A}{\alpha_n k_n'' J_1(\alpha_n)} \tag{9}$$

Now solving Eq. 6 for v_r and taking $r = R$ we find

$$v_R = \sum_n \frac{2iA}{R k_n''}\, e^{i k_n'' z - i\omega t} \tag{10}$$

From Eq. 3 and 4 we see the value of R may be adjusted with respect to λ to give $k_n'' = 0$. This condition gives a resonance and may occur for modes $n = 0, 1, 2, \ldots$. The corresponding values of R are:

$$R = .383\ \lambda,\ .879\ \lambda,\ 1.38\ \lambda,\ 1.88\ \lambda,\ \ldots \tag{11}$$

Figure 2 shows the amplitudes of v_R/A at $z = 0$ as a function of R/λ for modes $n = 0$ and 1.

From Eq. 3 we see if $R < .383\ \lambda$ then k_n'' will be imaginary making the wave damp out in the z direction as seen from Eq. 2. The amount of damping depends on how close to resonance the radius is. In Figure 3 v_R/A is graphed as a function of Z/λ. We see for the mode 0 the damping is less the closer R/λ is to the resonant value. We also see that the mode $n = 1$ for $R/\lambda = .38$ damps out more quickly than mode $n = 0$ even for R/λ as low as .22, about 40% lower than the resonant condition for that mode. We also see from Figures 1 and 2 that although the disc is being driven by a piston oscillating in the z direction the major motion can be radial.

From Eq. 6 we can also find the radial velocity as a function of r:

$$v_r = \sum_n \frac{2iA\, J_1(\alpha_n r/R)\, e^{i(k_n'' z - \omega t)}}{R\, k_n''\, J_1(\alpha_n)} \tag{12}$$

From Eq. 12 we see at $r = 0$ all modes are zero. For the $n = 0$ mode the maximum velocity occurs at about 75% of the maximum radius. A different situation would exist for an infinite strip of fluid between two planes. In that case the Bessel functions would be replaced by sin's and cos's and the maximum speed would occur at the fluid edge. For the $n = 1$ mode of oscillation the fluid for $r < .7R$ is out of phase with the outer section. Again the maximum speed for this mode does not occur at the edge but at about $r = .35R$.

B. Viscous Model

With the aid of the results we have obtained from Section IIA we may now proceed with a model closer to the physical system under study. Rather than an infinite column for the fluid we will assume a height H with the origin of Figure 1 moved along the z axis so the upper and lower boundaries occur at $z = H/2$ and $-H/2$ respectively. Since we are now including viscosity we will start with the Navier-Stokes equation:

$$\rho_o \left[\frac{\partial \vec{v}}{\partial t} + (\vec{v} \cdot \nabla)\vec{v} \right] = -c^2 \nabla\rho + \eta\nabla^2 \vec{v} + (\zeta + \frac{1}{3}\eta)\ \nabla\ (\nabla \cdot \vec{v}) \tag{13}$$

Since we are assuming the hydrodynamic variables may be expanded about their equilibrium values we will for now drop the higher order effects. We will take for a rectilinear coordinate system in component form:

$$\rho_o \frac{\partial v_i}{\partial t} = -c^2 \frac{\partial \rho}{\partial x_i} + \eta\nabla^2 v_i + (\zeta + \frac{1}{3}\eta) \frac{\partial}{\partial x_i} (\nabla \cdot \vec{v}) \tag{14}$$

If we operate on Eq. 2 with $\partial/\partial x_i$ and sum over i we have

$$\rho_o \frac{\partial \nabla \cdot \vec{v}}{\partial t} = -c^2 \nabla^2 \rho + \eta \nabla^2\ \nabla \cdot \vec{v} + (\zeta + \frac{1}{3}\eta) \nabla^2\ (\nabla \cdot \vec{v}) \tag{15}$$

The hydrodynamic variables must also obey the continuity equation:

$$\frac{\partial \rho}{\partial t} + \nabla \cdot (\rho \vec{v}) = 0 \tag{16}$$

where again to first order we have

$$\frac{\partial \rho}{\partial t} + \rho_o \nabla \cdot \vec{v} = 0 \tag{17}$$

Combining Eq's. 15 and 17 and assuming a time dependence $e^{i\omega t}$ we have

$$\Lambda_o \nabla^2 \rho = \rho \tag{18}$$

where

$$\Lambda_o = -\frac{i(\zeta + \frac{4}{3}\eta)}{\omega\rho_o} - \frac{c^2}{\omega^2} \tag{19}$$

The solution to Eq. 18 is

$$\rho = \sum_n \left[A_{1n} J_o (k_n r) e^{k_n'' z} + A_{2n} J_o (k_n r) e^{-k_n'' z} \right] e^{i\omega t} \tag{20}$$

where we have dropped the i from in front of the k_n'' factor since we will assume $R \leq .383 \lambda$ and from Section IA we know for that case the z dependence is real. We also have analogous to Eq. 3

$$k^2 = k''^2 - \frac{1}{A_o} \tag{21}$$

In order to simplify the solution of the Navier-Stokes equation we define two new functions according to

$$v_r = \frac{\partial \phi}{\partial r} + \frac{\partial \psi}{\partial z} \tag{22}$$

and

$$v_z = \frac{\partial \phi}{\partial z} - \frac{1}{r} \frac{\partial}{\partial r} (r\psi) \tag{23}$$

Now we have

$$\nabla \cdot \vec{v} = \nabla^2 \phi ; \tag{24}$$

so from Eq's. 17 and 18 we find ϕ may be related to ρ:

$$\phi = - \frac{i\omega \Lambda_o \rho}{\rho_o} \tag{25}$$

The z component of Eq. 13 to first order is

$$\rho_o \frac{\partial v_z}{\partial t} = -c^2 \frac{\partial \rho}{\partial z} + \eta \nabla^2 v_z + \left(\zeta + \frac{1}{3} \eta \right) \frac{\partial (\nabla \cdot \vec{v})}{\partial z} \tag{26}$$

Using Eq's. 17, 18, 19, and 22 we obtain

$$\frac{\eta}{i\omega \rho_o} \nabla^2 \xi = \xi \tag{27}$$

where

$$\xi = \frac{1}{R} \frac{\partial}{\partial r} (r\psi)$$

Taking

$$k_n^2 = k_n''^2 - \frac{i\omega \rho_o}{\eta} \tag{28}$$

the solution of Eq. 27 we take to be

$$\xi = \sum_n \left[A_{3n} J_o (k_n r)\, e^{k_n' z} + A_{4n} J_o (k_n r)\, e^{-k_n' z} \right] e^{i\omega t} \tag{29}$$

From Eq. 28 then

$$\psi = \sum_n \left[A_{3n} J_1 (k_n r)\, e^{k_n' z} + A_{4n} J_o (k_n r)\, e^{-k_n' z} \right] e^{i\omega t}/k_n \tag{30}$$

Eq's. 20, 25 and 30 may be used with Eq's. 22 and 23 respectively to obtain

$$v_r = \sum_n \frac{i\omega A_o k_n}{\rho_o} \left[A_{1n} e^{k_n'' z} + A_{2n} e^{-k_n'' z} \right] \tag{31}$$

$$+ \frac{k_n'}{k_n} \left[A_{3n} e^{k_n' z} - A_{4n} e^{-k_n' z} \right] \Bigg\} J_1 (k_n r) e^{i\omega t}$$

and

$$v_z = \sum_n \frac{-i\omega A_o k_n''}{\rho_o} \left[A_{1n} e^{k_n'' z} - A_{2n} e^{-k_n'' z} \right] \tag{32}$$

$$- \left[A_{3n} e^{k_n' z} + A_{4n} e^{-k_n' z} \right] \Bigg\} J_o (k_n r) e^{i\omega t}$$

Assuming a no-slip condition at $z = \pm H/2$ we must have $v_r = 0$ there. For the experiment we have performed $H/\lambda = .055$. From Figure 3 we see the amount of damping which has occurred as the wave traverses the vertical distance H of the disc. We will therefore take as an acceptable although not excellent approximation that $v_z = Ae^{-i\omega t}$ at $z = \pm H/2$. For these boundary conditions we find

$$A_{1n} = -A_{2n} = \frac{-2\rho_o k_n' A}{i\omega A k_n'' \rho_n J_1 (\alpha_n) (2k_n' - k_n^2 H)} \tag{33}$$

$$A_{3n} = A_{4n} = \frac{2 k^2 HA}{\alpha_n J_1 (\alpha_n) (2k_n' - k_n^2 H)\, e^{k_n' H/2}} \tag{34}$$

For the case under study $k_n' >> k_n^2 H$ and $k_n'' H << 1$. If we assume we are near the mode 0 resonance condition from Figures 2 and 3 we see we may drop the higher modes. Under these approximations we have

$$v_r = \frac{Ak_o}{\alpha_o J_1(\alpha_o)} \left\{ -2z + \frac{H}{e^{k_o' H/2}} \left(e^{k_o' z} - e^{-k_o' z} \right) \right\} J_1(k_o r) e^{i\omega t} \tag{35}$$

$$v_z = \frac{2 A J_o(k_o r) e^{i\omega t}}{\alpha_o J_1(\alpha_o)} \tag{36}$$

From Eq. 28 we see that k_o' is complex. For v_z what actually occurs is a cos ωt rather than the exponential. For the radial component:

$$v_r = \frac{Ak_o}{\alpha_o J_1(\alpha_o)} \left\{ -2z + H \left[e^{Re k_o' (z-H/2)} \cos \left[Im k_o' (z-H/2) + \omega t \right] \right. \right.$$

$$\left. \left. - e^{-Re k_o' (z+H/2)} \cos \left[Im k_o' (z+H/2) + \omega t \right] \right] \right\} x \, J_1(k_o r)$$

By setting r = R in the real form of v_r we may obtain a value of the radial amplitude of oscillation compared with that of the piston. For our sample we have H = .032 cm, Re k' = Im k' = 1112/cm and at resonance R = .22 cm. The resulting ratio of radial velocity to maximum piston velocity (which equals also the ratio of radial distance amplitude to vertical piston distance amplitude) is plotted as a function of z in Figure 4. The resulting maximum ratio shows for our case the radial motion has an amplitude less than 20% that of for the piston. Therefore, the infinite ratio for mode 0 shown in Figure 2 turns out to be of the order of .1 when viscous effects are considered. Also in Figure 4 a diagram is shown which depicts the deformation of the disc cross section. As the planes move upward the fluid bulges out at the bottom and in at the top. As the planes then move downward the opposite occurs.

Let us now return to Eq. 13 and examine the term we omitted. In light of the solutions, Eq's. 35 and 36, we see that each term of Eq. 13 oscillates sinusoidally in time. Although in Eq's. 35 and 36 we have used the complex exponential form, since the velocity is real the term we earlier omitted from Eq. 13, $\rho_o \vec{v} \cdot \nabla\vec{v}$, will have a factor of $\cos^2 \omega t$. Since $\cos^2 \omega t = (1 + \cos 2\omega t)/2$ if the time average of the omitted term is taken a non-zero static value results. Therefore, the time average of the other terms in the equation must also give non-zero static values. Since these other terms involve only the hydrodynamic variables to the first power we conclude a static value must be added to the values we obtained in Eq's. 35 and 36. This static flow is called acoustic streaming. We will denote the static addition to the variables with a subscript 2 signifying the second order solution: v_{r2}, ρ_2, v_{z2}. The time average of Eq. 13 to second order is

$$\rho \langle \vec{v} \cdot \nabla v_r \rangle = -c^2 \frac{\partial \rho_2}{\partial r} + \eta \nabla^2 v_{2r} + (\zeta + \frac{1}{3}\eta) \frac{\partial}{\partial r} (\nabla \cdot \vec{v}_2) \tag{37}$$

$$\rho \langle \vec{v} \cdot \nabla v_z \rangle = -c^2 \frac{\partial \rho_2}{\partial z} + \eta \nabla^2 v_{2z} + (\zeta + \frac{1}{3}\eta) \frac{\partial}{\partial z} (\nabla \cdot \vec{v}_2) \tag{38}$$

where the brackets denote a time average and merely involve replacing the $\cos^2 \omega t$ factor with 1/2. If we operate on Eq's. 37 and 38 by $\partial/\partial z$ and $\partial/\partial r$, respectively, subtracting the results we obtain

$$\rho \left\langle \frac{\partial}{\partial z} (\vec{v} \cdot \nabla v_r) - \frac{\partial}{\partial r} (\vec{v} \cdot \nabla v_z) \right\rangle = \eta \left[\frac{\partial}{\partial z} \nabla^2 v_{2r} - \frac{\partial}{\partial r} \nabla^2 v_{2z} \right] \tag{39}$$

Again invoking the approximations used to obtain Eq's. 35 and 36 along with $k_o' H \gg 1$ we find we may identify ∇^4 with $\partial^4/\partial z^4$ and obtain with the help of Eq's. 22 and 23

$$\psi_2 = \frac{\rho A^2 k_o^3 J_1(k_o r)}{2\eta \alpha_o^2 J_1(\alpha_o)} \cdot \frac{\partial J_1(k_o r)}{\partial (k_o r)} \left\{ -\frac{z}{4(R_e k_o')^3} \right. \tag{40}$$

$$\left. \times \left[e^{a}(\cos a - \sin a) + e^{-b}(\cos b + \sin b) \right] + c_1 z^3 + c_2 z^2 + c_3 z + c_4 \right\}$$

where

$$a = \mathrm{Re}\ k_o' \ (z - H/2) \tag{41}$$

$$b = \mathrm{Re}\ k_o' \ (z + H/2) \tag{42}$$

and where we have again taken the real part assuming $\mathrm{Re}\ k_o' = \mathrm{Im}\ k_o'$ as we find to be approximately true for our systems. The contribution from ϕ_2 can be shown to be small so that Eq's. 22 and 23 become

$$v_{2r} = \partial\psi/\partial z \tag{43}$$

$$v_{2z} = -\frac{1}{r}\frac{\partial}{\partial r}(r\psi_2)$$

The values of the C_i's may be found using the boundary conditions that both v_{2r} and v_{2z} equal zero at $z = \pm H/2$. Finally we obtain the second order contributions to the velocity:

$$v_{2r} = -\frac{\rho A^2 k_o^3 H J_1(k_o r)}{\eta \alpha_o^2 J_1^2(\alpha_o)} \cdot \frac{\partial J_1(k_o r)}{\partial(k_o r)} \left\{ \frac{z}{2(\mathrm{Re}\ k_o')^2} \left[e^{a} \sin a + e^{-b} \sin b \right] \right.$$

$$\left. - \frac{3z^2}{2(\mathrm{Re}\ k_o')^3 H^2} + \frac{3}{8(\mathrm{Re}\ k_o')^3} \right\} \tag{44}$$

$$v_{2z} = -\frac{\rho A^2 k_o^3}{2\eta \alpha_o^2 J_1^2(\alpha_o)} \frac{1}{r}\frac{\partial}{\partial r}\left(r J_1(k_o r) \frac{\partial J_1(k_o r)}{\partial (k_o r)} \right)$$

$$\times \left\{ -\frac{z}{4(\mathrm{Re}\ k_o')^3} \left[e^{a}(\cos a - \sin a) + e^{-b}(\cos b + \sin b) \right] \right.$$

$$\left. + \frac{3z}{8(\mathrm{Re}\ k_o')^3} - \frac{z^3}{2(\mathrm{Re}\ k_o')^3 H^2} \right\} \tag{45}$$

Eq's. 44 and 45 will be the basis of a comparison with the experimental results have obtained.

III. EXPERIMENT

A barium titanate crystal was used to produce the ultrasonic wave (cw) in the sample under study. The wave was transmitted from the crystal through the conducting glass electrode immediately above the crystal, through vacuum grease which was used to mount the sample holder, through the bottom glass slide, through the sample fluid disc, and on through the upper glass slide. Various fluids were used: water, a cholesteric liquid crystal, a nematic liquid crystal and a transparent vegetable oil. The oil's viscosity is closer to the nematic whose motion we will ultimately consider. Therefore, measurements reported here concern the velocity induced in the oil. To measure the magnitude of the flow in the disc the oil was doped with a hydrocarbon base ferrofluid (0.1% concentration). Aggregates of magnetite can then be seen in the oil by means of a polarizing microscope. By measuring the speed of these particles the speed of the oil may be determined. The particles were of the order of one micron in diameter. The thickness of the disc was .032 cm so the particle size was small compared to the distance over which the speed of the fluid changed appreciably. The diamter of the disc was from one to four mm, small compared to the 12.7 mm diameter of the barium titanate crystal. The microscope was calibrated so the vertical position of the particle whose speed was being measured could be determined when the microscope was focused on that particle. A sealed container was also used so that the ultrasonic wave would first travel through one cm of water before reaching the fluid disc. Using a capillary viscometer the ratio of viscosity to density of the oil was determined, $\eta/\rho = 0.66 \pm 0.03$ cm^2/sec. From Eq. 28 we see k_o' can now be determined if we know the frequency and wave speed. We take $c = 1.46 \times 10^5$ cm/sec and $f = .26$ MHz. We find the real part of $k_o'^2$ small so $k_o' = 1112\ (1 + i)$/cm.

From Eq. 44 we see that the radial flow goes to zero at r = 0 due to the $J_1(k_o r)$ factor. It becomes larger for larger values of r and then goes to zero near the edge r = R due to the derivative of $J_1(k_o r)$. The value of v_{2z} on the other hand is larger at r = 0 and decreases as r is increased and finally is larger but with a different sign near r = R. A diagram of the flows our equations predict is shown in Figure 5. The upper diagram, I, depicts the flow pattern although actually H is much smaller with respect to R than we have drawn. The lower pattern is not what we predict from our equations but the flow patterns that would pertain if the models proposed by other authors were applicable. If the fluid is observed at r = R/2 as one focuses from the top to the bottom the particles can be seen to flow toward the center near the top, toward the edge near the middle and toward the center near the bottom, in accordance with the pattern I which our equations predict. A more quantitative comparison is presented in Figure 6. The graph shows the fluid speed in the radial direction (toward the center is taken as positive) as a function of z. For the data shown $R/\lambda = .21$ and the frequency was .26 Mlz. The taller (labeled I) peaked curve in Figure 6 is the best fit of the quantity in brackets in Eq. 44 using our experimentally determined value for k'_o. Since everything in the brackets is determined a best fit was made of the data to a constant times the bracket. The constant so determined was $(13 \pm 1) \times 10^9$ cm^3 sec/micron and $\chi^2 = 2.3$. The smaller peaked curve (labeled II) in Figure 6 is a best fit where both k'_o and the constant are to be found. Their values are respectively 470 ± 10/cm and $2.0 \pm 0.1 \times 10^9$ cm^3 sec/micron with $\chi^2 = 0.3$. The later value of k'_o appears unacceptable in light of the small error on viscosity and the better fit we take to be fortuitous. It is noteworthy that the fit is so good since for the data plotted R/λ is about half of the resonant value for which Eq. 44 was derived. Notice the peak near the top of the disc, the one on the

right in Figure 6, is slightly less than the one on the left. The reason for the difference has to do with our assumption that $v_z = Ae^{i\omega t}$ both at the top and bottom of the disc. Making the boundary condition that $v_z = 0$ at the top decreases the top peak to about 20% of the bottom peak. The data seems to be in between these two extremes and it would appear we have taken the better approximation in allowing the upper boundary to move. Data was taken for R/λ equal to .21, .29, .30, .36, .39, and .45. All of the radial velocity profiles have the same basic pattern as those data shown in Figure 6.

Frequencies of .26, .77, .68, and 1.07 MHz were used both for direct contact of the sample holder with the barium titanate crystal and with the crystal in a cell so that the wave was propagated through about one cm of water before reaching the sample. All of the flow patterns observed in the microscope using the water cell were radial. For the direct contact case for certain frequencies and locations on the crystal it was possible to induce patterns of either two or four rather circular flow patterns. The discs became slightly distorted from circular to ellipsoidal in shape for these non-radial patterns. These patterns are assumed due to non-uniform oscillation of the crystal. For these cases the pressure in Eq. 1 must be assumed to be a function of angle. The solutions are similar to the well studied oscillating drumhead.

The radial velocity in Eq. 44 is proportional to A^2, the square of the piston velocity amplitude. But this amplitude should be proportional to the voltage applied to the barium titanate crystal. In Figure 7 therefore we have plotted the radial velocity measured at a fixed r and z as a function of voltage. The solid line is a fit to a voltage square curve.

REFERENCES (For Appendix III)

1. V. Vzolina, Trudy Lomonosov Inst. Akad. Nauk SSSR 8, 11 (1936)
2. J.L. Fergason, Proc. Second International Symposium on Acoustic Holography, 2, 53 (1970).
3. L.W. Kessler and S.P. Sawyer, Appl. Phys. Lett. 17, 440 (1970).
4. W. Helfrich, Phys. Rev. Lett. 29, 1583 (1972).
5. P. Greguss, Acustica 29, 52 (1973).
6. J.F. Dreyer, J. Acoust. Soc. Am. 55, 407 (1974).
7. C. Sripaipan, C.F. Hayes and G.T. Fang, Sixth International Liquid Crystal Conference, J-29 (1976).

   C. Sripaipan, C.F. Hayes and G.T. Fang, Phys. Rev. 15A, 1297 (1977).
8. S. Candau, A. Peters and S. Nagai, Sixth International Liquid Crystal Conference J-30 (1976).
9. J.L. Dion and F. DeForest, Sixth International Liquid Crystal Conference, K-18 (1976).
10. C.F. Hayes, Liquid Crystals and Ordered Fluids, 3, 287 (1978).
11. S. Nagai and K. Iizuka, Mol. Cryst. Liq. Cryst. 45, 83 (1978).
12. S. Nagai and Kozo Iizuka, Japan. J. Appl. Phys. 17, 723 (1978).

Figure 1. Diagram for calculations of the infinite non-viscous cylindrical fluid. The piston driving the oscillations is in the xy plane. For the viscous disc of height H the origin is moved along the z axis a distance H/2.

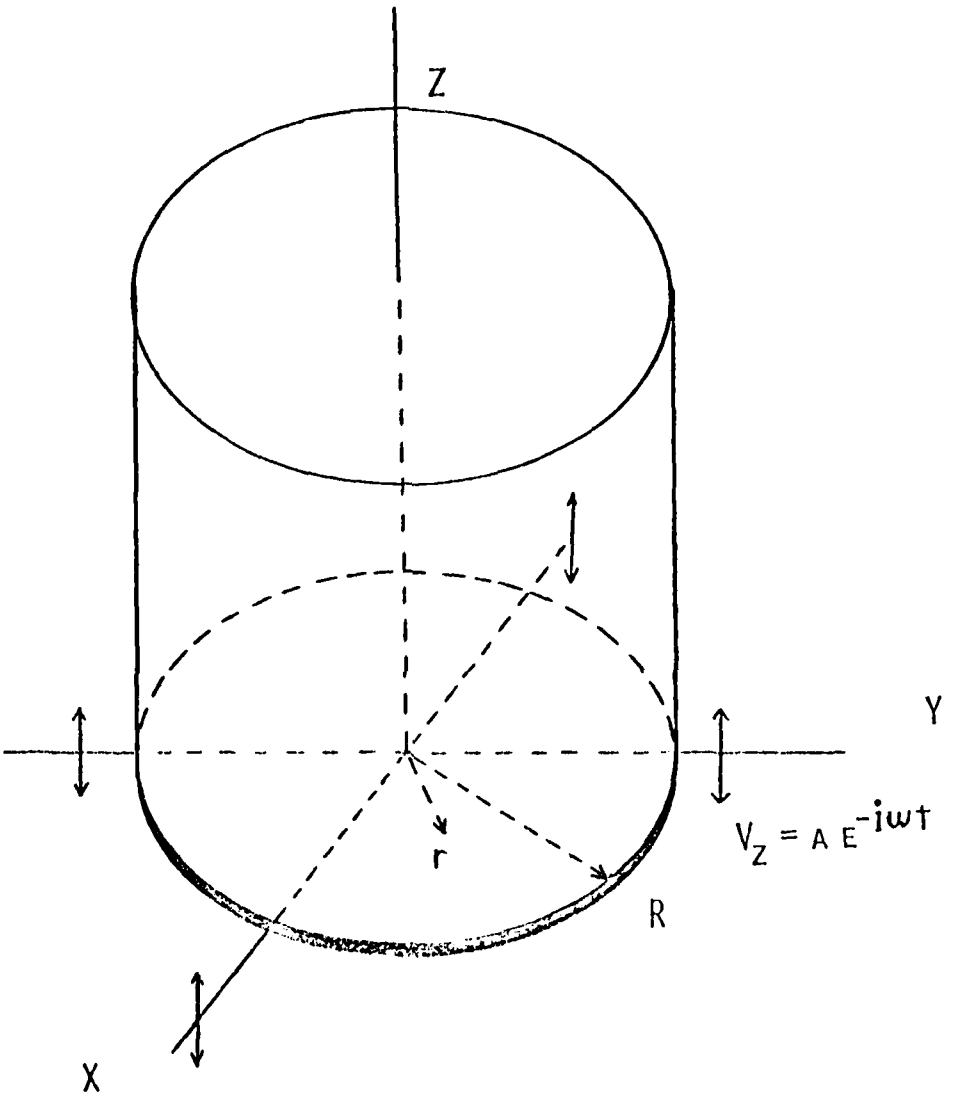
Z
Y
X
r
R
$V_Z = A E^{-i\omega t}$

Figure 2. Graph for the ratio of radial speed amplitude to piston speed amplitude versus the ratio of cylindrical radius to acoustic wavelength.

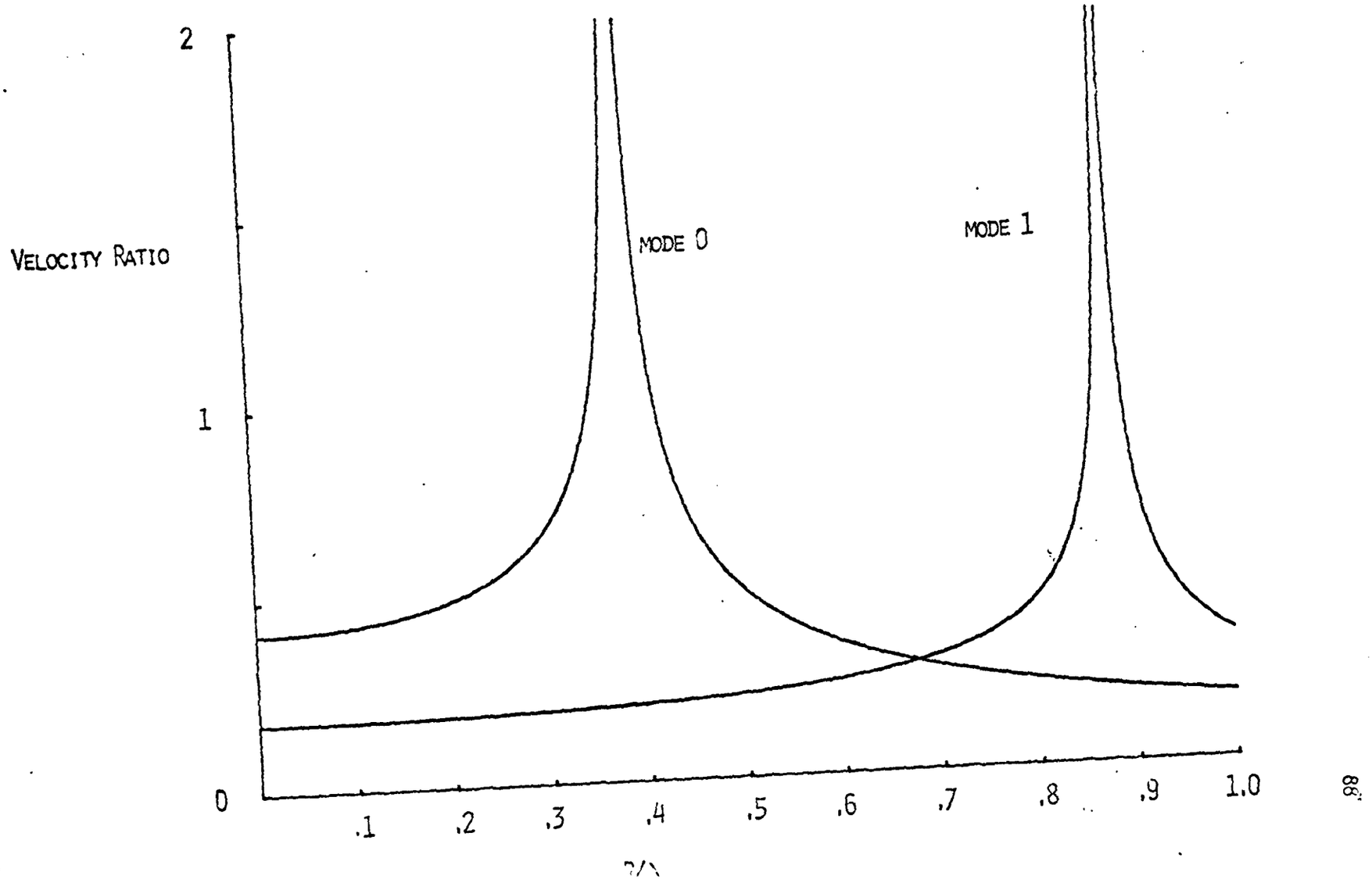
VELOCITY RATIO
2
1
0
MODE 0
MODE 1
.1
.2
.3
.4
.5
.6
.7
.8
.9
1.0

Figure 3. Graph of velocity ratio versus z/λ. The velocity ratio is the ratio of radial speed amplitude to piston speed amplitude.

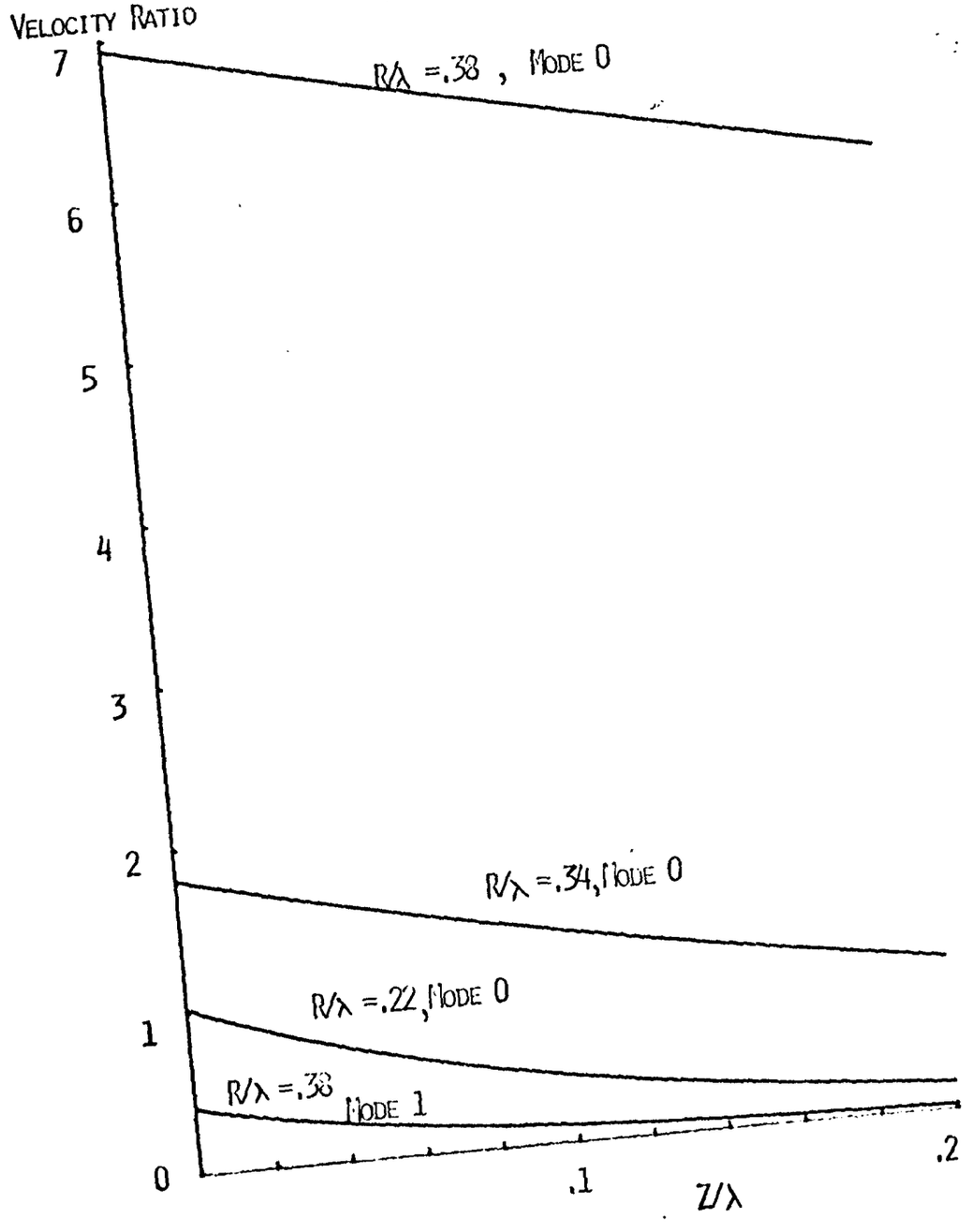
VELOCITY RATIO
7
6
5
4
3
2
1
0
R/λ =.38 , MODE 0
R/λ =.34, MODE 0
R/λ =.22, MODE 0
R/λ =.38 MODE 1
.1
.2
Z/λ

Figure 4. Velocity ratio (radial to piston's) versus distance along the z axis. The model assumes no-slip at the boundaries and incorporates viscosity.

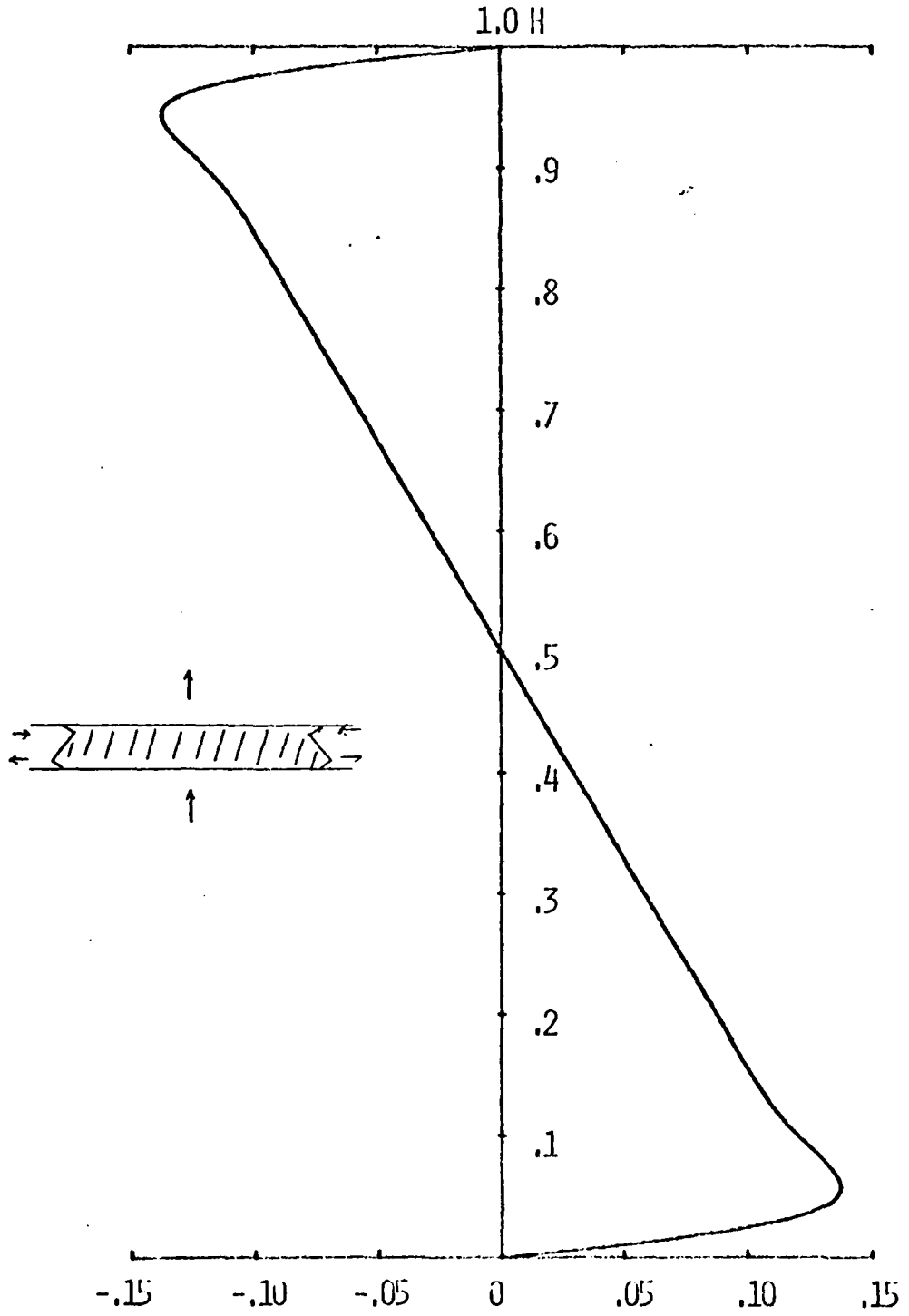
1.0 H
.9
.8
.7
.6
.5
.4
.3
.2
.1
-.15
-.10
-.05
0
.05
.10
.15
Velocity Ratio

Figure 5. Flow patterns in the disc due to acoustic streaming. The upper diagram, I, is the pattern predicted from our second order solutions. The lower pattern, II, is that assumed in other theories.

AD-A094 782 HAWAII UNIV HONOLULU DEPT OF PHYSICS AND ASTRONOMY F/G 20/6
A STUDY OF THE ACOUSTIC-OPTIC EFFECT IN NEMATICS,(U)
DEC 80 C F HAYES N00014-78-C-0417
UNCLASSIFIED 004 NL

2 OF 3
AD A094782

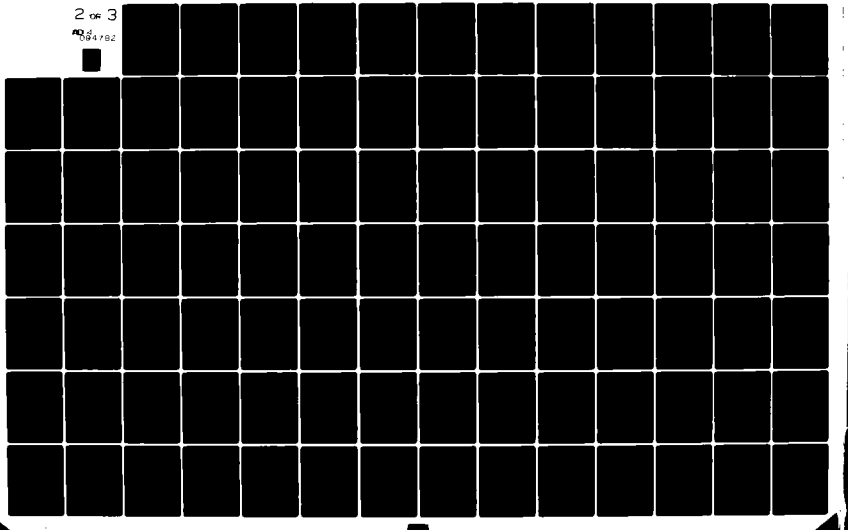

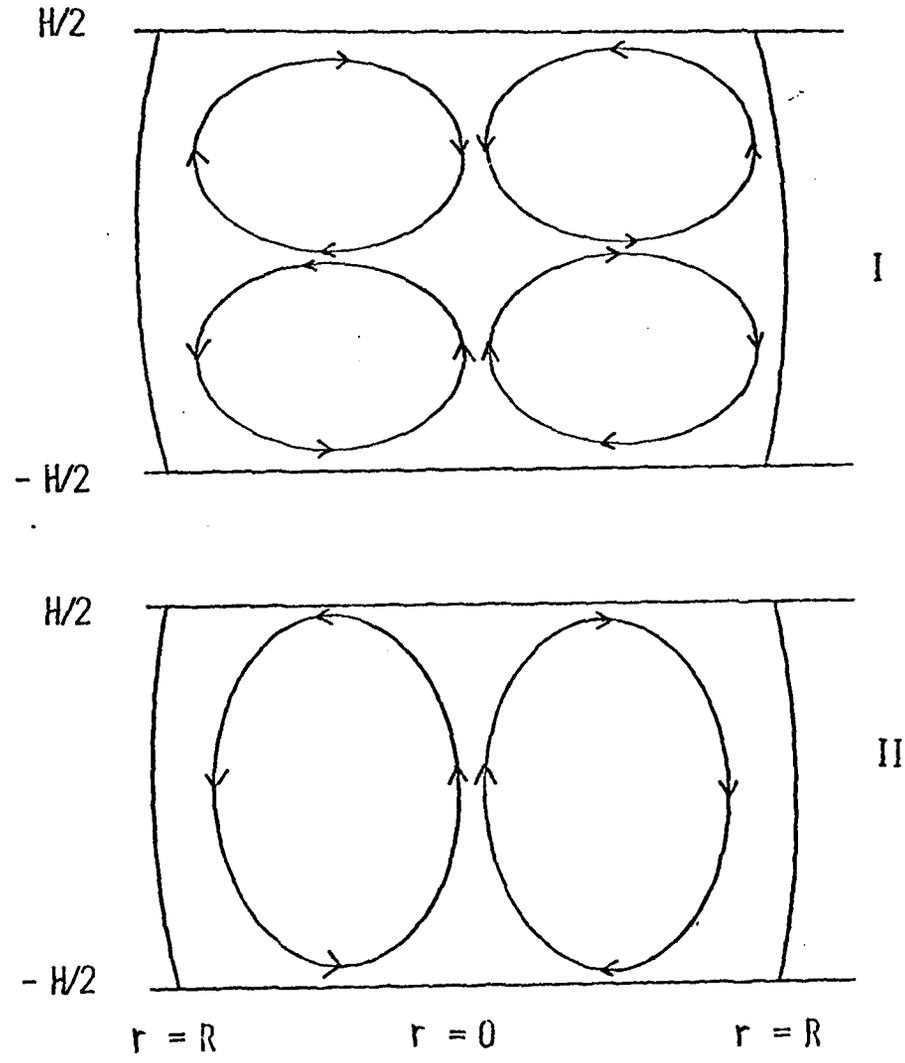
H/2
- H/2
I
H/2
- H/2
II
r = R
r = 0
r = R

Figure 6. Velocity of fluid due to acoustic streaming versus distance through the disc at r = R/2. Curve I is a best fit to the data using our measured value of k'_o. Curve II is a best fit allowing k'_o to be determined by the fitting process itself.

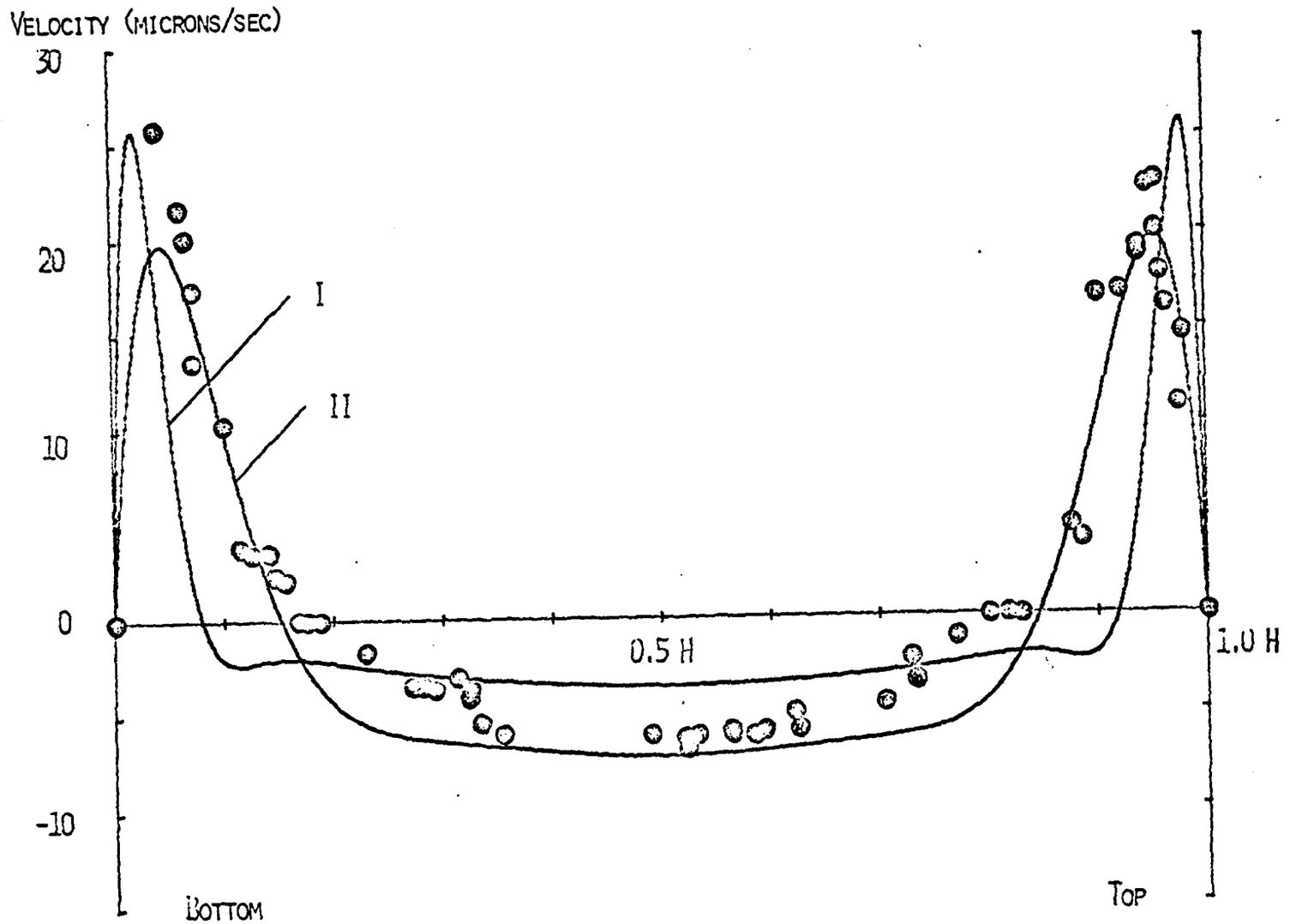
VELOCITY (MICRONS/SEC)
30
20
10
0
-10
I
II
0.5 H
1.0 H
BOTTOM
TOP

Figure 7. Velocity of the fluid due to acoustic streaming versus voltage applied to the transducer. The solid line is a best fit to a voltage square dependence.

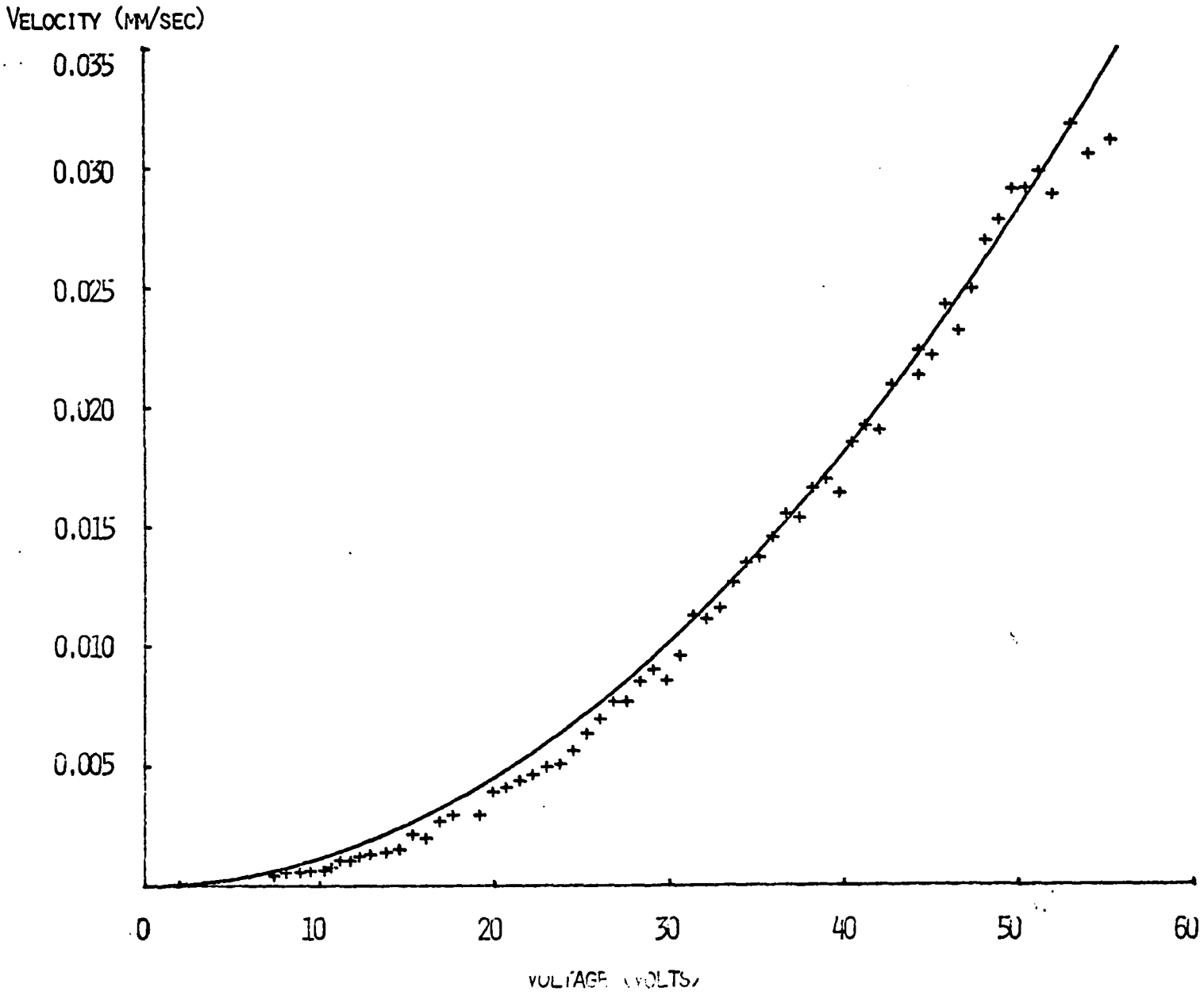
VELOCITY (MM/SEC)
0.035
0.030
0.025
0.020
0.015
0.010
0.005
0
10
20
30
40
50
60
VOLTAGE (VOLTS)

The Mathematical Description of a Nematic Liquid Crystal in an Acoustic Field

W. G. Laidlaw

Physics Department, University of Hawaii, Honolulu, Hawaii

I. INTRODUCTION

The recent literature attests to a growing interest in acoustically induced structures in liquid crystals[1]. The resulting optical effects are of potential use in display devices - for example as acoustic cameras[2]. Theoretical explanations have, until recently, been at odds with a number of experimental observations. Early attempts[3,4] attributed the sudden appearance of the "new" optical character for the system (see fig. 1) to the occurrence of an instability in the steady state regime generated by the imposed acoustic field. Unfortunately, the acoustic power, which these models predicted would bring about an instability, was as much as two orders of magnitude greater than the power which experiment showed would generate the new optical pattern[5]. More recently, experimental results have been explained satisfactorily[6,7] in terms of the gradual build up of an acoustic streaming pattern, (see fig. 2). In this explanation the sudden appearance of the optical pattern is simply a function of the complicated dependence of the optical effect on the acoustic streaming. This is illustrated in figure 3. One should emphasize that the acoustic streaming pattern invoked in this explanation eventually becomes unstable for, at sufficiently high input power, a turbulent flow pattern obtains with a concomitant sudden change in optical pattern.

This manuscript presents a rather simple analysis of the mathematical models which have been employed. Our hope is that of establishing the relation between them.

II. MATHEMATICAL MODEL (i) The Dynamic Equations

We undertake a description of the liquid crystal acoustic field system on a hydrodynamic scale. For this purpose we shall utilize the hydrodynamic equations expressing conservation of mass, conservation of energy and conservation of linear momentum. One must also introduce equations to describe any additional hydrodynamic scale variables, for example, the director variables which characterize the liquid crystal. For this latter purpose one commonly introduces the "Oseen equation" in the fashion of Leslie[8] and Eriksen[9]. Alternatively one may employ the "Broken Symmetry equations" as developed by Martin et al.[10] and Forster[11], or one may utilize the "torque model" of deGennes and collaborators[12]. The advantage of the Leslie-Eriksen equations is that they purport to treat the dynamics far from an equilibrium state and their equations, correct to second order, are readily available[13] and have been utilized by several authors[14]. For rather compelling reasions, discussed by Martin et al., there is a firmer theoretical basis for the "Broken Symmetry" approach. Unfortunately, the present literature contains the broken symmetry equations only in their linearized form although, in principal[15], they could also be written out in a nonlinearized form [For example see reference (16) where they have been obtained for a nematic liquid crystal.] Certainly the elegant conceptual frame work of the Martin and Forster approach (e.g., reactive fluxes,

dissipative fluxes etc.) is well worth utilizing (see reference (16) where they have been employed).

In any case the equations governing the dynamics of a nematic liquid crystal are a set of seven equations [from conservation of mass(1), linear momentum (3), energy (1) and the broken symmetry equations of the director (2)]. In terms of a complete set, {X}, of hydrodynamic scale variables $\alpha_i(\vec{r},t)$ they may be written formally as

$$i,=1\to 7 \; ; \; \frac{\partial}{\partial t}\alpha_i + \hat{G}(\{\alpha_i\}) + \hat{H}(\{\alpha_i\alpha_j\}) + \ldots = 0 \qquad (1)$$

Here $\hat{G}$ is a linear operator in which any member of the set of α_i appears only linearily, $\hat{H}$ is a linear operator in which members of $\{\alpha_i\}$ appear in a bilinear or quadratic form. We shall give further specifics of $\hat{G}$ and $\hat{H}$ as the need arises. It seems worthwhile to first discuss the method of the solution of eq. (1).

(ii) The Reference State

Because of their complexity the solutions of the set of eqs. in (1) is frequently carried out in terms of a reference state. The reference state is normally some readily obtained solution of eq. (1) for example the equilibrium state or some other appropriate "steady state" solution. Unfortunately, solutions of eq. (1) which would serve as appropriate reference states are sometimes not readily available! As we shall see this is certainly the case for the system under discussion. We introduce a reference state by writing, for all i

$$\alpha_i = \alpha_i^{\,r} + \delta\alpha_i \qquad (2)$$

where the superscript r denotes the known expression for the variable α_i in the reference state. The displacement $\delta\alpha_i$ is sometimes written

as a "power series"[17], giving, for eq. (2)

$$\alpha_i = \alpha_i^{0} + \alpha_i^{(1)} + \alpha_i^{(2)} + \ldots \tag{3}$$

The precise way in which eqs. (2) and (3) are chosen and utilized in the nematodynamic equations has a strong influence on the theoretical conclusions. Hence some simple applications would seem worthwhile at this point. For purposes of discussion imagine α_1 to be completely decoupled from the other hydrodynamic variables. We than take α_1 to be given by

$$\frac{\partial}{\partial t}\alpha_1 + a_1\alpha_1 + A_1\alpha_1^{2} = 0 \tag{4}$$

We introduce $\alpha^{(1)}$ as a solution of this equation with some specified boundary conditions. Substitution of eq. (2) into eq. (4) yields

$$\frac{\partial}{\partial t}\delta\alpha_1 + (a_1 + 2A_1\alpha_1^{r})\,\delta\alpha_1 + A(\delta\alpha_1)^{2} = 0 \tag{5}$$

If $A\delta\alpha_1$ can be taken to be small relative to the linear coefficient then we can neglect the last term to obtain the "linearized" and homogeneous equation

$$\frac{\partial}{\partial t}\delta\alpha_1 + \Gamma_1\delta\alpha_1 = 0,\ \Gamma_1 = a_1 + 2A_1\alpha_1^{r} \tag{6}$$

The quantity Γ_1 displays the nonlinear heritage of this equation through $2A_1\alpha_1^{r}$. However, if the reference state is chosen such that α_1^{r} is zero then $2A\alpha_1^{r} = 0$ and the linearized equation carries no information about the nonlinearity of the original equation. If on the other hand α_1^{r} is non zero this information is retained and solutions of the linearized form (eq. (6)) can reflect the nonlinear

character of the original equation. Indeed it is just this feature which allows linear stability theory to probe the solutions of non linear equations[18]. A particularily simple illustration is the use of a steady state solution of eq. (4) namely $\alpha_1^r = -a_1/A$. This gives $\Gamma_1 = -a$ so that the solution of eq. (6) is

$$\delta\alpha_1(t) = \delta\alpha_1(0)\, e^{at} \tag{7}$$

The implication of equation (7) for $a_1 > 0$ is that $\delta\alpha_1$ grows exponentially with time so that α_1 rapidly deviates from the reference description. One concludes that this reference solution of eq. (4) is absolutely unstable. More interesting instabilities would arise if α_1 were coupled to other variables and one shall have occasion to treat this in detail in a subsequent communication.

Turning now to the power series solution we substitute eq. (3) into eq. (4) and obtain the zero first and second order equations as

$$\partial/\partial t\ \alpha_1^{(0)} + a_1\alpha_1^{(0)} + A(\alpha^{(0)})^2 = 0 \tag{8}$$

$$\partial/\partial t\ \alpha_1^{(1)} + (a_1 + 2A\alpha^{(0)})\alpha_1^{(1)} = 0 \tag{9}$$

$$\partial/\partial t\ \alpha_1^{(2)} + (a_1 + 2A\alpha_1^{(0)})\alpha_1^{(2)} + A(\alpha_1^{(1)})^2 = 0 \tag{10}$$

An essential step in obtaining these equations is the assertion that $\alpha^{(m)}\alpha^{(n)}$ is of order $m + n$. The homogenous part of the second order equation is the same as that of the first order equation. Indeed if the reference state is such that $\alpha^{(0)}$ is zero then, in these homogeneous parts, all information about the nonlinearity of the original

equation is lost. As we shall see this is indeed the case for the analyses of acoustic streaming which select the equilibrium state i.e., no sound field ($v^{(0)} = 0$) as the reference solution and treat the steady sound field as first order and acoustic streaming as part of the second order contribution[17]. Theoretical analyses carried out in this fashion (Hayes[6], Candau[7]) would not even suggest an instability as arising from the homogeneous part of either the first or second order equations.

The set of nematodynamic equations are, of course, more complicated than this simple example. However, this should serve to illustrate the role of the nonlinearity and the reference state in both the linearized equation and in the first and second order equations of the power series approach.

(iii) Reference Descriptions

Even if one were not interested in instabilities it is clearly of some importance to select a reference solution with some case. Certainly solutions with all relevant $\alpha_i^r = 0$ emasculate the linearized form. Because of this various authors have utilized descriptions for which relevant α_i^r are not zero. However, at the same time, these reference descriptions may be solutions of only part of the original equation or their relation to the original equations may be less straightforward. For example, Chaban's[19] elegant analysis of the instability of a liquid crystal in an acoustic field utilizes a "pump solution" - an oscillating solution of the homogeneous part of the original equations. On the other hand Helfrich[3] and later Nagai[4] introduced a reference "state" which can perhaps be best characterized as a "shear-deformed" description but its relation to

the full nematodynamic equations is less than clear.

The implications of utilizing a reference solution $\{\alpha_i^r\}$ which is not a solution of the full equations can be illustrated by recourse once again to solutions of the simple relation given by eq. (4). Let α_1^r be such that it is a solution of the homogeneous part of eq. (4) namely that

$$\frac{\partial}{\partial t}\alpha_1{}^r + a_1\alpha_1{}^r = 0 \tag{11}$$

Then substitution of $\alpha_1 = \alpha_1^r + \delta\alpha_1$ into eq. (4) gives

$$\frac{\partial}{\partial t}\delta\alpha_1 + (a_1 + 2A\alpha_1{}^r)\delta\alpha_1 + A(\alpha_1{}^r)^2 + A(\delta\alpha_1)^2 = 0$$

The assertion that $(\delta\alpha_1)^2$ is small now leads to the inhomogenous equation

$$\frac{\partial}{\partial t}\delta\alpha_1 + \Gamma\delta\alpha_1 + A(\alpha_1{}^r)^2 = 0 \tag{12}$$

rather than the homogeneous form obtained earlier in eq. (6). Since eq. (11) requires that the only non zero $\alpha_1{}^r$ are time dependent the solution of eq. (12) becomes mathematically complicated (cf. Chaban [19]). In any case, the solution of the homogeneous part of eq. (12) may indicate stability; yet, because of the inhomogeneous term, $\delta\alpha_1$ may be substantially different than zero. To avoid the more complicated mathematics let us treat a case where the reference state $\{\alpha_i{}^r\}$ is time independent and non zero [Eq. (11) precludes this but it is easy to see that if α_1 were linearily coupled to another variable α_2 as in

$$\frac{\partial}{\partial t}\alpha_1 + a_1\alpha_1 + a_2\alpha_2 + A\alpha_1{}^2 + \ldots = 0$$

we could obtain a solution $\alpha_1{}^r \neq 0, \frac{\partial}{\partial t}\alpha_1{}^r = 0$]. Taking $\alpha_1{}^r$ to be

a constant means Γ_1 is a constant and we can immediately write the solution of eq. (12) as

$$\delta\alpha_1(t) = \delta\alpha_1(0)e^{-\Gamma_1 t} - e^{-\Gamma_1 t}\int_0^t e^{\Gamma t'} A(\alpha_1{}^r)^2 dt'$$

which integrates to

$$\delta\alpha_1(t) = \delta\alpha(0)e^{-\Gamma t} - \frac{A(\alpha_1^r)^2}{\Gamma}\left[1 - e^{-\Gamma t}\right]$$

and for $t \to \infty$ and $\Gamma > 0$ we have

$$\delta\alpha(t) \to \frac{-A}{\Gamma_1}(\alpha_1{}^r)^2$$

Hence α_1 could, with increasing $\alpha_1{}^r$ become quite different than just $\alpha_1{}^r$ even though Γ_1 remained positive, i.e, even though the system remains stable in terms of a decaying exponential $e^{-\Gamma_1 t}$. Of course, if $-2A\alpha_1{}^r$ were made sufficiently large Γ_1 could change sign, $\delta\alpha_1$, would increase dramatically with time and, the reference α_1^r would clearly be unstable. Whether one observes only this instability or one observes the gradual growth of the contribution $\frac{A}{\Gamma_1}(\alpha_1{}^r)^2$ will depend on how α_1 is probed experimentally. The instability may occur before this latter contribution becomes observable or $\frac{A}{\Gamma_1}(\alpha_1{}^r)^2$ may be observed prior to the instability.

(iv) Boundary Conditions

Although boundary conditions apply to the set of α_i the solution is carried out in terms of the separate parts of α_i (cf. eq. (2) or (3)). This presents few difficulties with $\alpha_i{}^r$ and $\delta\alpha_i$ in eq. (2) since $\alpha_i{}^r$ usually has well defined boundary conditions. However, in expansion to second order as in eq. (3) the selection of $\alpha_i{}^r = \alpha_i{}^o$

defines only the sum $\alpha_i^{(1)} + \alpha_i^{(2)} = \alpha_i - \alpha_i^{(0)}$. The separate conditions on $\alpha_i^{(1)}$ and $\alpha_i^{(2)}$ can be selected arbitrarily.

(v) Normal Modes

Given an appropriate reference description and its boundary conditions the solution of the nematodynamic equations may be addressed. The methodology of Rayleigh[20] followed, largely, by recent workers (cf. Hayes[6], Nagai[4], Candau[7]), proceeds directly to the expression for $\alpha_i^{(m)}(t)$. We have repeatedly seen (sections (ii) and (iii)) the role played by the solution of the homogeneous part of the dynamic equation. Where there are, in fact, several such coupled dynamic equations there are some advantages to solving the homogeneous equations in terms of their normal modes. This is particularly so in the case where the coefficients of the homogeneous equations are constants. The efficacy of a normal mode analysis is apparent even in the solution of inhomogeneous equations, for example equations of the form of eq. (10).

We shall illustrate their use by considering the set of second order nematodynamic equations denoted by

$$\frac{\partial}{\partial t}\underline{\alpha}^{(2)} + \underline{\underline{M}}\,\underline{\alpha}^{(2)} + \underline{F} = 0 \qquad (13)$$

Here $\underline{\alpha}^{(2)}$ is a column vector with elements $\alpha_i^{(2)}$, $\underline{\underline{M}}$ is a matrix with elements M_{ij} defined in terms of the operators $\frac{\partial}{\partial x_i}\frac{\partial}{\partial x_j}$ and phenomenological coefficients such as those for viscosity, ν_n, heat conductivity K, etc. The inhomogeneous part $\underline{F}$ is a column vector with elements F_i. This "force" F_i is defined in terms of products $\alpha_i^{(1)}\alpha_j^{(1)}$ where the latter are solutions of the homogeneous equation

$$\frac{\partial}{\partial t}\underline{\alpha}^{(1)} + \underline{\underline{M}}\,\underline{\alpha}^{(1)} = 0 \qquad (14)$$

We introduce normal modes γ_j by writing[21]

$$\gamma_j(t) = \gamma_j(0)e^{-\lambda_j t} \tag{15}$$

where the $\gamma_j(0)$ are elements of a column vector

$$\underline{\gamma} = \underline{\underline{V}}^{-1}\underline{\alpha} \tag{16}$$

Here $\underline{\underline{V}}$ is such that

$$\underline{\underline{V}}^{-1}\underline{\underline{V}} = \underline{\underline{1}} \text{ and } \underline{\underline{V}}^{-1}\underline{\underline{M}}\,\underline{\underline{V}} = \underline{\underline{\Lambda}} \tag{17}$$

and $\underline{\underline{\Lambda}}$ is a diagonal matrix with elements $\Lambda_{jj} = \lambda_j$. We should emphasize again that $\underline{\underline{M}}$ is the same for both the first and second order equations.

Given the definitions of eq. (16) and (17) we can rewrite the set of coupled inhomogeneous equations of the second order equation as a set of uncoupled inhomogeneous equations. We simply multiply from the left with $\underline{\underline{V}}^{-1}$[21] and use $\underline{\alpha} = \underline{\underline{V}}\,\underline{\gamma}$ on the right of $\underline{\underline{M}}$ to obtain

$$\partial/\partial t\ \underline{\underline{V}}^{-1}\underline{\alpha} + \underline{\underline{V}}^{-1}\,\underline{\underline{M}}\,\underline{\underline{V}}\,\underline{\gamma} + V^{-1}F = 0$$

or

$$\partial/\partial t\ \gamma_j + \lambda_j\gamma_j + F_j^{\gamma} = 0 \tag{18}$$

where $F_j^{\gamma} = \Sigma\ V_{ji}^{-1}\ F_i$ (19)

The complete solution of eq. (18) can be immediately written down as

$$\psi_j \equiv \gamma_j(t) = \gamma_j(0)e^{-\lambda_j t} - e^{-\lambda_j t}\int_0^t e^{\lambda_j t'} F_j^{\gamma}(t')\,dt' \tag{20}$$

(note we use ψ_j for the complete solution of eq. (18)).

In treatments[17] where the acoustic streaming is taken to be part of the second order solution one asserts that F_j contains a

constant term and the remaining terms are of less importance. Under these conditions eq. (20) integrates to give

$$\psi_j(t) = \gamma_j(0)e^{-\lambda_j t} - \frac{F_j^{\gamma}}{\lambda_j}\left[1 - e^{-\lambda_j t}\right] \qquad (21)$$

Consequently one can describe the solution of eq. (13), i.e., the second order equation, in terms of the "modes" γ_j given by eqs (15)-(17). The description in terms of the variables $\alpha_1^{(2)}$ (i.e., $v_x^{(2)}$, $p^{(2)}$, etc.) is obtained by simply inverting eq. (16) to give

$$\alpha_i^{(2)}(t) = \Sigma V_{ij}\psi_j(t) \qquad (22)$$

(vi) The Characteristics of the Second Order Solution

We shall discuss only those cases where the inhomogeneous term is constant and the eigenvalues λ_i of $\underline{\underline{M}}$ have positive real parts. In these circumstances the response and long time characteristics are of interest. From eq. (21) we see that as $t \to \infty$ we have

$$\psi_j = -\frac{F_j^{\gamma}}{\lambda_j} \qquad (23)$$

Thus ψ_j reaches a steady value which we might remark is simply that obtained from the second order equation (eq. (18)) on ignoring $\partial\gamma_i/\partial t$. For the long time steady value of say α_i we have

$$\alpha_i = \Sigma\, V_{ij}F_j^{\gamma}/\lambda_j = \sum_{jk} V_{ij}V_{jk}F_K/\lambda_j \qquad (24)$$

It is this solution which corresponds to the steady acoustic streaming solutions of Hayes[6] and others. We shall emphasize that once one has the eigenvalues, λ_i, and eigen vectors, V_i,

of the first order equation then all one needs to complete the solution is the "forces" F_i of the second order equation.

The response time of the second order solution can characterize either growth (τ_G) or decay τ_D. In the case of growth we take the initial state to have $\gamma_j(0)$ [recall section (iv) and note that this implies all $\alpha_i^{(2)} = 0$ at time $t = 0$ so that $\alpha(0) = \alpha_i^{(0)}(0) + \alpha_i^{(1)}(0)$]. Hence eq. (21) is just

$$\psi_j^G(t) = -\frac{F_j}{\lambda_j}^{\gamma}\left[1 - e^{-\lambda_j t}\right] \tag{25}$$

We can write τ_G as $\tau_G = \left|\frac{\partial \psi_j^G / \partial t}{\psi_j^G(t) - \psi_j^G(\infty)}\right|^{-1}$ which gives for eq. (25) $\tau_G = \lambda_j^{-1}$.

The growth of the individual $\alpha_i^{(2)}$ is of course characterized by several response times. If all $\alpha_i^{(2)}(0) = 0$ eq. (22) gives

$$\alpha_i^{(2)} = \sum_j V_{ij}\left[\frac{F_j}{\lambda_j}^{\gamma}\left(1 - e^{-\lambda_j t}\right)\right] \tag{26}$$

and in anology with eq. (25) we see that there are several response times $\tau_{G,j} = 1/\lambda_j$. Which of these $\tau_{G,j}$ appears dominant will depend on the elements of $(V_{ij}F_j^{\gamma}/\lambda_j)$.

Alternatively one can enquire as to the decay of, say, the steady long time value of ψ_j^{ss}. when the inhomogeneous term (which we think of as a "force" which had maintained this steady state) is suddenly shut off. This means that in eq. 21 we can take $\gamma_j(0) = \gamma_j^{ss}$ at the instant the forces F_i are set of zero and write eq. (21) for decay (D) as

$$\psi_j^D(t) = \psi_j^{ss} e^{-\lambda_j t} \tag{27}$$

Defining the response time τ_{Dj} as $\left| \frac{\partial \psi_j^D / \partial t}{\psi_j^D(t) - \psi_j^D(\infty)} \right|^{-1}$ gives

$$\tau_{Dj} = \lambda_j^{-1}$$

As with growth, we would expect that decay of a given $\alpha_j^{(2)}$ would be characterized by several decay times as in

$$\alpha_j^{(2)} = \Sigma\, V_{ij} \gamma_j^{ss} e^{-\lambda_j t} = \Sigma\, V_{ij}\, V_{jk}\, F_k \left(\frac{e^{-\lambda_j t}}{\lambda_j} \right) \tag{28}$$

We must remark that the decay time of a given mode ψ_j is the same as its response time. Further it should be clear that the decay times λ_j^{-1} do not depend on the "forces" F^{γ}. The γ_j are the roots of $\underline{\underline{M}}$ and in the power series expansion utilizing an equilibrium reference (i.e., no sound) the matrix $\underline{\underline{M}}$ can be shown [cf. eqs. (8) to (10)

with $\alpha_1^r = 0$) to reduce to that of the equilibrium case. For this reason one would not expect this method to predict a response time λ_j^{-1} which depended on the sound field.

A word of caution is, however, in order if the response times are probed[7] in terms of the individual $\alpha_i^{(2)}$. Notice that in both eq. (26) and (28) the forces F_j enter as coefficients of terms with different exponential decay characteristics (16). Now these forces F_i do not depend in precisely the same way on a given external stress, e.g., electric or even the acoustic field. Hence changing these external stresses will change the relative contributions of the various terms in these expressions for growth and decay of $\alpha_i^{(2)}$ in a complicated way. As a result the apparent decay time can depend more than just λ_j^{-1}, it could depend on the external stress in a complicated way[22].

The long time behaviour and response times of acoustic streaming when the reference state is chosen as something other than equilibrium can differ from that given above. For example, if the reference state is a "pump" solution[19] or an acoustically strained description[4] then in the linearized equation,

$$\left[\frac{\partial}{\partial t}\,\delta\,\underline{\alpha} + \underline{\underline{M}}\delta\underline{\alpha} + \underline{F} = 0\right] \quad ;$$

where $\underline{\underline{M}}$ now retains information about the reference state - i.e., about the imposed acoustic field-in contrast to the cases discussed above. If the reference is such that $\underline{\underline{M}}$ is time dependent the mathematics is complicated (cf. Chaban) but if $\underline{\underline{M}}$ is constant it is easy to see that the analysis of the previous few paragraphs goes through in the same way. Now, however, the characteristic "response" times λ_j^{-1} could be directly dependent on the imposed acoustic field. Assuming stability the long time steady state results should, however, be the same.

III. CONCLUSIONS

For a nematic liquid crystal in an acoustic field the power series solution carried to second order from a reference state of zero acoustic power (i.e., equilibrium) is incapable of displaying an exponential growth (instability) of the characteristic solution. Other reference descriptions could display such an instability. However, the use of reference descriptions which are not solutions of the full nematodynamic equations leads to solutions which may deviate significantly from the reference description yet still exhibit stability of the characteristic solution. Depending on the mode structure the response times may show a complicated dependence on the acoustic or other external fields.

IV. ACKNOWLEDGEMENT

The present work was stimulated by and benefitted from numerous discussions with C. F. Hayes.

REFERENCES (For Appendix IV)

1. For reviews see: S. Candau and V. Letcher Adv. Liq. Crystal. 3, 167 (1978), or O. Kapustina Sov. Phys. Acoust. 20, 1 (1974).
2. Preprint, C. F. Hayes. Physics Dept. Univ. of Hawaii.
3. W. Helfrich, Phys. Rev. Lett. 29, 1583 (1972).
4. S. Nagai and K. Iizuka, Jpn. J. Appl. Phys., 13, 189 (1974).
5. 25 W/cm^2 as the predicted value[3] vs. 1-10 milliwatts/cm^2 utilized by, for example, P. Gregus, Acustica, 29, 52 (1973).
6. C. F. Hayes, Phys. Rev. A, 15, 1297 (1977).
7. S. Nagai, A. Peters and S. Candau, Rev. de Phys. Appl. 12, 21 (1977).
8. F. M. Leslie, Quart. J. Mech. Appl. Math., 19 357 (1966).
9. J. L. Eriksen, Arch. Ration. Mech. Analy., 4, 231 (1960).
10. P. C. Martin, O. Parodi and P. S. Pershan, Phys. Rev. A., 6, 2401 (1972).
11. D. Forster, "Hydrodynamic Fluctuations, Broken Symmetry and Correlation Functions", Benjamin (1975).
12. P. de Gennes, "The Physics of Liquid Crystals", Clarendon Oxford (1974).
13. M. J. Stephen and J. P. Straley, Rev. Mod. Phys., 46, 617 (1974).
14. C.Fan,L.Kramer, and M.J.Stephen,Phys.Rev.A 2,2482 (1970).
15. Ref. 11 p. 280 or K. Kawasaki Ann. Phys., 61, 1 (1971).
16. W. G. Laidlaw unpublished.
17. W. L. Nyborg in "Physical Acoustics" ed. W. B. Mason, Vol. 2. Part B, Academic (1970).
18. S. Chandrasekar, "Hydrodynamics and Hydromagnetic Stability", Clarendon Press (1961).

19. I. A. Chaban, Akust. Zh., 24, 260-270 (1978).

20. J. W. S. Rayleigh, "Theory of Sound", Dover (1945).

21. D. L. Carle, W. G. Laidlaw and H. N. W. Lekkerkerker J. Chem. Soc. (Faraday Trans.)II, 7, 1158 (1978).

22. See ref. 7, fig. 7.

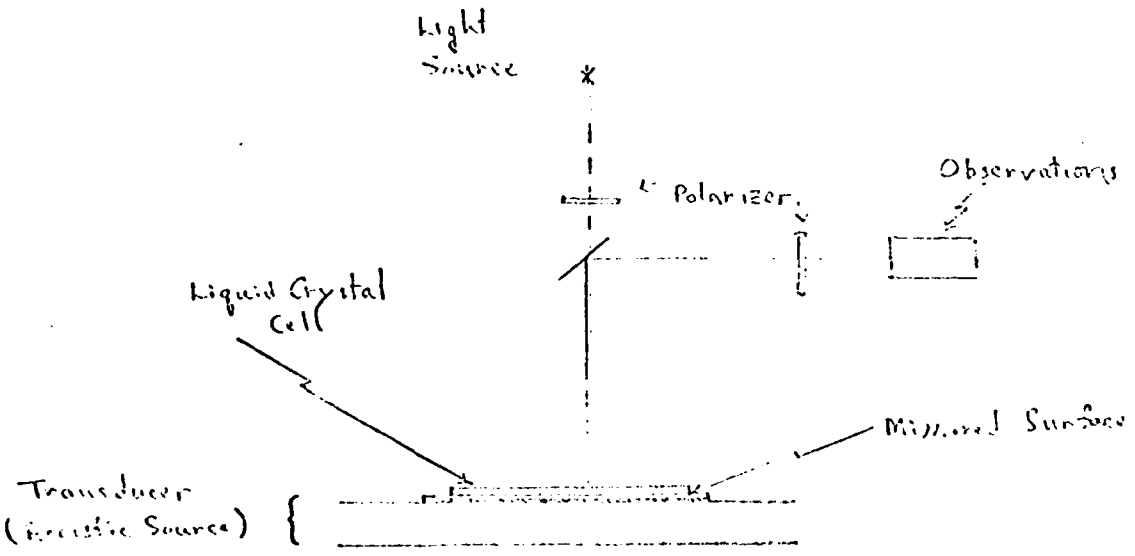

Fig. 1. Experimental Configuration for Observation of the Acousto-Optical Effect

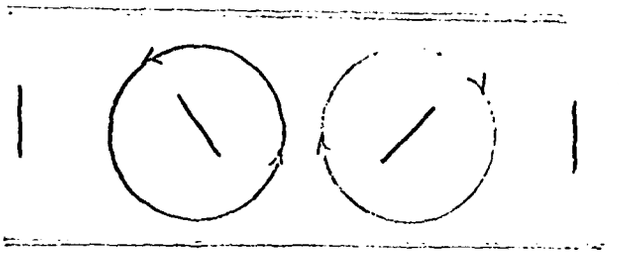

(a) Candau[7]

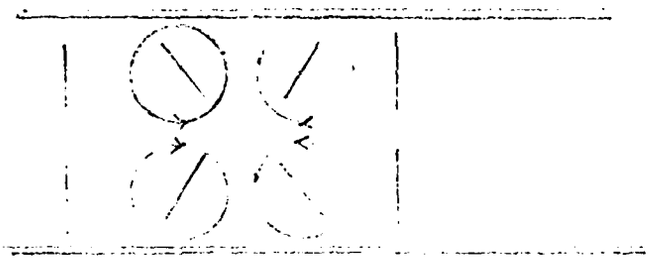

(b) Hayes[6]

Fig. 2 Acoustic Streaming Pattern in a Nematic Liquid Crystal

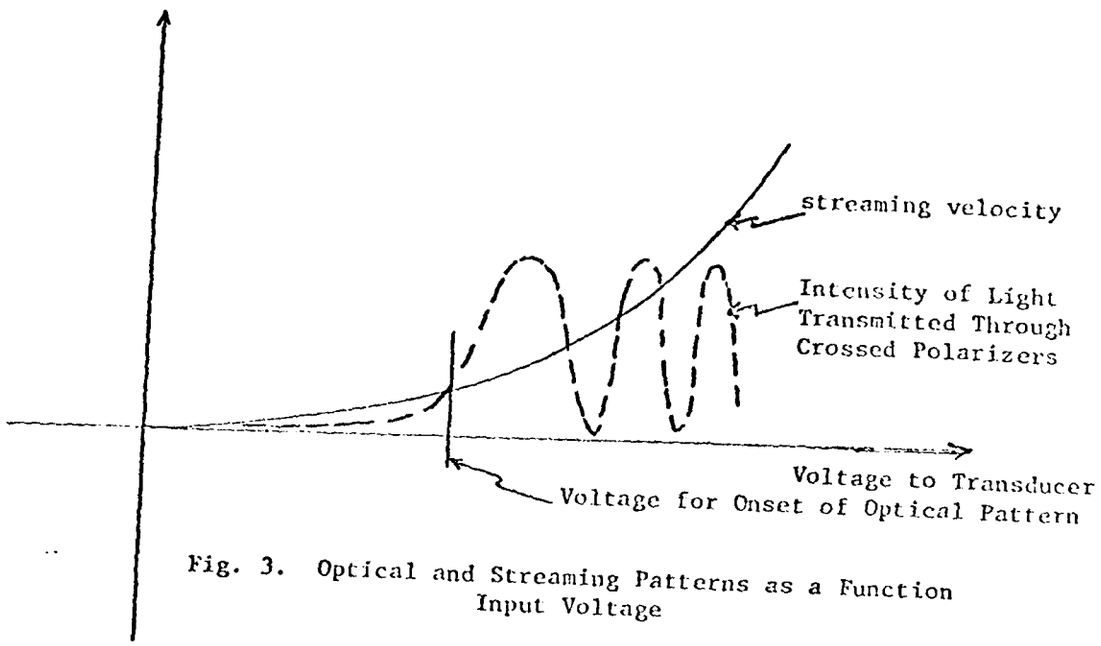

Fig. 3. Optical and Streaming Patterns as a Function Input Voltage

TECHNICAL REPORT: 003

ANGULAR DEPENDENCE OF LIQUID CRYSTAL BASED NEMATIC ACOUSTIC FIELD IMAGING DEVICES

C. F. HAYES

DEPARTMENT OF PHYSICS AND ASTRONOMY

UNIVERSITY OF HAWAII

HONOLULU, HAWAII 96822

APRIL, 1980

I. INTRODUCTION

The acousto-optic effect is a phenomenon occuring in a nematic liquid crystal in the presence of both an ultrasonic wave and a linearly polarized light wave. The nematic cell is constructed by inserting the liquid crystal between two sheets of glass chemically treated to promote homeotropic alignment. Lecithin is a typical chemical agent which causes the long axes of the nematic molecules to become oriented perpendicular to the glass sheets. Normally no light is transmitted if the cell is observed between crossed polarizers. However, if an ultrasonic wave is directed to the cell, light will be transmitted through the second polarizer.

Since 1976 it has been known[1] that the mechanism causing the effect is acoustic streaming. However, the dependence of the effect upon the incident acoustic angle is not understood. In 1978, Letcher, Lebrun, and Candau[2] reported for their cells the effect took place in a relatively narrow range of incident angles, 27 to 30 degrees. In 1977, Nagai, Peters and Candau[3] and, in 1978, Nagai and Iizuka[4] reported the acoustic frequency dependence of the angular variation of sensitivity and gave preliminary results which indicated the transmitted light intensity increased with increased acoustic transmission. In 1979, Perbet, Hareng, and LeBerre[5] reported strong light transmission at incident acoustic angles of maximum and minimum acoustic transmission. Also, in 1979, Lebrun, Candau, and Letcher[6] reported the narrow angular range for the effect becomes broadened when thin glass is used for the cell.

In this report we describe the study we have undertaken to analyze the angular dependence of the acousto-optic effect. In Section II a theory is developed which gives the acoustic transmission of the cell as a function of

incident acoustic angle, frequency, speed of the acoustic wave in the fluid(s) surrounding the cell, density of the cell, density of the fluid(s) surrounding the cell, density of the glass, speeds of the longitudinal and transverse waves in the glass, thickness of the glass layer, thickness of the liquid crystal and acoustic speed in the liquid crystal. Since each of these quantities are measurable, as well as the actual transmission, the final equation can be rigorously tested experimentally. The results of such testing is reported in Section III for both a single sheet of glass and the liquid crystal cell. A comparison is also made in this section between the acoustic transmission and sensitivity of the acousto-optic effect. This comparison gives insight into the results mentioned above by other researchers. We also obtain results for the angular dependence of lines which often appear in cells exhibiting the acousto-optic effect. In the final sections conclusions are drawn from these observations. Appendix A contains a computer program for evaluation of the acoustic transmission for a given set of the above mentioned parameters. Appendices B and C contain graphs of the transmission for typical cells as a function of angle for various frequencies.

II. THEORY

To obtain an expression for the transmission of an acoustic wave through a liquid crystal cell, we will use the coordinate system of Figure 1. Although experimentally we will immerse the cell in water the expression will allow the fluid on each side of the cell to be different.

Since fluids support no shear waves we will only have one wave function in the water and liquid crystal regions, a wave function for the compression wave:

$$\phi = (\phi' e^{i\alpha z} + \phi'' e^{-i\alpha z})\, e^{i(\sigma x - \omega t)} \tag{1}$$

In the glass we will have an additional function for shear:

$$\Psi = (\Psi' e^{i\beta z} + \Psi'' e^{-i\beta z})\, e^{i(\sigma x - \omega t)} \tag{2}$$

We note that the x component of the wave number, σ, is the same for both types of waves. Due to Snell's law we further see σ is the same in each medium.

The material speeds may be found from

$$v_x = \frac{\partial \phi}{\partial x} - \frac{\partial \Psi}{\partial z} \tag{3}$$

and

$$v_y = \frac{\partial \phi}{\partial x} + \frac{\partial \Psi}{\partial z} \tag{4}$$

The wave speeds may be expressed in terms of the Lame' parameters (λ,μ) and the density, ρ. The longitudinal speed is given by

$$c = \sqrt{\frac{\lambda + 2\mu}{\rho}} \tag{5}$$

and the shear speed by

$$b = \sqrt{\frac{\mu}{\rho}} \tag{6}$$

For the fluid region the only stress is the pressure, since $\mu = 0$, but for the glass regions we must generalize to

$$z_z = \lambda \left(\frac{\partial u}{\partial x} x + \frac{\partial u}{\partial z} z \right) + 2\mu \frac{\partial u}{\partial x} z \tag{7}$$

$$z_x = \mu \left(\frac{\partial u_x}{\partial z} + \frac{\partial u_z}{\partial x} \right) \tag{8}$$

where u_x and u_z are material displacements from equilibrium in the x and z directions, respectively. These displacement components are related to the speed components by

$$u_x = \frac{iv}{\omega} x \tag{9}$$

$$u_z = \frac{iv}{\omega} z \tag{10}$$

As indicated in Figure 1 we use the subscript 1 to denote the water glass interface at $z = d$. We let

$P = \alpha d = \omega d \cos\theta / c$ and $Q = \beta d = d \cos\gamma / b$

Combining Equations 1 - 4 and 7 - 10 we have

$$\begin{pmatrix} v_{x_1} \\ v_{z_1} \\ z_{z_1} \\ \frac{1}{2\mu} z_{x_1} \end{pmatrix} = \Lambda \begin{pmatrix} \phi' + \phi'' \\ \phi' - \phi'' \\ \psi' - \psi'' \\ \psi' + \psi'' \end{pmatrix} \tag{11}$$

where

$$A = \begin{pmatrix} i\omega \cos P & -\alpha \sin P & -i\beta \cos Q & \beta \sin Q \\ -\alpha \sin P & i\alpha \cos P & -\sigma \sin Q & i\sigma \cos Q \\ -\frac{i}{\omega}(\lambda k^2 + 2\mu\alpha^2)\cos P & \frac{1}{\omega}(\lambda k^2 + 2\mu\alpha^2)\sin P & \frac{-2i\mu\sigma}{\omega}\beta \cos Q & \frac{2\mu\sigma\beta}{\omega}\sin Q \\ \frac{\alpha\sigma}{\omega}\sin P & \frac{-i\alpha\sigma}{\omega}\cos P & \frac{1}{2\omega}(\alpha^2 - \beta^2)\sin Q & \frac{i(\beta^2 - \sigma^2)}{2\omega}\cos Q \end{pmatrix} \quad (12)$$

For interface 2 we write a similar equation:

$$\begin{pmatrix} v_{x2} \\ v_{z2} \\ z_{z2} \\ \frac{1}{2\mu} z_{x2} \end{pmatrix} = B \begin{pmatrix} \phi' + \phi'' \\ \phi' - \phi'' \\ \psi' - \psi'' \\ \psi' - \psi'' \end{pmatrix} \quad (13)$$

where B is obtained from A by letting P=Q=0. Of more interest is the inverse of B:

$$B^{-1} = \begin{pmatrix} \frac{-2i\sigma}{K^2} & 0 & \frac{i\omega}{\mu K^2} & 0 \\ 0 & \frac{-i(-\sigma^2 + \beta^2)}{\alpha K^2} & 0 & \frac{2i\sigma\omega}{\alpha K^2} \\ \frac{i(\lambda k + 2\alpha^2\mu)}{\beta\mu K^2} & 0 & \frac{i\sigma\omega}{\beta\mu K^2} & 0 \\ 0 & -2i\sigma/K^2 & 0 & \frac{-2i\omega}{K^2} \end{pmatrix} \quad (14)$$

We are using the notation of Brekhovskikh[7] and Spielvogel.[8] We take

$$k^2 = \sigma^2 + \alpha^2 \tag{15}$$

$$K^2 = \sigma^2 + \beta^2 \tag{16}$$

and use

$$\mu K^2 = k^2(2\mu + \lambda) \tag{17}$$

from Equations 5 and 6.

Combined Equations 11 and 13 we have

$$\begin{pmatrix} v_{x1} \\ v_{z1} \\ z_{z1} \\ \frac{1}{2\mu} z_{x1} \end{pmatrix} = A\beta^{-1} \cdot \begin{pmatrix} v_{x2} \\ v_{z2} \\ z_{z2} \\ \frac{1}{2\mu} z_{z2} \end{pmatrix} = a \cdot \begin{pmatrix} v_{x2} \\ v_{z2} \\ z_{z2} \\ \frac{1}{2\mu} z_{x2} \end{pmatrix}$$

we let $\sin\theta = \sigma/k$ and $\sin\gamma = \sigma/k$ so the components of a are

$$a_{11} = 2\sin^2\gamma \cos P + \cos 2\gamma \cos Q \tag{19}$$

$$a_{12} = i(\tan\theta \cos 2\gamma \sin P - \sin 2\gamma \sin Q) \tag{20}$$

$$a_{13} = \frac{\sin\theta}{\rho c} (\cos Q - \cos P) \tag{21}$$

$$a_{14} = -2ib(\tan\theta \sin\gamma \sin P + \sin Q \cos\gamma) \tag{22}$$

$$a_{21} = i\left[\frac{b\cos\theta \sin 2\gamma \sin P}{c \cos\gamma} - \tan\gamma \cos 2\gamma \sin Q\right] \tag{23}$$

$$a_{22} = \cos 2\gamma \cos P + 2\sin^2\gamma \cos Q \tag{24}$$

$$a_{23} = \frac{-i}{\rho c} (\cos\theta \sin P + \tan\gamma \sin\theta \sin Q) \tag{25}$$

$$a_{24} = 2b \sin\gamma (\cos Q - \cos P) \tag{26}$$

$$a_{31} = 2\rho b \sin\gamma \cos 2\gamma \, (\cos Q - \cos P) \tag{27}$$

$$a_{32} = -i\rho \left(c \frac{\cos^2 2\gamma}{\cos\theta} \sin P + 4b \cos\gamma \sin^2\gamma \sin Q \right) \tag{28}$$

$$a_{33} = \cos 2\gamma \cos P + 2 \sin^2\gamma \cos Q \tag{29}$$

$$a_{34} = 2i\rho b^2 \, (\cos 2\gamma \tan\theta \sin P - \sin 2\gamma \sin Q) \tag{30}$$

$$a_{41} = -i \left(\frac{2}{c} \cos\theta \sin^2\gamma \sin P + \frac{\cos^2 2\gamma \sin Q}{2b \cos\gamma} \right) \tag{31}$$

$$a_{42} = \frac{\sin\theta \cos 2\gamma}{c} \, (\cos Q - \cos P) \tag{32}$$

$$a_{43} = \frac{i}{2\rho} \left(\frac{\sin 2\theta \sin P}{c^2} - \frac{\cos 2\gamma \tan\gamma \sin Q}{b^2} \right) \tag{33}$$

$$a_{44} = 2 \sin^2\gamma \cos P + \cos 2\gamma \cos Q \tag{34}$$

The last component of Equation 18 is

$$\frac{1}{2\mu} z_{x_1} = a_{41} v_{x2} + a_{42} v_{z2} + a_{43} z_{z2} + a_{44} z_{x2}/2\mu \tag{35}$$

This equation describes what happens at the glass fluid interface. However, since there can be no transverse stress in the fluid we must also have no transverse stress in the glass at the boundary: $z_{x1} = z_{x2} = 0$. Therefore Equation 35 reduces to

$$a_{41} v_{x2} + a_{42} v_{z2} + a_{43} z_{z2} = 0 \tag{36}$$

Incorporating Equation 36 into Equation 18 we obtain

$$v_{x1} = \left(a_{12} - \frac{a_{11} a_{42}}{a_{41}} \right) v_{z2} + \left(a_{13} - \frac{a_{11} a_{43}}{a_{41}} \right) z_{z2} \tag{37}$$

$$\begin{pmatrix} v_{z1} \\ z_{z1} \end{pmatrix} = \begin{pmatrix} M_1 & M_2 \\ M_3 & M_4 \end{pmatrix} \begin{pmatrix} v_{z2} \\ z_{z2} \end{pmatrix} \tag{38}$$

where

$$M_1 = a_{22} - a_{21}\ a_{42}/a_{41} \tag{39}$$

$$M_2 = a_{23} - a_{21}\ a_{43}/a_{41} \tag{40}$$

$$M_3 = a_{32} - a_{31}\ a_{42}/a_{41} \tag{41}$$

$$M_4 = a_{33} - a_{31}\ a_{43}/a_{41} \tag{42}$$

In a fluid b = 0 and $\gamma = 0$ so to relate v_z and z_z between interfaces 2 and 3 we have analogous to Equation 38:

$$\begin{pmatrix} v_{z2} \\ z_{z2} \end{pmatrix} = \begin{pmatrix} a_{22}' & a_{23}' \\ a_{32}' & a_{33}' \end{pmatrix} \begin{pmatrix} v_{z3} \\ z_{z3} \end{pmatrix} \tag{43}$$

where

$$a_{22}' = \cos P_{LC} \tag{44}$$

$$a_{23}' = \frac{-i \sin P_{LC} \cos\theta_{LC}}{\rho_{LC}\ C_{LC}} \tag{45}$$

$$a_{32}' = \frac{-i\rho_{LC}\ C_{LC} \sin P_{LC}}{\cos\theta_{LC}} \tag{46}$$

$$a_{33}' = \cos P_{LC} \tag{47}$$

where the LC subscript refers to the value of these parameters in the liquid crystal region.

We have for the second glass region:

$$\begin{pmatrix} v_{z3} \\ z_{z3} \end{pmatrix} = \begin{pmatrix} M_1 & M_2 \\ M_3 & M_4 \end{pmatrix} \begin{pmatrix} v_{z4} \\ z_{z4} \end{pmatrix} \tag{48}$$

where the M_i's are given in Equations 39-42.

Equations 38, 43, and 48 combine to give

$$\begin{pmatrix} v_{z1} \\ z_{z1} \end{pmatrix} = \begin{pmatrix} C_1 & C_2 \\ C_3 & C_4 \end{pmatrix} \begin{pmatrix} v_{z4} \\ z_{z4} \end{pmatrix} \tag{49}$$

where

$$\begin{pmatrix} C_1 & C_2 \\ C_3 & C_4 \end{pmatrix} = \begin{pmatrix} M_1 & M_2 \\ M_3 & M_4 \end{pmatrix} \begin{pmatrix} a_{22}' & a_{23}' \\ a_{32}' & a_{33}' \end{pmatrix} \begin{pmatrix} M_1 & M_2 \\ M_3 & M_4 \end{pmatrix} \tag{50}$$

Equation 49 relates the z component of stress and velocity of interface 1, the first interface the incident wave encounters, to interface 4, the final interface of the cell. We may now match the incident wave with interface 1 and the transmitted wave with interface 4 and thereby find the acoustic transmission of the cell. We will change the origin of the coordinate system in Figure 1 so it lies in interface 4 and take the complete cell thickness from 1 to 4 to be H. Then for the initial wave we have

$$\phi_a = \left[\phi_a' \, e^{i\alpha_a(z-H)} + \phi_a'' \, e^{-i\alpha_a(z-H)}\right] e^{-i(\sigma_a x-\omega t)} \tag{51}$$

$$\Psi_a = 0 \tag{52}$$

where ϕ'' is the amplitude of the incident wave and ϕ' the amplitude of the reflected wave. The wave is traveling in the negative z direction.

Similarly for fluid b

$$\phi_b = \phi_b''' \, e^{-i\alpha_b z} \, e^{i(\sigma_a x-\omega t)} \tag{53}$$

for the wave transmitted through the cell. Using Equations 3,4, and 7-10 and omitting the common factor of $e^{i(\sigma x-\omega t)}$ we have

$$v_{xa} = i\sigma_a \left(\phi_a' + \phi_a''\right) \tag{54}$$

$$v_{za} = i\alpha_a \left(\phi_a' - \phi_a''\right) \tag{55}$$

$$z_{xa} = 0 \tag{56}$$

$$z_{za} = -i\omega\rho_a \left(\phi_a' + \phi_a''\right) \tag{57}$$

$$v_{xb} = i\sigma_b \, \phi_b''' \tag{58}$$

$$v_{zb} = i\alpha_b \, \phi_b''' \tag{59}$$

$$z_{zb} = i\omega\rho_b \, \phi_b''' \tag{60}$$

From Equation 49 we have

$$\begin{pmatrix} -\alpha_a \left(\phi_a' - \phi_a''\right) \\ \omega\rho_a \left(\phi_a' + \phi_a''\right) \end{pmatrix} = \begin{pmatrix} C_1 & C_2 \\ C_3 & C_4 \end{pmatrix} \begin{pmatrix} \alpha_b & \phi_b''' \\ \omega\rho_b & \phi_b''' \end{pmatrix} \tag{61}$$

We define the transmission coefficient as

$$D = \rho_b \, \phi_b'''/\rho_a \, \phi_a''' \tag{62}$$

and the reflection coefficient as

$$V = \phi_a'/\phi_a'' \tag{63}$$

Equation 61 provides the means by which these coefficients may be evaluated. To calculate the transmitted acoustic intensity we must evaluate $|D|$. Care must be take in doing so, however. The longitudinal speed in the glass is over three times the speed in the water. Use of Snell's law shows the critical angle for the two types of glass we use occurs at 15 degrees and 15.5 degrees. Similarly, the shear wave speed in the glass is over twice the

longitudinal speed in the water. For the two types of glass we use the critical angle for this type of wave is exceeded at 25.5 and 27 degrees. Therefore, we find three regions for the angle of incidence. A separate equation for the transmission must be found for each region: the region where no critical angle is exceeded, where only the critical angle for the longitudinal wave is exceeded and where both critical angles are exceeded. For example, in the second region taking 0 to be the angle for the compression wave in the glass and θ_a in the water we have from Snell's law

$$\sin\theta = \frac{C \sin\theta_a}{C_a} \qquad \text{so if} \quad \frac{C \sin\theta_a}{C_a} > 1 \quad \text{then}$$

$$\cos\theta \to i\sqrt{\sin^2\theta - 1} \tag{64}$$

$$\sin P \to i \sinh |P| \tag{65}$$

$$\cos P \to \cosh |P| \tag{66}$$

Similarly, if both critical angles are exceeded we must make changes in cos γ, sin Q, and cos Q.

Therfore, certain terms which are real in the matrices for one region will be imaginary in another. Nevertheless we do find for all regions:

$$|D|^2 = \frac{4\omega^2\rho_b^2/\alpha_b^2}{\left[\frac{\omega\rho_b}{\alpha_b}|C_4| + \frac{\omega\rho_a|C_1|}{\alpha_a}\right]^2 + \left[|C_3| + \frac{\omega^2\rho_a\rho_b|C_2|}{\alpha_a\alpha_b}\right]^2} \tag{67}$$

although the form for $|C_i|$ will change for each region.

Equation 67 will be the basis of comparison for the measurements we will make for the amount of ultrasound transmitted through the liquid crystal cell. It should be noted that Equation 67 does not include any damping due to either

viscosity or surface waves in the cell. Furthermore, we have omitted the small anisotropy for the speed of sound which occurs in liquid crystals. The latter simplification appears to be less severe than the former ones.

III. EXPERIMENT

A. Single Layer Verification

To test Equation 67 experimentally, we start with the simple case of a single sheet of glass rather than the liquid crystal cell mentioned above. For this case the $|C_i|$ reduce to the $|M_i|$ of Equations 39-42.

Two Panametrics Model V302 transducers are used for the transmitter and hydrophone. The transmitter is driven by a Hewlett-Packard Model 3312A function generator in the amplitude modulation mode externally modulated by a Hewlett-Packard Model 3310A pulse generator. Pulses were typically 25 μ sec in width containing approximately 20 cycles per pulse. The frequency is measured using a Hewlett-Packard Model 5326A timer/counter. The glass sheet is placed in the center of a water tank 30cm x 40 cm x 60 cm. The acoustic transmitter is located 8 cm from the glass sheet with the hydrophone approximately the same distance on the other side. The glass is suspended by an angular positioning device allowing orientation to the nearest degree to be specified. Initial alignment is facilitated by a laser. The signal from the hydrophone is amplified and sent to both a PAR Model 160 boxcar integrator and Tektronix 564 oscilloscope. For the data on the graphs presented in this section the values are read from the oscilloscope.

The glass sheets are 15 cm x 15 cm x 0.16 cm and 15 cm x 15 cm x 0.0146 cm, respectively. The diameter of both the transmitter and hydrophone are 2.5 cm. By noting the time of the various pulses displayed on the oscilloscope the reflection source may be identified. As the orientation of the glass changes the times between the reflection pulses and main pulse changes. The largest reflected pulse amounts to 10% of the main pulse.

The following constants are used for the thicker glass, longitudinal and shear speeds: 5.61×10^5 cm/sec and 3.32×10^5 cm/sec, respectively, with a

density of 2.54 gm/cm^3. For the thin glass these values are 5.81 x 10^5 cm/sec, 3.48 x 10^5 cm/sec and 2.51 gm/cm^3, respectively. The thicker glass is float glass obtained from PPG Industries. The manufacturer supplied the values of Young's modulus, 1.0 x 10^7 lb/in^2, and the Poisson ratio, 0.23, from which the above acoustic speeds are obtained. The thin glass is obtained from Corning Glass Co. which supplied the shear modulus, 4.4 x 10^6 psi, and Poisson ratio, 0.22, from which the acoustic speeds for the thin glass are calculated.

Figure 2 is a graph of the ratio of the hydrophone voltage with the glass present to that without. The abscissa is the angle between the normal to the glass plate and that of the acoustic beam. The crosses are the experimental values obtained approximately every degree. The solid line is the theoretical result from Equation 67 for $|D|$ using the above constants.

It should be noted that there are no adjustable parameters used in this graph since each constant of Equation 67 is known. There are two peaks of 100% transmission in the theoretical plot at 16.5 degrees and at 35.4 degrees, as well as a dip to zero transmission at 15.9 degrees. Experimentally the crosses in the graph show the upper peak, though shifted to 34.5 degrees and reduced from 100% to 70% transmission. The lower peak and dip are missing, however. These discrepancies are due in part to the finite acceptance angle of the hydrophone. Figure 3 is identical to Figure 2 except each point on the theoretical plot is averaged over the values for 3 degrees on each side. The averaging brings the upper peak down to a maximum of 82.9% and places it at 35.2 degrees as well as greatly reducing the lower peak and almost eliminating the dip. This averaging will be performed in the subsequent graphs.

Figure 4 shows the comparison of theory and experiment for a single sheet of the thin glass. The theory appears to uniformly predict two to three

percent higher transmission than what is realized experimentally, in agreement with Figure 3. Considering we have omitted any dissipation of the sound wave we would expect such a result. A frequency of 0.858 MHz is used for Figures 2 and 3 and 0.857 MHz for Figure 4. For the thicker glass the resulting wavelengths for the longitudinal and shear waves are, respectively, 0.65 cm and 0.39 cm. The ratio of wavelength to glass thickness is 0.25 and and 0.41, respectively. For the thinner glass the longitudinal and shear wavelengths are 0.021 and 0.036, respectively. It is this smaller ratio for the thin glass which makes it suited for the nematic cell exhibiting the acousto-optic effect. We shall see the uniform higher sound transmission allows for a greater light transmission in the acousto-optic effect with less angular sensitivity.

B. Liquid Crystal Cell Investigation

The nematic liquid crystal is 4 - cyano - 4' - n hexyl biphenyl commonly known as K18. The transition temperature for the crystal to nematic phase transition occurs at 14.5° C and the nematic to isotropic transition at 20.4° C. It is obtained from Atomergic Chemetals Corp. and used without further purification.

Each cell is constructed by coating two glass sheets with lecithin to promote homeotropic alignment of the liquid crystal. The coated sides are placed next to one another with 80 μm spacers at the edges. The liquid crystal is then introduced at the glass edges between the spacers and pulled into the cell by capillary action.

After the cell has been filled with the nematic the edges are coated with wax. Epoxy is then applied at all edges. The wax is used to prevent the nematic from reacting chemically with the epoxy. For cells made with the thin glass the cell is mounted in a plexiglass frame for added support.

The acoustic wave for these cells is generated by the method described above or with a Medi Sonar Model 1100 ultrasonic generator. The latter operates at 1 MHz and is used when greater power is required. Intensities of 1.1 Watts/cm^2 may be obtained with this unit.

For measurement of the light transmitted by the acousto-optic effect a 150 Watt lamp is used. Light passes through the liquid crystal cell, a second polarizer with an axis oriented at 90 degrees to the first, and to a photomultiplier. The signal from the photomultiplier is amplified and sent to a digital voltmeter.

Figure 5 shows the ratio of voltage to the hydrophone, with and without the liquid crystal cell, as a function of angle. For Figure 5 the cell is constructed of the thicker glass and an acoustic frequency of 1 MHz is used. The crosses are the experimental ratios and the solid line is the theoretical value of $|D|$ from Equation 67. The details of the program used for the evaluation of Equation 67 is found in Appendix A. The solid points on the graph are for the light intensity in arbitrary units transmitted via the acousto-optic effect.

It would appear the acousto-optic effect is operative when the cell configuration allows maximum transmission of sound. This result appears to explain the results of Letcher, Lebrun and Candau[2] who reported a strong optical signal for only a narrow range of incident angles, 27 to 30 degrees. This result is also in agreement with Nagai, Peters and Candau[3] who found a correlation with experimental acoustic and optical transmission. Equation 67 also explains their results for acoustic transmission versus film thickness, their Figure 7. Also, the broadening of the transmission for thin glass as reported by Lebrun, Candau and Letcher[2] is explained. This result is in disagreement to that of Perbet, Hareng and LeBerre[5] who report an

optical signal for large acoustic reflection. We find no optical signal for large acoustic reflection.

If we conclude that Equation 67 may be used to predict maximum acoustic transmission and therefore maximum transmitted light from the acousto-optic effect it would appear the equation could be used to prescribe how a given cell should be made for a particular acoustic frequency. Or if the cell size is determined by other considerations, Equation 67 could be used to prescribe the acoustic frequency which should be used. For instance, for the thicker glass cell used in Figure 5, assuming an incident angle of zero, Equation 67 is used to determine the acoustic transmission. See Figure 6. The results indicate that an acoustic frequency of around 500 kHz would give the best results.

For Figure 7 the cell was constructed of the thinner glass sheets. Again we see as the acoustic transmission increases more light is transmitted. In comparing Figure 7 with Figure 4 and Figure 5 with Figure 3 we see the difference in the theoretical sound transmission and experimental sound transmission increases as one changes from a single glass sheet to a liquid crystal cell. The increase is reasonable since the means of dissipation has increased. The flows induced in the liquid crystal which give rise to the acousto-optic effect are in fact an added means of dissipation of the acoustic energy.

Another means of dissipation is the surface wave generated. Figure 8 shows a series of photographs for the cell viewed between crossed polarizers. The photographs labeled A to F have the incident acoustic beam at angles 0^{o}, 4^{o}, 12.5^{o}, 15^{o}, -17^{c} (from the right rather than the left), and 33^{o}. The dark circle with the knob on the left in the photographs is the acoustic transmitter. The small tilted rectangle in each picture is a spacer. In each picture vertical lines are shown. In the absence of acoustic waves these

lines disappear. The light transmitted in each line is the result of acoustic streaming in the liquid crystal (i.e. the acousto-optic effect). As the angle of incidence increases the distance between the lines decreases. Figure 9 is a graph of the line spacing as a function of angle. If we imagine a plane wave of incident angle, θ, coming to the cell surface the component, d, of the wavelength along the surface is given by

$$d = \frac{\lambda}{\sin\theta} \tag{68}$$

We would expect a surface wave to be generated and the distance between the lines to be proportional to d. Since for normal incidence Equation (68) shows d to become infinite we generalize the equation to

$$\text{line space} = a/\sin(\theta + b) \tag{69}$$

where a and b are constants. The constant b should result from the divergence of the incident acoustic beam. The continuous curve in Figure 9 is for Equation 69 with a = 1.25 mm and b = 14.38 degrees. Lines similar to these have been reported by Perbet, Hareng, and LeBerre.[5] The angular dependence we observe lends support to their claim that the lines result from surface waves.

From Equations 38, 43, 48, 59, and 60 we find the ratio of v_{z2} to v_{z3},

$$\frac{v_2}{v_3} = \Lambda_1 + \Lambda_2 \frac{\left[M_3 + \frac{\rho_b C_b M_4}{\cos\theta_b}\right]}{\left[M_1 + \frac{\rho_b C_b M_2}{\cos\theta_b}\right]}$$

Since this ratio is complex it contains information concerning the phase. The two surfaces, labeled 2 and 3, are the liquid crystal boundaries. If this phase is 180 degrees we have a peristaltic wave traveling along the liquid crystal layer. If the phase is zero degrees we have an ordinary flexural wave. In Figures 10 and 11 the phase calculated from Equation 70 is plotted as a function of incident acoustic angle for the thick glass and the thin glass cells respectively. Referring to Figure 5 we see there is a significant amount of light from the acousto-optic effect for incident angles in the range of 29 to 33 degrees. From Figure 10 we see the boundaries are out of phase (50 to 140 degrees) in this region giving rise mainly to a peristaltic wave. From Figure 7 we find for the thin glass cell the light intensity increases with angle and from Figure 11 the phase difference becomes smaller with angle to a phase of around 20 degrees at an incident angle of 40 degrees generating mainly a flexural wave. It would appear therefore the important feature giving rise to the acousto-optic effect is the amplitude of vibration for the liquid crystal boundaries as indicated above rather than the relative phase.

It is of interest therefore to see how the angular transmission changes as a function of the acoustic frequency for the cells. Appendix B is a series of graphs which show the theoretical value of $|D|$ from Equation 67 as a function of angle for the thick glass cell. For low frequencies, 100 kHz, for which the ratio of acoustic wavelength to thickness of a single glass plate is about 0.03 the curve is fairly flat with a transmission greater than 50% for all angles less than 60 degrees. As the frequency is increased to 300 kHz the lower angle transmission decreases and a peak appearks at higher angles. The peak becomes narrower at 400 kHz and appears at a lower angle. By 500 kHz a peak has appeared at lower angles, as well,

and is seen to increase in location at 600 kHz. These peaks continue to approach one another and are nearly superimposed at one MHz.

In Appendix C a series for a thin glass cell is presented. For the first graph the frequency is 1.0 MHz which still gives an acoustic wavelength to glass thickness of about 0.03 since the glass is so thin. Again we see a rather flat curve with the transmission above 60% for all angles. At 2 MHz a peak appears and at 3 MHz a second one. At 4 MHz the two peaks have narrowed and merged. The narrowing continues to 8 MHz.

In Figure 12 the theoretical plot of amplitude ratio versus the thickness of the nematic layer is plotted for an acoustic frequency of 1 MHz and zero acoustic incident angle. It would appear from the sound transmission the best thickness for a cell made of the thin glass would occur at 200 micrometers. For higher frequencies the peak occurs at lower thicknesses and is narrower. At 1.9 MHz the peak occurs at 70 micrometers.

In Figure 13 the theoretical amplitude is given as a function of acoustic frequency, for a cell of the thin glass with zero acoustic incident angle. The decrease in ratio above 3 MHz continues up through 8 MHz, as seen in Appendix C. It would appear the best frequency occurs at 1.9 MHz. Therefore, we conclude the best cell for the thin glass and for zero incident acoustic angle would occur for a frequency of 1.9 MHz and find the optimum nematic thickness to be 70 micrometers.

IV. CONCLUSIONS

We have developed an equation to allow evaluation of the acoustic transmission through a liquid crystal cell as a function of incident acoustic angle, frequency and thickness, density and acoustic speeds of the materials in the cell. Although a number of simplifying assumptions are made in the derivation, such as omitting viscous dissipation, we find good agreement between the theoretical prediction and the experimental realization for acoustic transmission. We also find a positive correlation between the maximum acoustic transmission and the maximum sensitivity for the acousto-optic effect. Therefore, the transmission equation may be used to prescribe cell structure and acoustic frequency for the utilization of the acousto-optic effect. Appendices B and C contain examples of how one may use the equation in this way. The maximum acoustic transmission of the cell occurs at those angles where the component of the incident wavelength along the glass surface matches the wavelength of a flexural or peristaltic wave along the glass at the imposed acoustic frequency. Therefore, the maximum acoustic transmission occurs when the liquid crystal boundaries have their largest amplitudes of oscillation. The result is important for the resolution of a visualized acoustic wavefront pattern. To increase the resolution we must not only dampen the lateral flow of the liquid crystal but we must dampen the lateral flexural or peristaltic wave induced in the glass walls. There are several means of inducing such damping. We are presently attempting to increase the cell resolution by increasing the lateral damping.

Acknowledgement- This work was supported by the Office of Naval Research, contract N00014-78-C-0417.

REFERENCES

1. C. Sripaipan, C.F. Hayes and G.T. Fang, Sixth International Liquid Crystal Conference, J-29 (1976).

   C. Sripaipan, C.F. Hayes and G.T. Fang, Phys. Rev. 15A, 1297 (1977).

   K. Miyano and Y.R. Shen, Appl. Phys. Lett. 28, 473 (1976).

   S. Candau, A. Peters and S. Nagai, Sixth International Liquid Crystal Conference, J-30 (1976).

2. S. Letcher, J. Lebrun and S. Candau, J. Acoust. Soc. Am. 63, 55 (1978).

3. S. Nagai, A. Peters and S. Candau, Revue Phys. Appl. 12, 21 (1977).

4. S. Nagai and K. Iizuka, Japan. J. Appl. Phys. 17, 723 (1978).

5. J.N. Perbet, M. Hareng and S. LeBerre, Rev. Phys. Appl. 14, 569 (1979).

6. J. Lebrun, S. Candau, S.V. Letcher, Jour. Phys. C3, 298 (1979).

7. L.M. Brekhovskikh, Waves in Layered Media (Academic, New York, 1960), pp. 56 ff.

8. L.Q. Spielvogel, Jour. Appl. Phys. 42, 3667 (1971).

APPENDIX A

Appendix A contains a program in Basic to give the acoustic transmission through a liquid crystal cell as a function of incident acoustic angle.

```
10 V1=0
20 REM DENSITY R1(H20),    R(GLASS),    R3(L.C.),   R4(AIR OR H20)
30 REM SPEED   C1(H20),  C(GLASS),  B(GLASS),  C3(L.C.),  C4(AIR OR)
40 REM DISTANCE  D1(L.C.),   D2(GLASS)
50 REM ANGLE  V1(H20) = THE INITIAL ANGLE
160 R3=1
170 R4=1
180 R1=1
190 C4=150000
200 F=900000
210 R=2.54
220 C1=150000
230 C=560845
240 B=332216
250 C3=150000
260 D1=.008
270 D2=.0146
300 IF C*SIN(V1)/C1>1 THEN 400
310 GOTO 1000
400 IF B*SIN(V1)/C1>1 THEN 5000
410 GOTO 3000
1000 S8=C*SIN(V1)/C1
1010 S9=B*SIN(V1)/C1
1020 C8=SQRT(1-1*S8^2)
1030 C9=SQRT(1-1*S9^2)
1040 C7=2*C9^2-1
1060 P=2*3.14159*F*D2*C8/C
1070 Q=2*3.14159*F*D2*C9/B
1080 S6=SIN(P)
1090 C6=COS(P)
1100 S5=SIN(Q)
1110 C5=COS(Q)
1120 J1=2*B*C8*S6*S9/C-S9*C7*S5/C9
1130 J2=C7*C6+2*S9^2*C5
1140 J3=-S8*S9*S5/(C*R*C9)-C8*S6/(C*R)
1150 K1=-2*B*R*S9*C7*C6+2*B*R*S9*C7*C5
1160 K2=-4*B*R*S9^2*C9*S5-C*R*C7^2*S6/C8
1170 K3=C7*C6+2*S9^2*C5
1180 L1=-1*C7^2*S5/(2*B*C9)-2*S9^2*C8*S6/C
1190 L2=-S8*C7*C6/C+S8*C7*C5/C
2000 L3=-S9*C7*S5/(2*B^2*R*C9)+S6*S8*C8/(C^2*R)
```

```
2010 M1=J2-J1*L2/L1
2020 M2=J3-J1*L3/L1
2030 M3=K2+K1*L2/L1
2040 M4=K3-K1*L3/L1
2050 T8=C3*SIN(V1)/C1
2060 U8=SQRT(1-T8^2)
2070 P1=2*3.14159*F*D1*U8/C3
2080 A1=COS(P1)
2090 A2=-SIN(P1)*U8/(R3*C3)
2100 A3=-R3*C3*SIN(P1)/U8
2110 A4=A1
2120 E1=-M1*M2*A3-M1*M3*A2-M2*M3*A4+M1*M1*A1
2130 E2=M1*M2*A1+M1*M4*A2+M2*M4*A4-M2*M2*A3
2140 E3=M1*M3*A1+M1*M4*A3+M3*M4*A4-M3*M3*A2
2150 E4=-M2*M3*A1-M2*M4*A3-M3*M4*A2+M4*M4*A4
2160 Z1=R1*C1/COS(V1)
2170 Z4=R4*C4/SQRT(1-1*(C4*SIN(V1)/C1)^2)
2180 T2=4*Z4^2/((Z4*E4+Z1*E1)^2+(E3+Z1*Z4*E2)^2)
2189 T2=SQRT(T2)
2190 PRINT INT(10*V1*180/3.14)/10,T2,TAB(15+50*T2),"*"
2200 V1=V1+3.14159/180
2210 IF V1>70*3.14/180 THEN 8000
2220 GOTO 300
3000 S8=C*SIN(V1)/C1
3010 S9=B*SIN(V1)/C1
3020 C8=SQRT(S8^2-1)
3030 C9=SQRT(1-1*S9^2)
3040 C7=2*C9^2-1
3050 P=2*3.14159*F*D2*C8/C
3060 Q=2*3.14159*F*D2*C9/B
3070 S6=(EXP(P)-EXP(-P))/2
3080 C6=(EXP(P)+EXP(-P))/2
3084 S5=SIN(Q)
3085 C5=COS(Q)
3090 J1=-B*C8*S6*2*S9/C-S9*C7*S5/C9
3100 J2=C7*C6+2*S9^2*C5
3110 J3=-S8*S9*S5/(C*R*C9)+C8*S6/(C*R)
3120 K1=-2*D*R*S9*C7*C6+2*B*R*S9*C7*C5
3130 K2=-4*D*R*S9^2*C9*S5-C*R*C7^2*S6/C8
3140 K3=C7*C6+2*S9^2*C5
3150 L1=-1*C7^2*S5/(2*D*C9)+2*S9^2*C8*S6/C
3160 L2=-S8*C7*C6/C+S8*C7*C5/C
3170 L3=-S9*C7*S5/(2*D^2*R*C9)-S6*S8*C8/(C^2*R)
3180 GOTO 2010
```

```
5000 S8=C*SIN(V1)/C1
5010 S9=B*SIN(V1)/C1
5020 C8=SQRT(S8^2-1)
5030 C9=SQRT(S9^2-1)
5040 C7=-2*C9^2-1
5050 P=2*3.14159*F*D2*C8/C
5060 Q=2*3.14159*F*D2*C9/B
5070 S6=(EXP(P)-EXP(-P))/2
5080 C6=(EXP(P)+EXP(-P))/2
5090 S5=(EXP(Q)-EXP(-Q))/2
5100 C5=(EXP(Q)+EXP(-Q))/2
5110 J1=-B*C8*S6*2*S9/C-S9*C7*S5/C9
5120 J2=C7*C6+2*S9^2*C5
5130 J3=-S8*S9*S5/(C*R*C9)+C8*S6/(C*R)
5140 K1=-2*B*R*S9*C7*C6+2*B*R*S9*C7*C5
5150 K2=4*B*R*S9^2*C9*S5-C*R*C7^2*S6/C8
5160 K3=C7*C6+2*S9^2*C5
5170 L1=-1*C7^2*S5/(2*B*C9)+2*S9^2*C8*S6/C
5180 L2=-S8*C7*C6/C+S8*C7*C5/C
5190 L3=-S9*C7*S5/(2*B^2*R*C9)-S6*S8*C8/(C^2*R)
5200 GOTO 2010
8000 END
```

APPENDIX B

Appendix B contains the computer print-out for the acoustic transmission as a function of angle for a liquid crystal cell using glass 1.6 mm thick and a liquid crystal layer 0.08 mm thick. The frequencies used vary from 100 kHz to 1 MHz.

```
RUN

FREQUENCY =  100000
ANGLE   SQ.ROOT T2
 0 .53031519
 2 .53049074
 4 .53101764
 6 .5318928
 8 .53310191
 10 .53458961
 12 .53614786
 14 .53671979
 16 .50364879
 18 .55621914
 20 .55744664
 22 .56194362
 24 .5678085
 26 .57475542
 28 .58273586
 30 .59176335
 32 .60187158
 34 .61309946
 36 .62548237
 38 .63904676
 40 .65380648
 42 .66976124
 44 .68688188
 46 .70511943
 48 .7243843
 50 .74456355
 52 .7654945
 54 .7869849
 56 .80879108
 58 .83065597
```

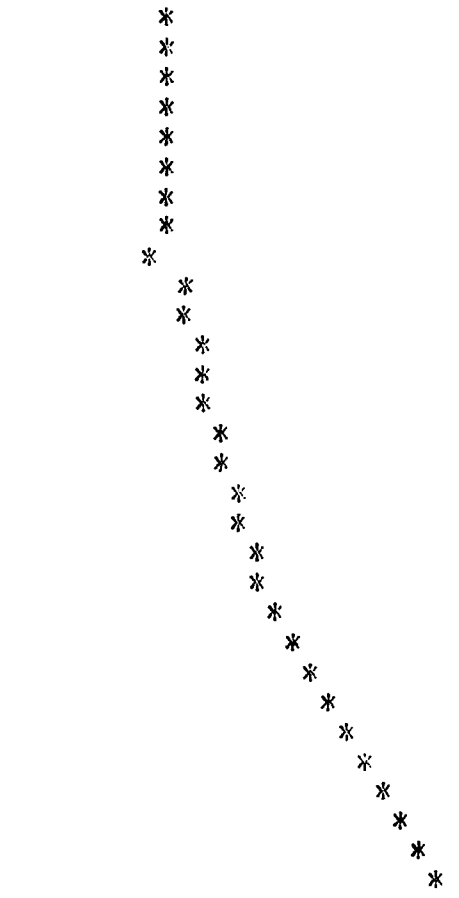

FREQUENCY = 200000

ANGLE	SQ.ROOT T2
0	.34651734
2	.34652966
4	.34656605
6	.34661781
8	.34664528
10	.34650293
12	.34565976
14	.34146675
16	.26142596
18	.3775428
20	.37185871
22	.37389204
24	.37855748
26	.38512721
28	.39352561
30	.40387373
32	.41638878
34	.43135173
36	.44909945
38	.47001909
40	.49453893
42	.52311694
44	.55619384
46	.59413948
48	.63713051
50	.68497456
52	.73688352
54	.79120591
56	.84526676
58	.89552709

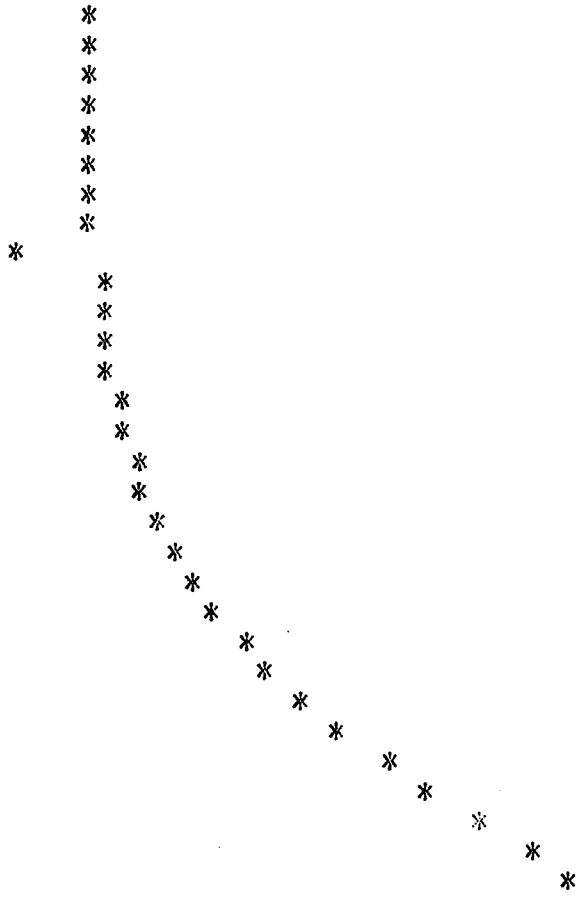

FREQUENCY = 300000

ANGLE	SQ.ROOT T2
0	.32365379
2	.32349096
4	.32298899
6	.32209405
8	.32066008
10	.31828903
12	.31372772
14	.30122937
16	.15743477
18	.37393455
20	.35301396
22	.349408
24	.35052289
26	.35454088
28	.36123751
30	.37090848
32	.38415687
34	.40186889
36	.4252746
38	.45605482
40	.49648752
42	.54959308
44	.61903527
46	.70804023
48	.81524999
50	.92433679
52	.99392697
54	.98251658
56	.90117879
58	.79729963

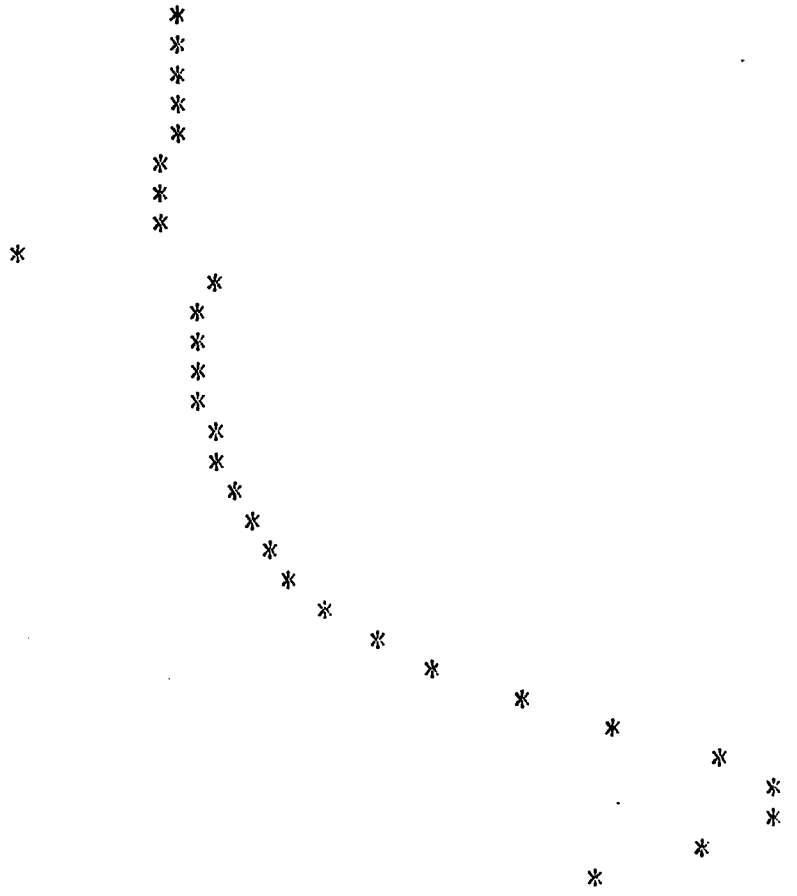

```
FREQUENCY =  400000
ANGLE    SQ.ROOT T2
 0 .44575546                          *
 2 .44550411                          *
 4 .4446042                           *
 6 .44258774                          *
 8 .43854122                         *
 10 .43071006                        *
 12 .41496347                       *
 14 .37567037                    *
 16 9.9410913E-02  *
 18 .57428437                              *
 20 .49033762                         *
 22 .45981837                         *
 24 .44093094                         *
 26 .42797399                        *
 28 .42019843                        *
 30 .41826343                       *
 32 .42357769                        *
 34 .43836952                        *
 36 .4661941                          *
 38 .51296621                          *
 40 .58873302                              *
 42 .7088387                                   *
 44 .87912815                                        *
 46 .99979624                                             *
 48 .87226826                                        *
 50 .64427637                                  *
 52 .47698099                          *
 54 .37026756                    *
 56 .30125195                  *
 58 .25502811              *
```

FREQUENCY = 500000

ANGLE	SQ.ROOT T2
0	.9975715
2	.99701681
4	.99530841
6	.99285562
8	.99154948
10	.99454156
12	.99999471
14	.94080152
16	6.2643351E-02
18	.86642261
20	.99819855
22	.9556492
24	.83643918
26	.71178303
28	.61440708
30	.54968327
32	.51535038
34	.51080818
36	.54167181
38	.62599924
40	.80105178
42	.99890843
44	.75957952
46	.45576596
48	.296223
50	.21062089
52	.16009318
54	.12793822
56	.10637034
58	.09137821

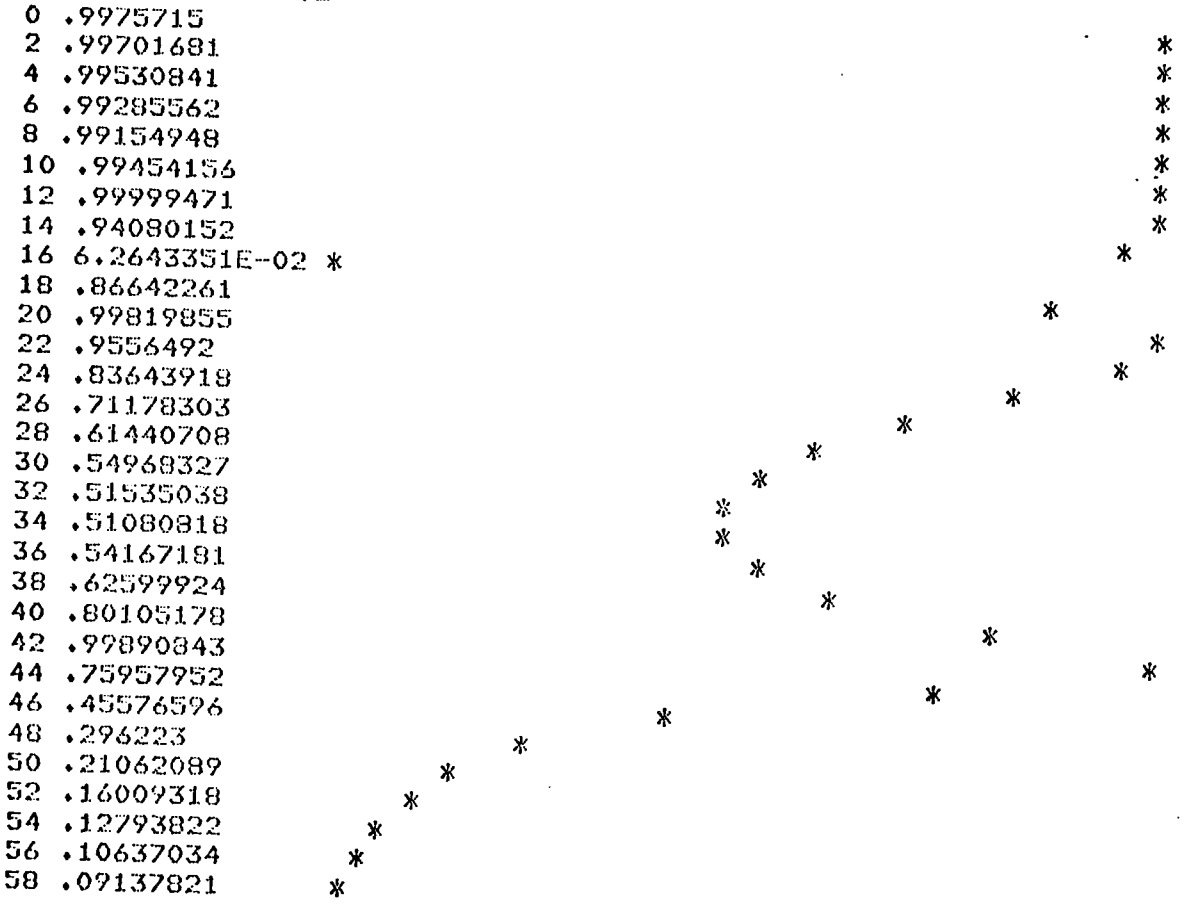

FREQUENCY = 600000

ANGLE	SQ.ROOT T2
0	.30500073
2	.30179229
4	.29326018
6	.28215715
8	.2718099
10	.26538554
12	.26626798
14	.28324073
16	3.8622229E-02
18	.30400601
20	.36175208
22	.46167116
24	.63904649
26	.90453746
28	.97731108
30	.78256852
32	.6412908
34	.59504245
36	.64279457
38	.83487677
40	.95840298
42	.80310603
44	.26612626
46	.16407183
48	.11207212
50	8.2105742E-02
52	6.3350093E-02
54	5.0914309E-02
56	4.2331909E-02
58	3.6242261E-02

```
FREQUENCY =  700000
ANGLE    SQ.ROOT T2
 0 .14614023           *
 2 .14398759           *
 4 .13934244          *
 6 .1310977           *
 8 .12417377          *
 10 .11882437        *
 12 .11532526        *
 14 .1114234         *
 16 3.6084021E-02*
 18 .17296716           *
 20 .18446955            *
 22 .22275625              *
 24 .29682343                *
 26 .4481302                       *
 28 .77005966                                *
 30 .98714771                                          *
 32 .76241145                                *
 34 .67384193                            *
 36 .79491955                                *
 38 .95902435                                        *
 40 .41070682                      *
 42 .19101633            *
 44 .10856379        *
 46 6.9545699E-02 *
 48 .04819727     *
 50 3.5364793E-02*
 52 .02713297    *
 54 2.1596886E-02*
 56 1.7743446E-02*
 58 .01499378   *
```

FREQUENCY = 800000

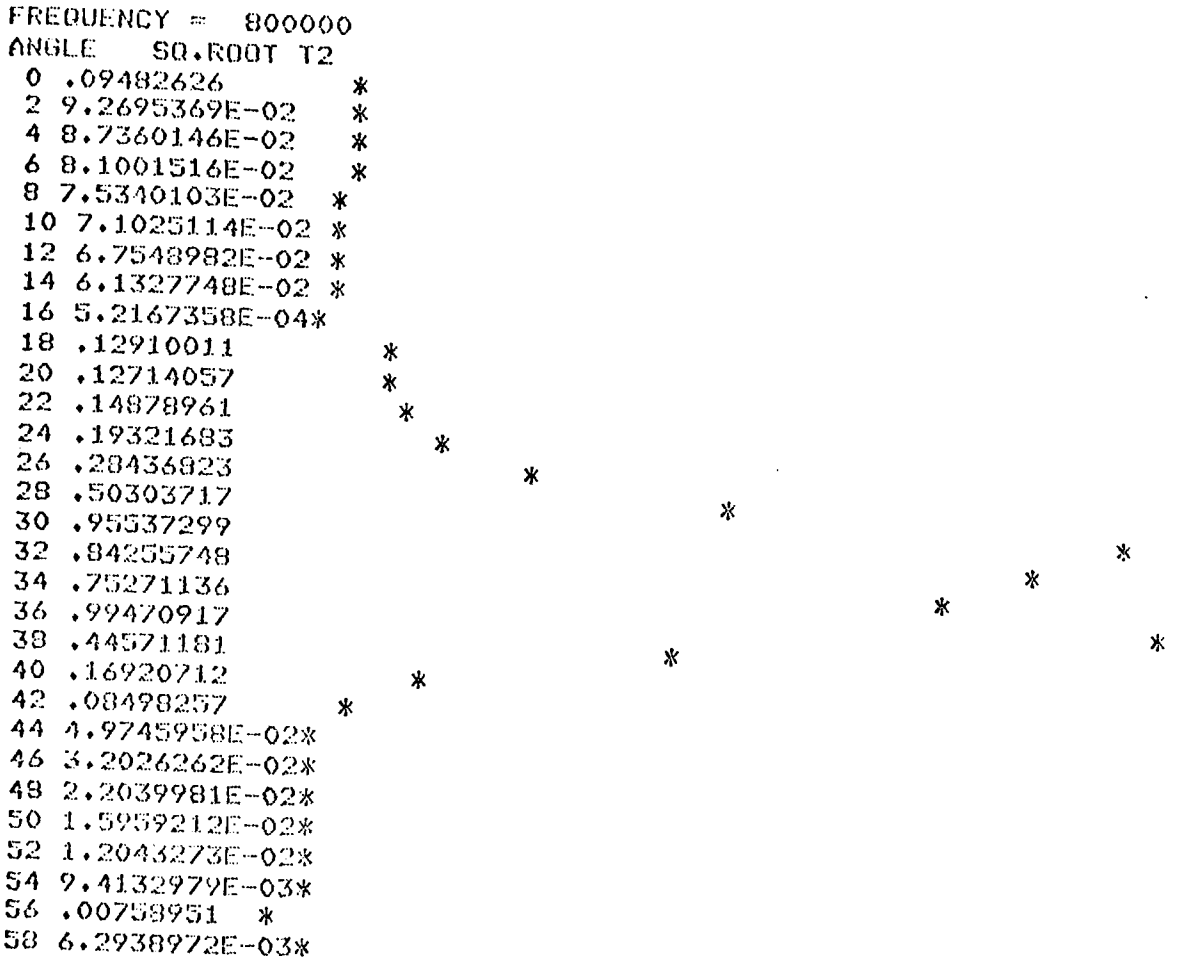

```
RUN

FREQUENCY =  1000000
ANGLE   SQ.ROOT T2
 0 .062             *
 2 .054            *
 4 .044            *
 6 .039           *
 8 .037           *
 10 .035          *
 12 .034          *
 14 .027          *
 16 .012         *
 18 .119              *
 20 .097            *
 22 .107              *
 24 .133               *
 26 .188                   *
 28 .331                        *
 30 .795                                                  *
 32 .895                                                     *
 34 .992                                                        *
 36 .312                        *
 38 .094             *
 40 .04            *
 42 .021          *
 44 .012         *
 46 .007         *
 48 .004         *
 50 .003         *
 52 .002         *
 54 .001         *
 56 .001         *
 58 .001         *
```

APPENDIX C

Appendix C contains the computer print-out for the acoustic transmission as a function of angle for a liquid crystal cell using glass 0.146 mm thick and a liquid crystal layer 0.08 mm thick. The frequencies used vary from 1 MHz to 8 MHz.

```
RUN

FREQUENCY =  1000000
ANGLE    SQ.ROOT T2
 0  .697
 2  .697
 4  .697
 6  .697
 8  .697
 10  .697
 12  .697
 14  .694
 16  .724
 18  .705
 20  .705
 22  .706
 24  .708
 26  .711
 28  .714
 30  .718
 32  .722
 34  .728
 36  .734
 38  .742
 40  .75
 42  .759
 44  .77
 46  .781
 48  .793
 50  .807
 52  .821
 54  .835
 56  .851
 58  .866
```

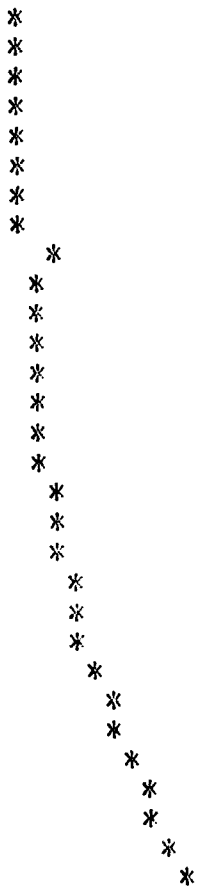

FREQUENCY = 2000000

ANGLE	SQ.ROOT T2
0	.855
2	.856
4	.86
6	.867
8	.877
10	.889
12	.906
14	.928
16	.903
18	.953
20	.974
22	.99
24	.998
26	.998
28	.988
30	.968
32	.942
34	.912
36	.882
38	.856
40	.834
42	.818
44	.809
46	.808
48	.813
50	.825
52	.844
54	.867
56	.893
58	.92

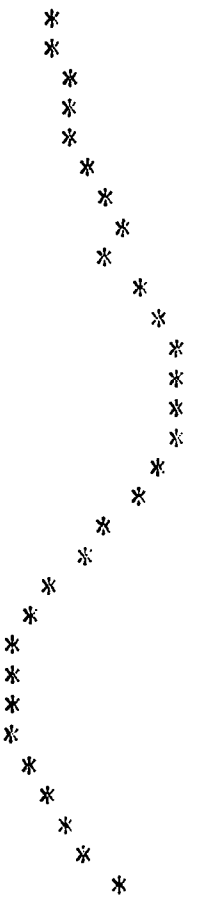

FREQUENCY = 3000000

ANGLE	SQ.ROOT T2
0	.158
2	.159
4	.159
6	.16
8	.161
10	.163
12	.165
14	.167
16	.208
18	.194
20	.204
22	.22
24	.243
26	.274
28	.317
30	.378
32	.462
34	.58
36	.732
38	.89
40	.986
42	.995
44	.964
46	.94
48	.94
50	.962
52	.99
54	.998
56	.96
58	.881

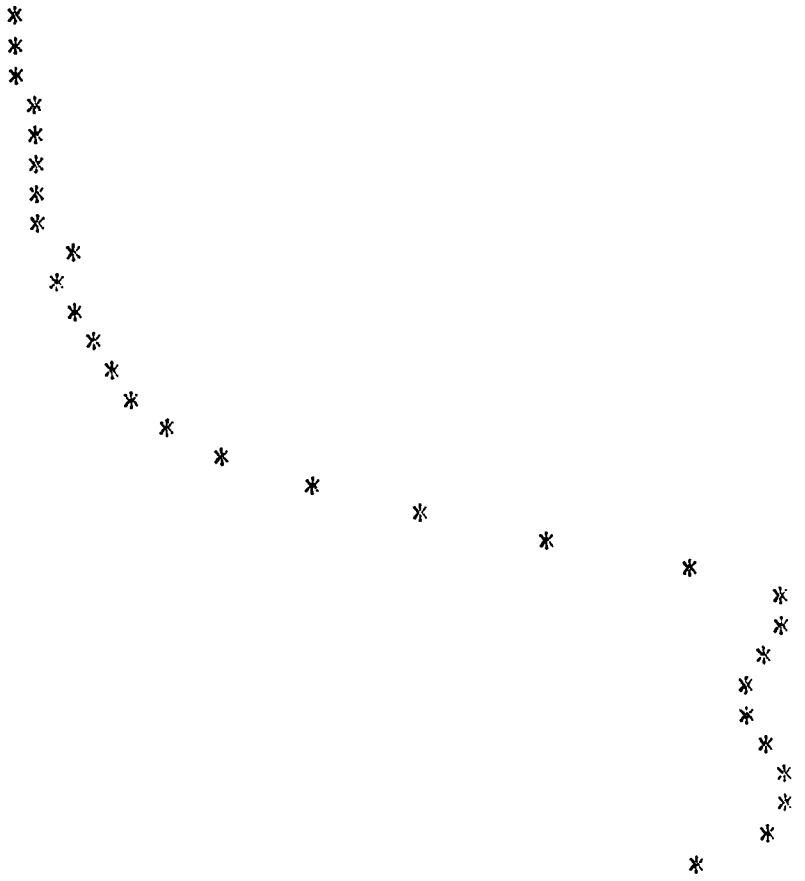

FREQUENCY = 4000000

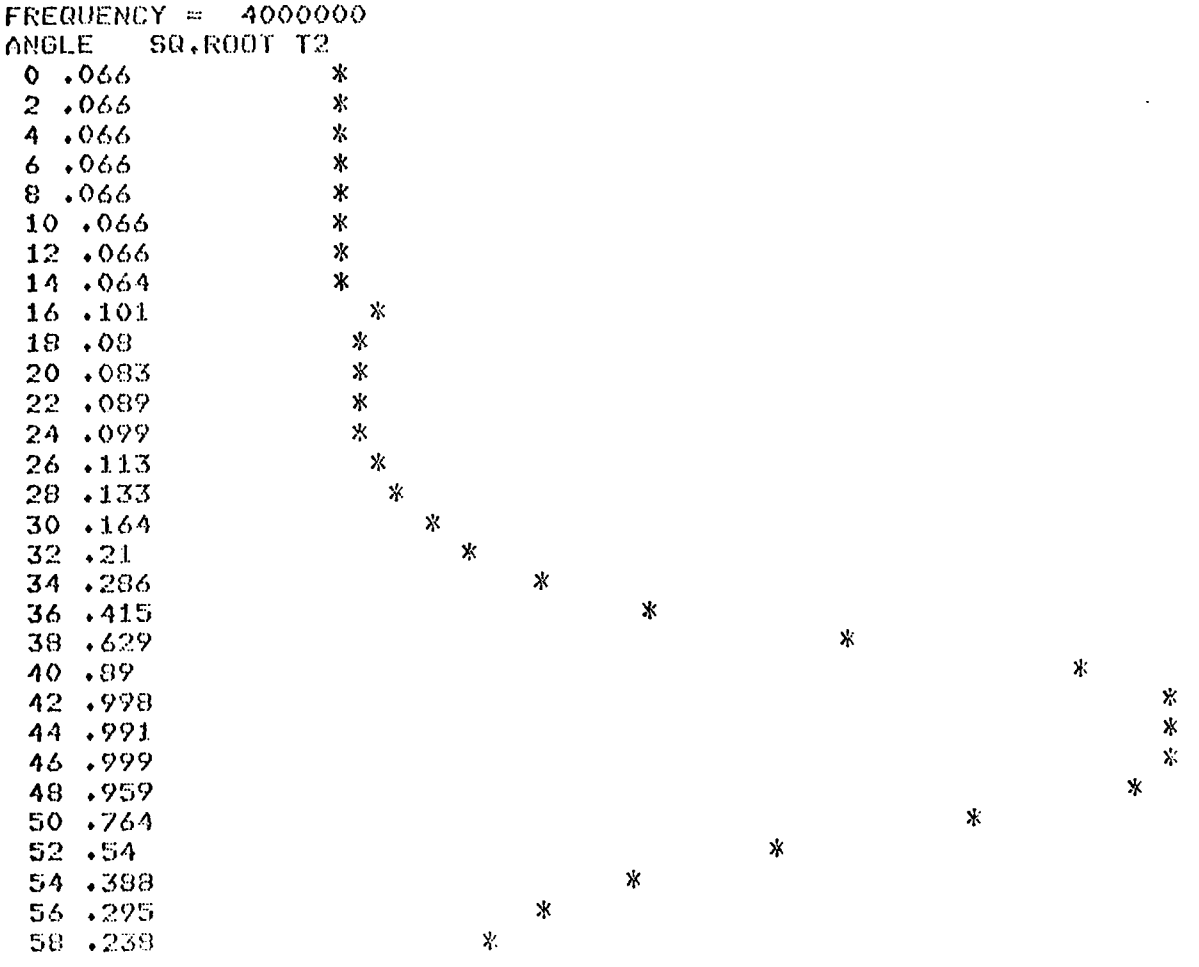

FREQUENCY = 5000000

ANGLE	SQ.ROOT T2
0	.041
2	.041
4	.04
6	.04
8	.04
10	.039
12	.038
14	.036
16	.077
18	.05
20	.051
22	.055
24	.061
26	.072
28	.087
30	.111
32	.152
34	.227
36	.381
38	.694
40	.979
42	.999
44	.924
46	.567
48	.311
50	.191
52	.131
54	.098
56	.078
58	.066

FREQUENCY = 6000000

ANGLE	SQ.ROOT T2
0	.033
2	.033
4	.032
6	.031
8	.031
10	.03
12	.029
14	.026
16	.08
18	.04
20	.04
22	.044
24	.049
26	.058
28	.073
30	.098
32	.144
34	.244
36	.501
38	.944
40	.999
42	.752
44	.316
46	.154
48	.09
50	.06
52	.043
54	.033
56	.027
58	.023

```
FREQUENCY =  7000000
ANGLE    SQ.ROOT T2
 0  .033          *
 2  .033          *
 4  .032          *
 6  .031          *
 8  .03           *
 10  .029         *
 12  .027         *
 14  .023         *
 16  .116             *
 18  .041          *
 20  .04           *
 22  .043          *
 24  .048          *
 26  .058          *
 28  .074           *
 30  .104            *
 32  .166              *
 34  .329                  *
 36  .812                                  *
 38  .994                                                *
 40  .781                                 *
 42  .255                    *
 44  .108            *
 46  .058          *
 48  .036         *
 50  .024         *
 52  .018        *
 54  .013        *
 56  .011        *
 58  .009        *
```

FREQUENCY = 8000000

ANGLE	SQ.ROOT T2
0	.046
2	.045
4	.044
6	.042
8	.039
10	.036
12	.033
14	.025
16	.277
18	.055
20	.051
22	.053
24	.059
26	.069
28	.089
30	.128
32	.221
34	.529
36	.924
38	.979
40	.349
42	.112
44	.051
46	.028
48	.017
50	.012
52	.008
54	.006
56	.005
58	.004

Figure 1 gives the coordinate system for the liquid crystal cell. The origin is at the first glass-liquid crystal interface for the initial matrix calculation and is moved for the final matrix calculation to the lower glass-fluid B interface.

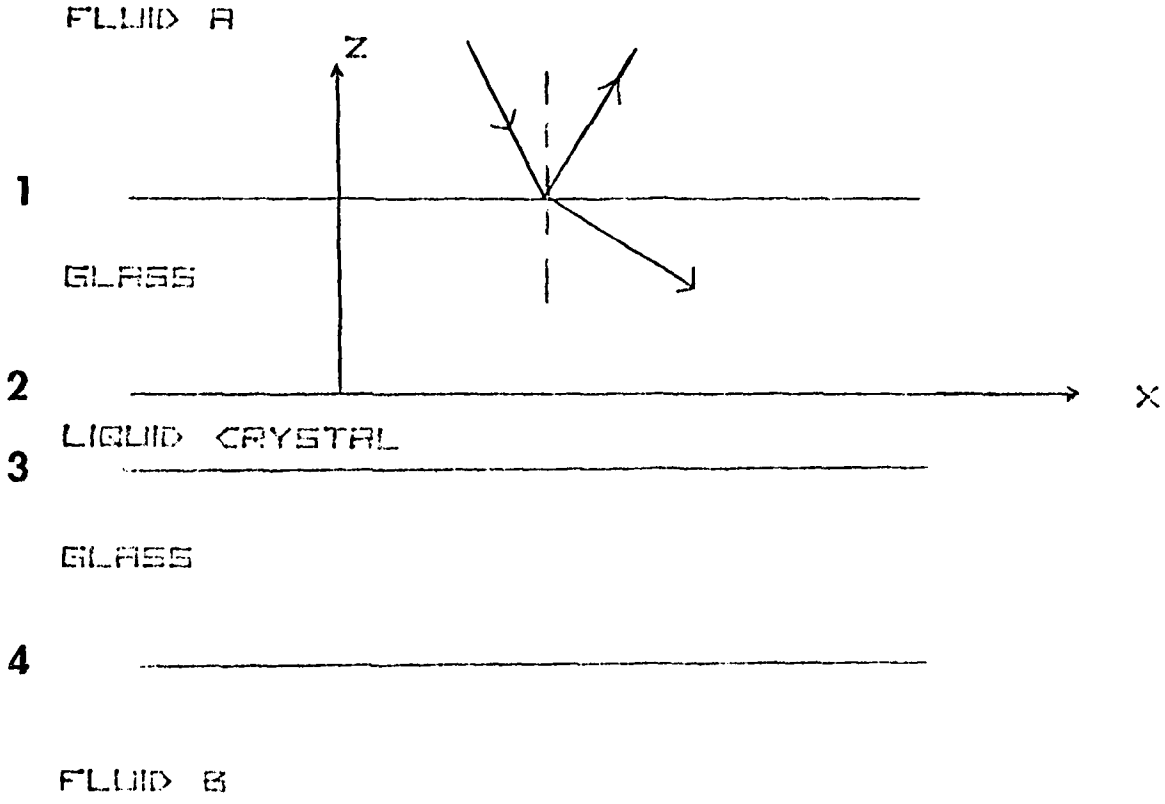
FLUID A
Z
1
GLASS
2
X
LIQUID CRYSTAL
3
GLASS
4
FLUID B

Figure 2 is a graph of the ratio of voltages from the hydrophone with and without a single sheet of 1.6 mm thick glass as a function of angle. Therefore, this graph shows the acoustic transmission of the glass as a function of angle. The crosses are experimental points. The solid line is from Equation 67 for $|D|$. Since each factor in the equation is measured there are no adjustable parameters used to induce the fit. Therefore, the graph represents a severe testing of the theory. For this graph the thicker glass cell is used and a frequency of 0.858 MHz. No correction is made for the finite acceptance angle of the hydrophone.

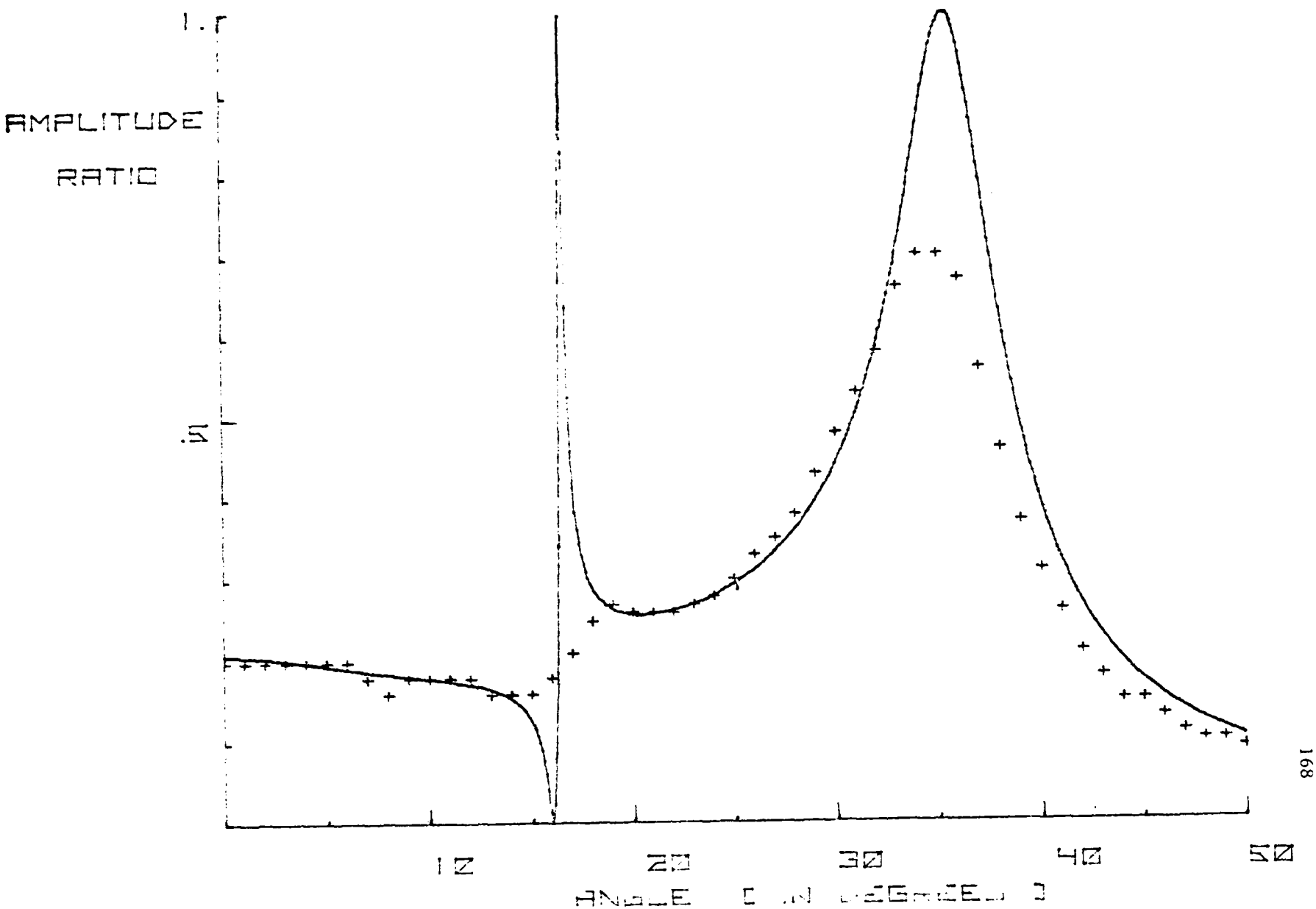
AMPLITUDE
RATIO
1.0
.5
10
20
30
40
50
ANGLE [IN DEGREES]

Figure 3 is identical to Figure 2 only correction is made for the finite acceptance angle of the hydrophone.

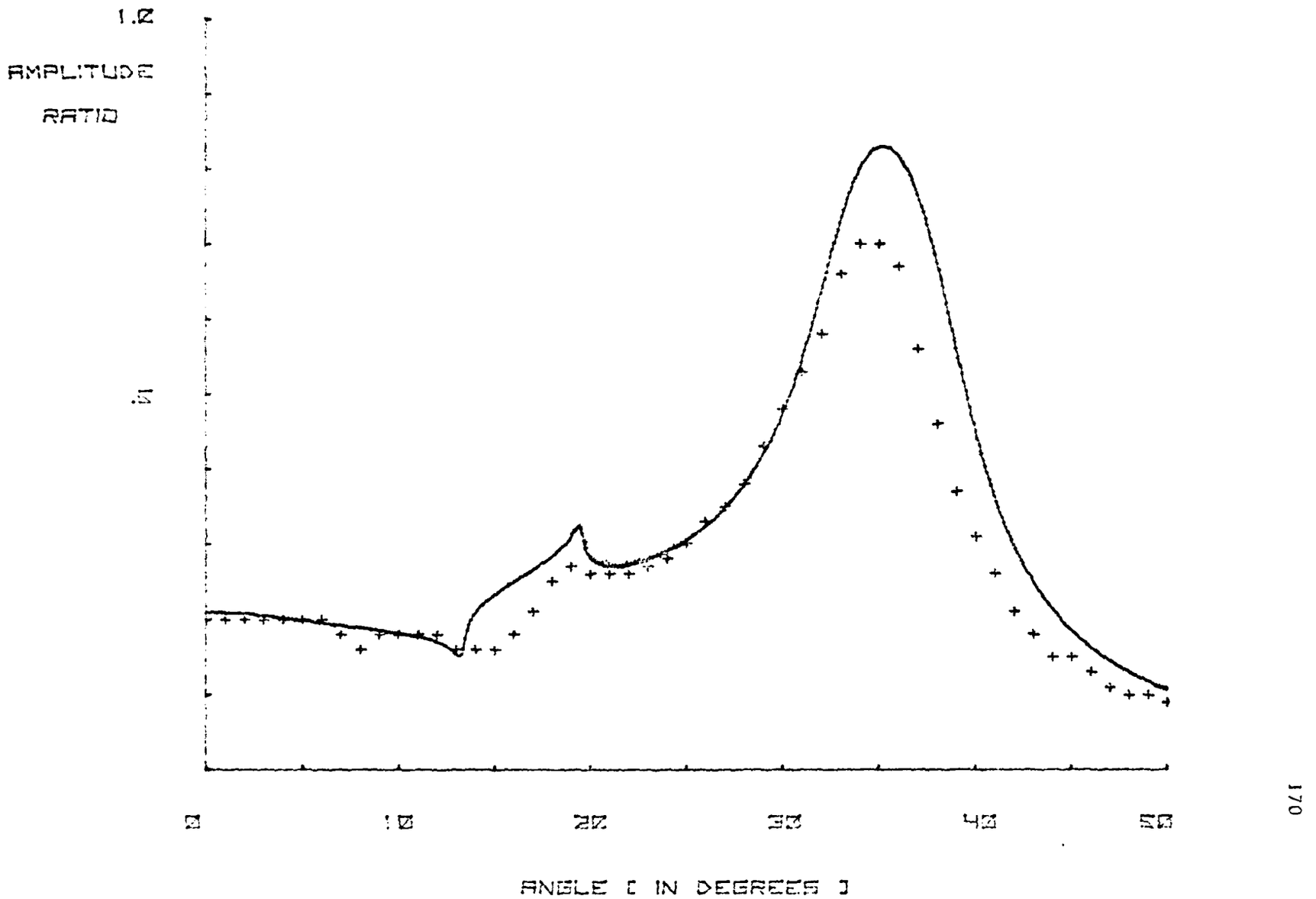
1.0
AMPLITUDE
RATIO
.5
0
10
20
30
40
50
ANGLE (IN DEGREES)

Figure 4 is a graph of the ratio of voltages from the hydrophone with and without a single sheet of 0.146 mm thick glass as a function of angle. The frequency is 0.857 MHz.

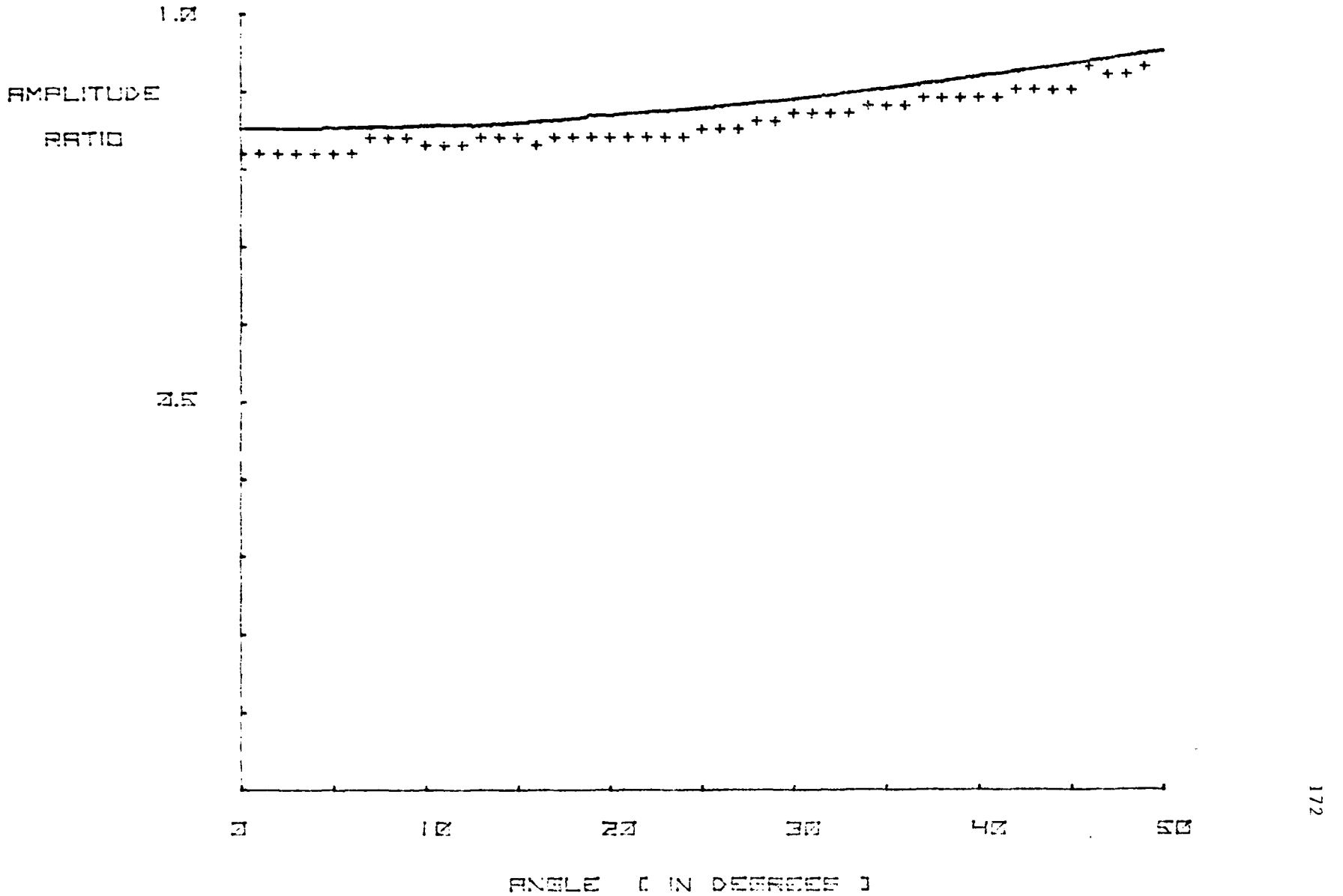
1.0
AMPLITUDE
RATIO
0.5
0
10
20
30
40
50
ANGLE [IN DEGREES]

Figure 5 is a graph of acoustic transmission through a liquid crystal cell made of the 1.6 mm thick glass as a function of incident acoustic angle. The acoustic transmission is measured as the ratio of voltage from the hydrophone with and without the presence of the liquid crystal cell. The solid line is the theoretical value of $|D|$ from Equation 67. The crosses are the measured values of acoustic transmission. The filled circles are measured values of transmitted light intensity via the acousto-optic effect using arbitrary linear units. It should be noted that the maximum light intensity occurs at the incident angle for maximum acoustic transmission.

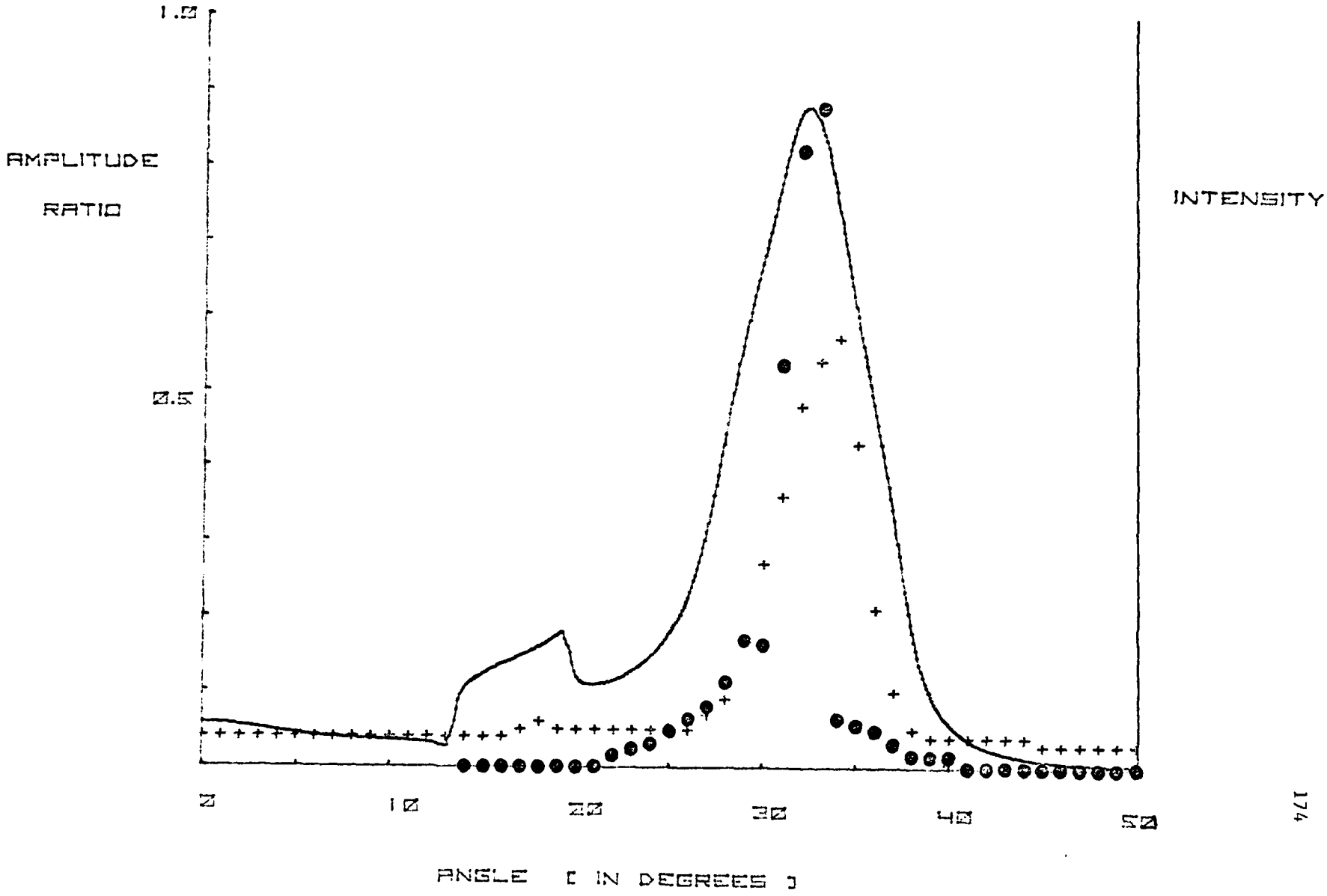
1.0
0.5
AMPLITUDE
RATIO
INTENSITY
0
10
20
30
40
50
ANGLE (IN DEGREES)

Figure 6 is a graph of acoustic transmission as a function of acoustic frequency. The solid line is the theoretical value from Equation 67. The crosses are the experimental values. There are no adjustable parameters used to induce the fit since each parameter in Equation 67 is known or measured. A liquid crystal cell made of 1.6 mm thick glass is used for these results.

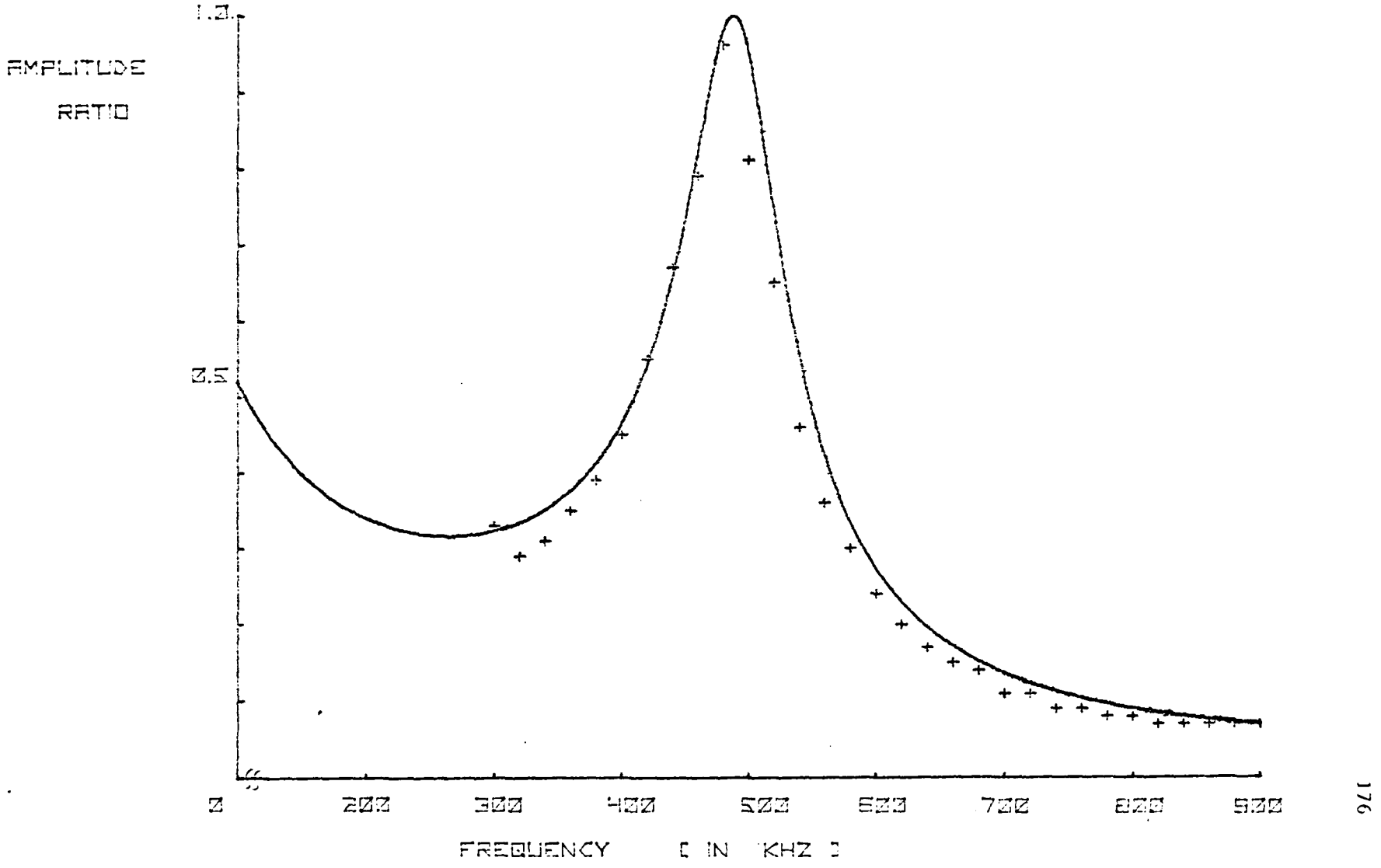
AMPLITUDE
RATIO
1.0
0.5
0
200
300
400
500
600
700
800
900
FREQUENCY (IN KHZ)

Figure 7 is similar to Figure 5 only the liquid crystal cell is constructed of thinner glass, 0.0146 mm thick. The filled circles represent measured values of transmitted light intensity via the acousto-optic effect.

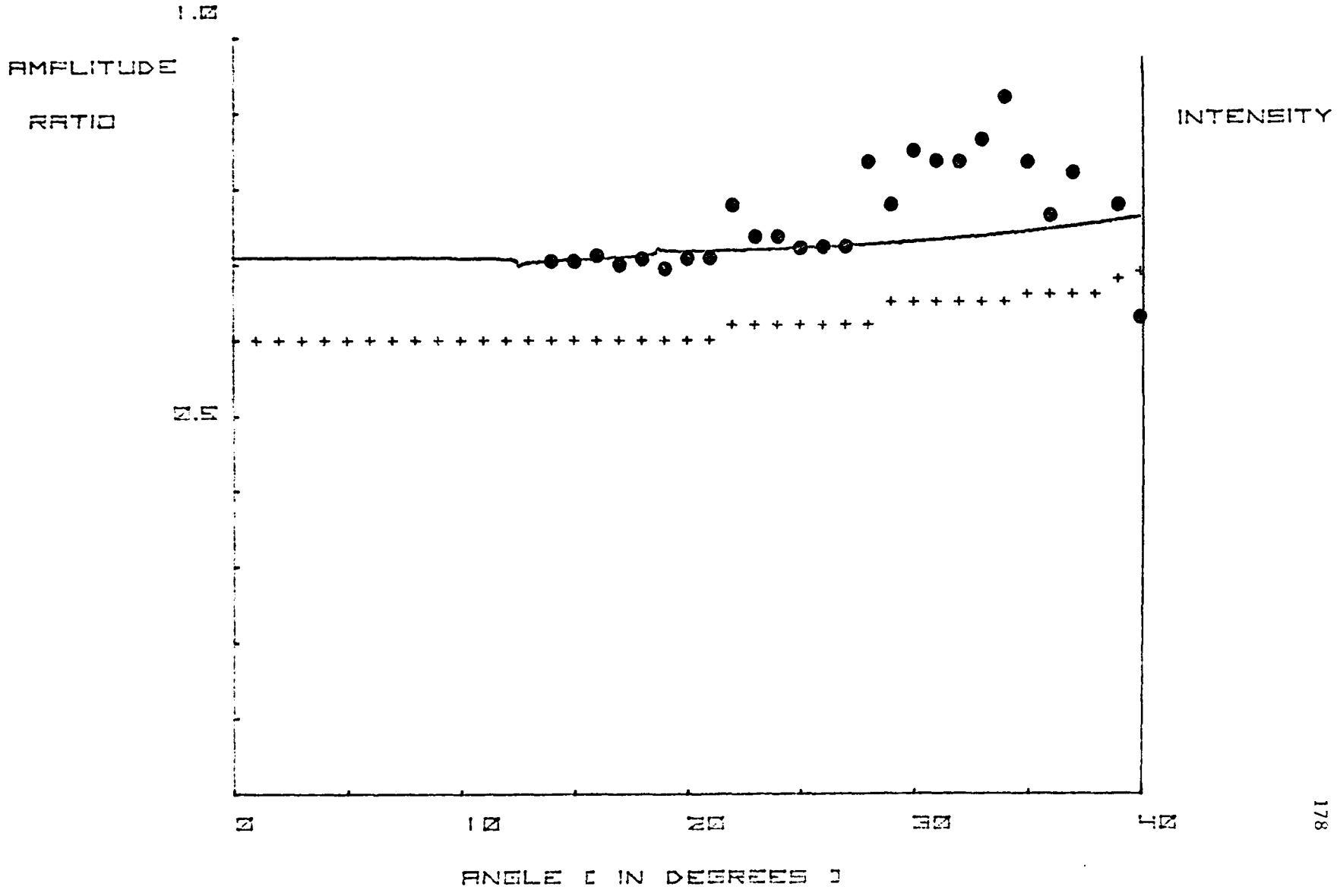
1.0
AMPLITUDE
RATIO
INTENSITY
0.5
0
10
20
30
40
ANGLE (IN DEGREES)

Figure 8 is a series of pictures of the liquid crystal while excited by an ultrasonic wave. The spacing between the resulting vertical lines is seen to decrease with increasing acoustic angle. The angle of incidence for each picture is:

A. zero degrees
B. four degrees
C. twelve and one half degrees
D. fifteen degrees
E. negative seventeen degrees (from the right rather than left)
F. thirty three degrees

A

B

C

D

E

F

Figure 9 is a graph of the distance between the lines such as those shown in Figure 8 as a function of incident angle. The solid line is the fit from Equation 69.

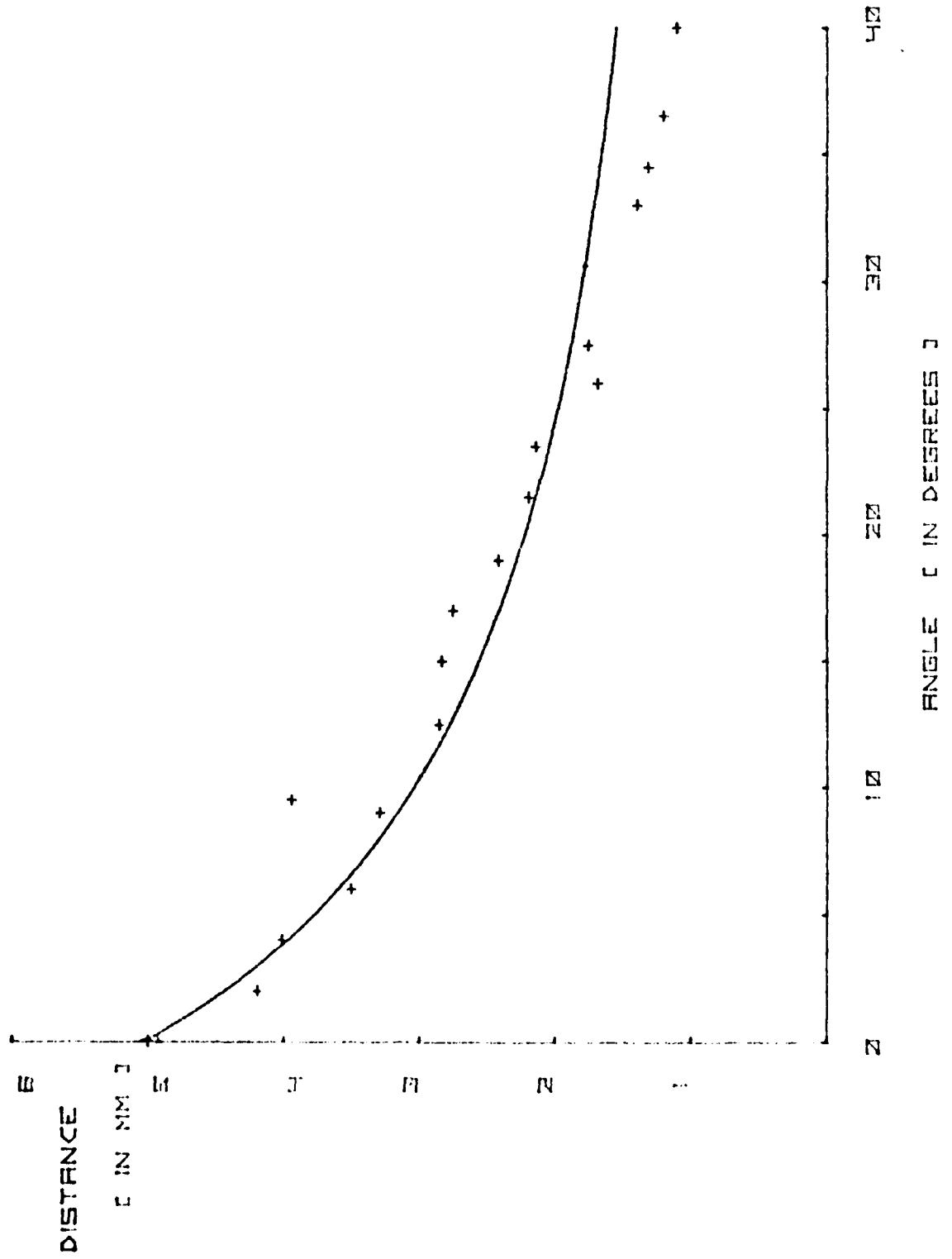
DISTANCE
ANGLE

Figure 10 is a graph of the phase angle of one liquid crystal glass surface with respect to the other versus incident wave angle for a liquid crystal cell constructed of 1.6 mm thick glass. Equation 70 is used for these values.

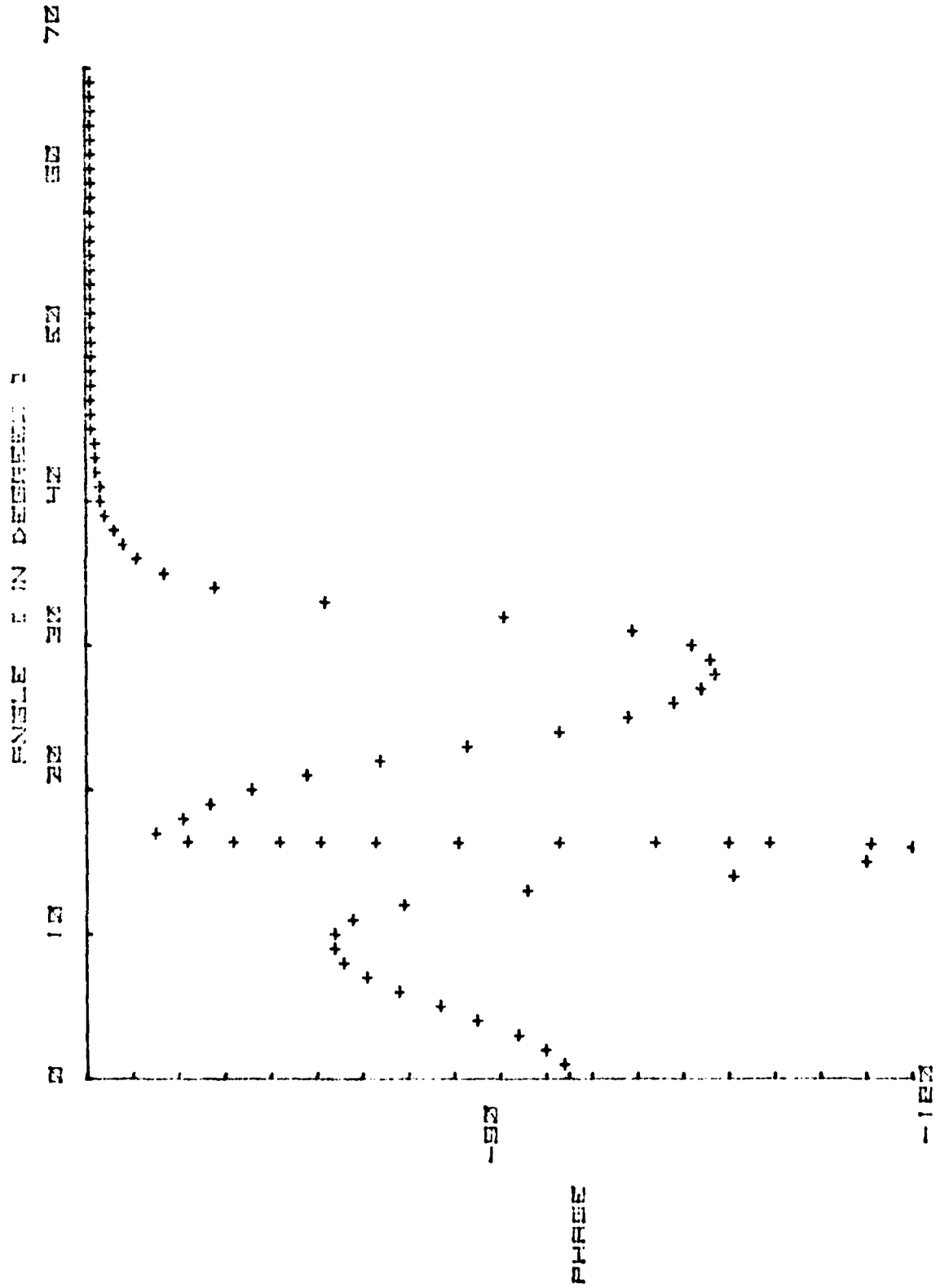
ANGLE IN DEGREES
PHASE

Figure 11 is similar to Figure 10 only for a cell made with 0.0146 mm thick glass.

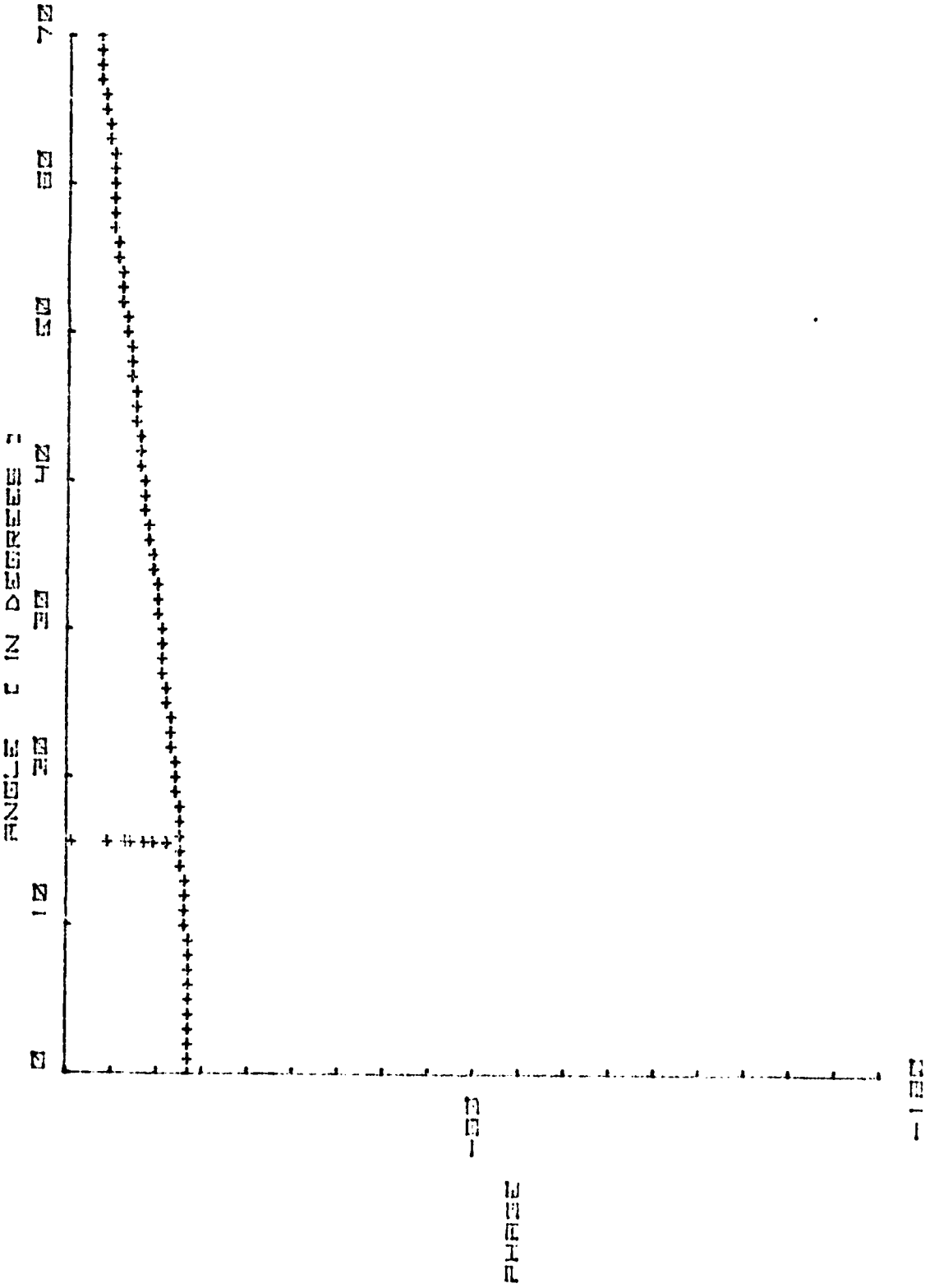
ANGLE U IN DEGREES
0
15
30
45
60
75
TIME

Figure 12 is a graph of acoustic transmission from Equation 67 as a function of liquid crystal layer thickness for a cell of 1.5 mm thick glass. A frequency of 1 MHz and incident angle of zero degrees is used.

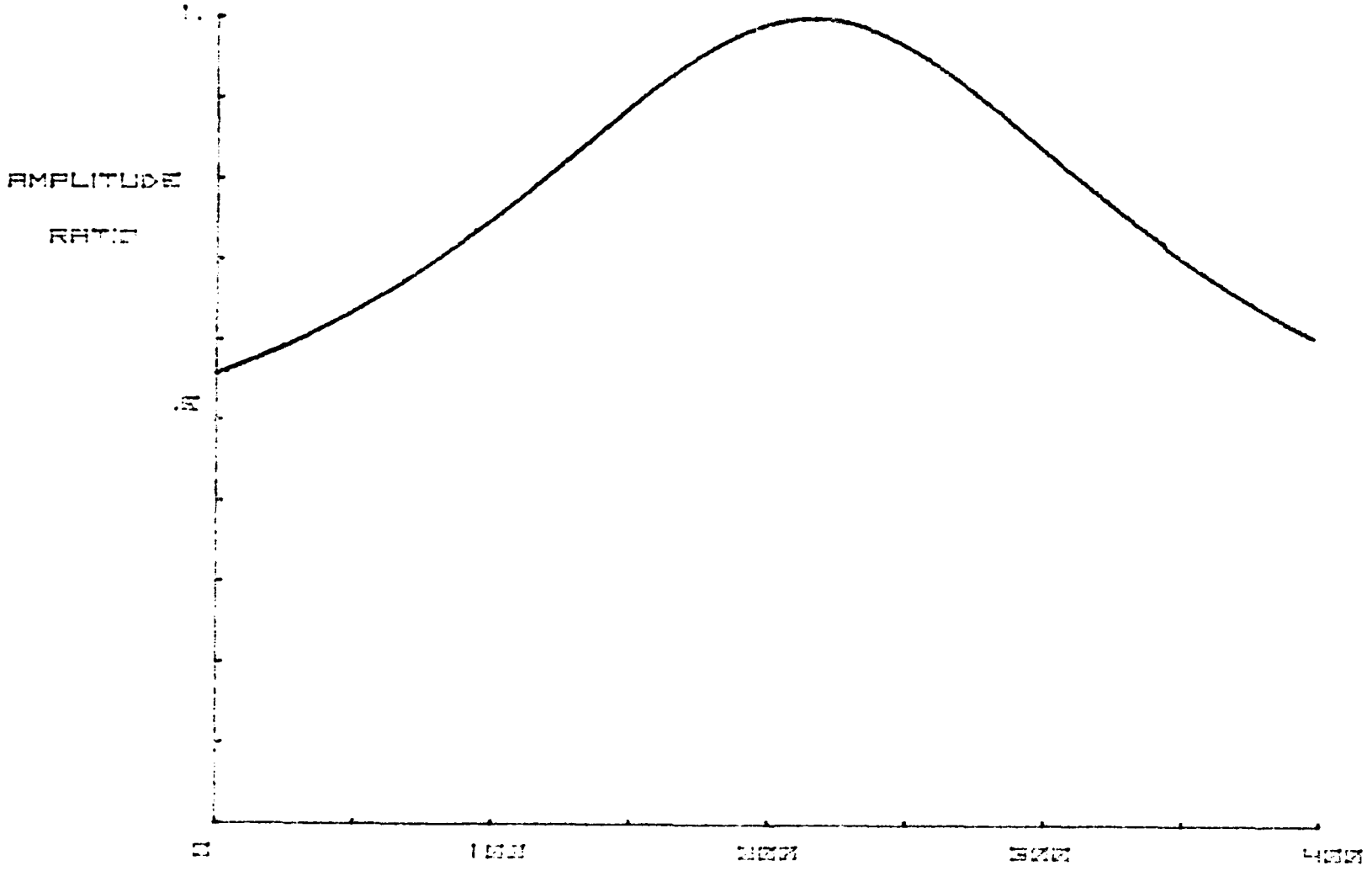

NEMATIC THICKNESS [IN MICROMETERS]

Figure 13 is the acoustic transmission for a cell made with 0.0146 mm thick glass versus frequency.

AD-A094 782 HAWAII UNIV HONOLULU DEPT OF PHYSICS AND ASTRONOMY F/G 20/6
A STUDY OF THE ACOUSTIC-OPTIC EFFECT IN NEMATICS.(U)
DEC 80 C F HAYES N00014-78-C-0417
UNCLASSIFIED 004 NL

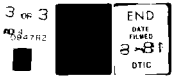

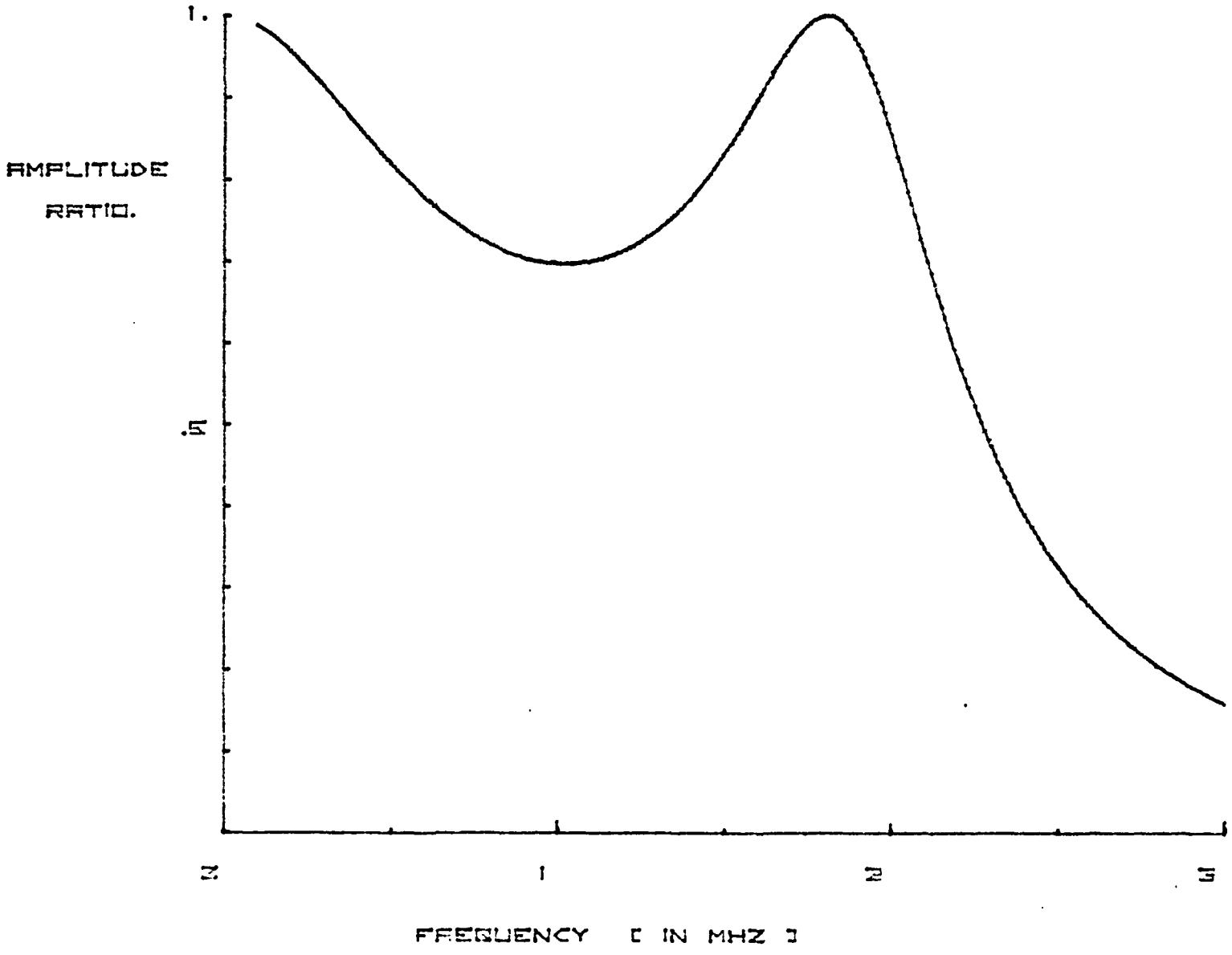
AMPLITUDE
RATIO.
1.
.5
0
1
2
3
FREQUENCY [IN MHZ]